QUANTITATIVE APPROACHES FOR UNDERSTANDING AND MINIMIZING CHEMOTHERAPY-INDUCED PERIPHERAL NEUROPATHY

By

XIAOWEI ZANG

A dissertation submitted to the

School of Graduate Studies

Rutgers, The State University of New Jersey

In partial fulfillment of the requirements

For the degree of

Doctor of Philosophy

Graduate Program in Pharmaceutical Science

Written under the direction of

Leonid Kagan

And approved by

_____

_____

_____

_____

New Brunswick, New Jersey

January, 2019

ABSTRACT OF THE DISSERTATION

Quantitative Approaches for Understanding and Minimizing Chemotherapy-induced Peripheral Neuropathy

by XIAOWEI ZANG

Dissertation Director:

Leonid Kagan

In 2016, it was estimated that more than 15.5 million cancer survivors were living in the US, and this number will increase to more than 20 million by 2026. Highly effective treatments have been developed, and the increase in survival demands more attention to patient's quality of life and management of adverse effects. Chemotherapy-induced peripheral neuropathy (CIPN) is a dose-limiting adverse effect of various cancer therapies, such as paclitaxel and cisplatin. CIPN is one of the most challenging pain conditions with poor response to pharmacotherapy; therefore, discontinuation of chemotherapy or dose reduction often remains the only clinical solution.

The thesis focused on using quantitative approach for improving our understanding of the relationships between tissue distribution of the chemotherapeutic agents and CIPN development. In an introductory Chapter 1, an overview of the chemotherapeutics, CIPN, formulations, and modeling approaches is presented. In Chapter 2, a physiologically-based pharmacokinetic (PBPK) model was developed to characterize the whole-body disposition of paclitaxel following administration of a commercially available formulation (Taxol®). Pharmacokinetic data of paclitaxel in mice from multiple publications was collected and used for model development. Interspecies scaling approaches were incorporated in the model and provided reasonable prediction of tissue disposition of

paclitaxel in rats and plasma pharmacokinetics in humans. In Chapter 3, a nanoparticle formulation of paclitaxel was developed. The neurotoxicity development in rats was significantly reduced after administration of the PEGylated liposomal paclitaxel compared to Taxol®. The formulation has also significantly altered paclitaxel disposition into tissues. In Chapter 4, a quantitative relationship between the dose, plasma pharmacokinetics, and paclitaxel-induced peripheral neurotoxicity was established by evaluating the paw withdrawal threshold to mechanical stimuli after intravenous administration of Taxol® to rats using experimental data and published literature. Indirect response models adequately described the pharmacokinetic-pharmacodynamic relationship. In Chapter 5, a PBPK model of cisplatin (another neurotoxic compound) was developed based on multiple published data sets from preclinical species. The model included the uncommon metabolism and binding pattern of cisplatin, and an interspecies scaling approach based on protein turnover rate was developed. The model successfully predicted cisplatin pharmacokinetics in humans. Collectively, the studies provided important insights into quantitative relationships for neurotoxic chemotherapeutics. Translational PBPK and PK-PD modeling approaches can be further utilized for optimization of therapy with neurotoxic chemotherapeutics.

ACKNOWLEDGEMENT

My journey at Rutgers has been a memorable one because of all the help and support from the most wonderful people in my life. First and foremost, I would like to express my sincere gratitude to my advisor Dr. Leonid Kagan for his immense support, guidance, and motivation for my Ph.D. project. As my mentor and advisor, he has taught me more than I could ever give him credit for. He has shown me what a great person, scientist, supervisor should be. His intelligence, enthusiasm, and proactivity inspired me throughout my graduate study, and certainly years to come.

I would like to thank my committee members, Professor Tamara Minko, for her continuous support on my project and serving on my committee. And I would like to thank Dr. Arash Hatefi, and Dr. Simon Zhou for their valuable comments, advice, and critical review on my dissertation.

I am also thankful to Gregory Voronin and Raymond Rosa for their education and help with my animal studies. I am especially thankful for Dr. John Sun and Dr. David Cragin, who have been supportive and insightful of my career goals and who worked actively to provide me with advices to pursue those goals.

Graduate studies are not only a compilation of research work, but also a testimony of teamwork and collaboration. I am grateful to all the current and previous fellow students and colleagues in Dr. Kagan's lab, Dr. Luigi Brunetti, Dr. Helene Chapy, Manting Chiang, Grace Chong, Kiran Deshpande, Xizhe Gao, Dr. Katarzyna Kosicka, Dr. Jong Bong Lee, Sarah Oh, Andrew Shen, Andrew Wassef. Their kindness, friendship, encouragement make my journey so enjoyable and unforgettable.

I would like to present my special thanks to the administrative team in the Department of Pharmaceutics for their support, Ms. Hui Pung, Fei Han, Marianne Shen, and Sharana Taylor. I also acknowledge the financial support from Department of

Pharmaceutics, Department of Pharmacy Practice & Administration, Ernest Mario School of Pharmacy and NIH R01 grant (CA209818) during the entire graduate study.

I am very lucky to be surrounded with some of the most wonderful friends at Rutgers and US. I would like to thank Manting Chiang, Maryam Khojasteh, Jong Bong Lee, Uijin Jeong, Helene Chapy, Andrew Kuzmov, Obeid Malekshah, Qian Zhang, Shuting Fang, Zhi Yang, Tianxin Wu, Hao Li, and Mian Wang for the fun times we had together. I would like to express my gratitude to Sino-American Pharmaceutical Professional Association for providing a platform to improve my interpersonal, leadership, and communication skills.

This dissertation is dedicated to my beloved mom and dad, who has been an immense source of relentless love and support. I could not have gone this far without their encouragement to help me overcome the most desperate circumstances. The dissertation is also dedicated to my husband, Xiang, who has shown his unconditional love and encouragement. Your critical thinking, proactivity, and patience has motivated me to be a better person. The love and support from my entire family in China has supported me so much through every step along my way.

DEDICATION

To My Beloved Parents and Husband

TABLE OF CONTENTS

LIST OF TABLES

LIST OF ILLUSTRATIONS

Chapter 1 Introduction

1.1 Chemotherapy-Induced Peripheral Neuropathy (CIPN)

1.1.1 Peripheral Neuropathy

It was estimated that over 15.5 million cancer survivors were living in the US in 2016, and this number will increase to more than 20 million by 2026 (1). Based on recent data from the Center of Disease Control and Prevention, about 650,000 cancer patients receive chemotherapy in an outpatient oncology clinic in the US each year. Although highly effective treatments have been developed in oncology field, new approaches are needed to manage and prevent severe adverse effects associated with these treatments and to improve patients' quality of life.

Neuropathy (and especially neuropathic pain) is a challenging clinical problem with 8% of the population worldwide suffering from this condition (2). Neuropathy is defined as "pain caused by a lesion or disease of the somatosensory nervous system". Neuropathic pain may have a much greater impact on patients compared to people with other types of chronic pain; and significantly more patients with neuropathy rated their quality of life as "worse than death", according to a generic health-related quality of life study (3). Chemotherapy treatment often cause both acute and chronic peripheral neuropathy – chemotherapy-induced peripheral neuropathy (CIPN).

1.1.2 CIPN

CIPN is caused by various chemotherapeutic agents including taxanes (paclitaxel, docetaxel), platinum-based compounds (cisplatin, oxaliplatin, carboplatin), vinca alkaloids (vincristine, vinblastine), epothilones (ixabepilone), proteasome inhibitors (bortezomib) and immunomodulators (thalidomide) (4). Although chemotherapy is often highly effective, many cancer survivors suffer from CIPN during and after the treatment. CIPN is a major

dose limiting side effect that often leads to dose reduction or discontinuation of treatment (5). In a meta-analysis on 31 studies from 4179 patients, CIPN prevalence was 68% when measured in the first month after chemotherapy, 60% at 3 months, and 30% at 6 months after chemotherapy (6). The incidence of CIPN usually depends on the cumulative dose and the type of the chemotherapeutic agent, with reported prevalence rates ranging from 19% to 85% (7). CIPN is more common in patients with preexisting nerve damage, such as previous CIPN and diabetic neuropathy (8).

The mechanisms of toxicity and molecular targets in CIPN vary and depend on chemotherapeutic drug; and most agents cause neuronopathy, axonopathy, myelinopathy, mitochondrial dysfunction and/or oxidative stress (9, 10). Several cellular mechanisms in the peripheral nervous system are affected by chemotherapeutic agents, including neuronal and/or mitochondrial DNA and gene expression, axonal transport, ion channel expression and function, and neuroimmune system (4). Notably, peripheral nerves contain a variety of nerve fibers with the longest nerves having the greatest vulnerability and consequently first affected by neurotoxic agents (11). Therefore, a typical clinical symptom observed in patients with CIPN is occurs in a “glove and stocking” pattern, where the predominantly sensory syndrome is first observed in the hands and feet of patients, including numbness, paresthesia, ongoing/spontaneous pain, and hypersensitivity to mechanical and/or cold stimuli (2). Patients with CIPN will experience extreme difficulties in essential daily activities including difficulty in fine finger movement, such as picking up coins (numbness), walking with pain (mechanical hypersensitivity), inability to retrieve food from a refrigerator (cold hypersensitivity). Sometimes chemotherapeutics causes “coasting” symptom, which represents either worsening of mild neuropathy or development of new neuropathy after cessation of the treatment (2, 4). Such symptom will continue to impact the quality of life of patients even after discontinuation of chemotherapy (often for many years after therapy). CIPN is also associated with a substantial economic

burden because of the healthcare costs, resource use, and work-loss of patients to treat and manage the severe symptoms (12).

1.1.3 Clinical Treatment and Prevention of CIPN

CIPN is a challenging clinical syndrome without effective preventive or curative options. American Society of Clinical Oncology clinical practice guideline did not recommend any agent for the prevention of CIPN, based on a systematic literature review of randomized controlled trials for the treatment of CIPN (13). Preventive drugs also may potentially counteract the desired effect of chemotherapy. Such phenomena have been observed with multiple preventive therapies, including vitamins B and E, glutathione, alpha lipoic acid, acetylcysteine, amifostine, calcium and magnesium (5). Furthermore, the effectiveness of preventive approaches is often questionable. For example, preventive drugs did not work on CIPN induced by platinum drugs (14). Current treatment options for CIPN are mostly based on experience from managing other types of chronic neuropathy, rather than specifically designed for CIPN based on its mechanisms (2). Anticonvulsants, antidepressants, and opioids have been used for symptomatic treatment of neuropathy (5), yet there is scarce evidence for their clinical utility. For example, in an uncontrolled clinical trial of 75 patients with CIPN from the first-line chemotherapy, patients who received 800 mg/day of gabapentin reported significant improvement in pain compared with patients who refused to take gabapentin (15). However, another crossover randomized trial of 115 patients with CIPN showed no difference between the control group and patients who received 900 mg of gabapentin three times a day (16). Similarly, amitriptyline, nortriptyline, and lamotrigine failed to demonstrate any effect on CIPN in several randomized controlled trials (17-19). Topical preparations are often used off-label, such as 0.025% capsaicin cream, 8% capsaicin and 5% lidocaine patches with questionable benefit (20).

1.1.4 Methods of assessment of CIPN (in animals and humans)

1.1.4.1 Difference between pain and nociception

Pain is defined by the International Association for the Study of Pain (IASP) as “an unpleasant sensory and emotional experience associated with actual or potential tissue damage or described in terms of such damage”. Different from pain, nociception is a result of central nervous system processing of the physiological signal from of the peripheral nervous system responding to potential harmful stimuli (21, 22). In other words, the ability to detect a harmful or potentially harmful stimulus is called nociception, which is a fundamental physiological function in humans and animals. Pain, on the other hand, is an experience that encompasses both sensory and emotional components, which is one of many end points of nociception and the term cannot interchange with nociception.

1.1.4.2 Measurement of Pain and Nociception in Humans

There are no widely accepted and standardized assessment tools to reliably classify patients with CIPN. Several clinician-administered grading scales are available to assess CIPN clinically, including grading benchmarks from the World Health Organization, Eastern Clinical Oncology Group, National Cancer Information Center-Common Toxicity Criteria, and Common Terminology Criteria for Adverse Events (23). Majority of the grading systems rely on the patient’s self-report of symptoms, from grade 0 at no symptom to higher grade levels as the symptom gets more severe. In addition to grading the neurotoxicity levels, patients are also evaluated on how CIPN affects their lives. The most common self-report measurement is the Functional Assessment of Cancer Therapy/Gynecologic Oncology Group Neurotoxicity. This assessment evaluates the severity of symptoms by reporting scores range from 0 to 44 points, where a higher score is associated with a higher quality of life (23).

1.1.4.3 Nociception in Animals

Pain assessment is difficult and often subjective in humans, and study of pain is limited by ethical considerations. Various animal models (mostly rats and mice) to study pain/nociception have been developed (24). However, to appropriately quantify behavioral responses in animals that translates to various degree of pain in humans is extremely challenging. Some possible surrogate end points include but not limited to withdrawal reflexes, vegetative and hormonal responses, and vocalization (25). It should be noted that none of the assessments in animals directly measured pain, but an enhanced nociception because animals cannot provide verbal feedback of a painful experience. This distinction between measurement of nociception in animals and assessment of pain in humans often leads to lack of effective translation between preclinical and clinical settings.

Instead of measuring CIPN directly in animals, “pain-like” behaviors, such as paw withdrawal from a nociceptive stimulus, are commonly used to quantify nociception in animal models (26). If the animal withdraws from a stimulus that does not normally evoke a withdrawal response, the animal is considered to have allodynia. If the animal withdraws with an exaggerated response from a normally noxious stimulus, the animal is considered to have hyperalgesia. However, it is very difficult to differentiate between allodynia and hyperalgesia in animals, and these two terms are often being used incorrectly or interchangeably in the literature. Therefore, in this work, the term “sensitivity” is used instead of hyperalgesia or allodynia. Similarly, nociception and pain are often used interchangeably in the literature, although the term “pain” should not be used in animal studies.

The outcomes of most behavioral studies are subjective and somewhat biased. For example, the investigator must determine if paw withdrawal occurred because of aversive nature of applied stimulus or other reasons, such as tickle, grooming, or ambulation. Therefore, preferred method of behavioral studies is blinding the treatment

groups from the investigator and performing randomization of treatment groups by a different investigator (26). The behavioral methods can be divided into three stimulus-evoked modalities: mechanical, heat, and cold stimuli. Commonly used methods to assess nociception in animals are listed in **Table 1.1**. In the current study, electronic Von Frey and Hargreaves tests were used to evaluate development of CIPN in animals.

1.1.4.3.1 Measurement of animal response to mechanical stimuli - Electronic Von Frey

Electronic Von Frey systems were developed based on the “gold standard” manual Von Frey test introduced by the physiologist Maximilian von Frey (26). The main advantage of electronic Von Frey compared to manual Von Frey is that the threshold is determined by a single, un-bending filament with a continuously increasing mechanical force. The force is automatically recorded by the apparatus when paw withdrawal response is elicited. In addition, the experimental time is also significantly reduced compared to manual Von Frey test. However, the investigator needs to be experienced to differentiate a true response from other responses (tickle, grooming, or ambulation). Several electronic Von Frey systems are commercially available, the dynamic plantar aesthesiometer (Ugo Basile, Italy) was selected in the current study because it is very robust and user-friendly. The dynamic plantar aesthesiometer comes with a perforated platform with plastic enclosures on top of it (**Figure 1.1a**). Animals are placed inside the plastic enclosures for ~20 min of habituation before the actual measurement. A metal filament (0.5 mm diameter) is placed under the mesh screen floor to apply a continuous linearly increasing mechanical force to the plantar surface on the hind paw at 2.5 g/s, with a cut-off time of 20 seconds to prevent damage. A withdrawal threshold in grams is automatically recorded, either when the animal withdraws the paw in response to the mechanical stimuli or at the cut-off force. The measurement is repeated at least 3 times with a 5 min interval.

1.1.4.3.2 Measurement of animal response to thermal stimuli - Hargreaves Test (Plantar Test)

Hargreaves test, also known as plantar test, was developed to quantify response to heat in the hind paw of rodents by applying a beam of radiant or infrared heat (27). Similar to the electronic Von Frey test, animals are placed inside the plastic enclosures for ~20 min of acclimation before measurement (**Figure 1.1b**). A radiant or infrared heat generator is positioned underneath the glass floor, directly below the plantar surface of hind paws. The time of withdrawal from the heat stimulus is recorded automatically as the withdrawal latency. The cut-off time is 20 seconds to prevent potential tissue damage. The measurement is repeated at least 3 times with a 5 min interval. The intensity of the heat is constant during the experiment, and it should be adjusted to produce a withdrawal latency of 10-12 s in naïve animals. The disadvantage of this test is that the withdrawal latency is recorded rather than directly measuring the response temperature. The paw withdrawal temperature can be derived from the response time (27). A modified Hargreaves test has been reported to determine the actual withdrawal temperature (28). However, this method takes much time consuming and it is not commercially available.

Table 1.1 Common methods for assessment of pain-like behaviors in rodents*

	Name	Test Methods	Testing Sites	Outcome Parameter
Mechanical Stimuli	Manual Von Frey	Application of non-noxious calibrated static hairs on skin	Hindpaw	Force threshold of paw withdrawal
	Electronic Von Frey	Application of linearly increasing mechanical force in non-noxious range on skin	Hindpaw	Force threshold of paw withdrawal
	Randall-Selitto	Application of linearly increasing mechanical force in noxious range on skin	Hindpaw, tail	Force threshold of paw withdrawal
Heat Stimuli	Tail Flick	Application of radiant heat on tail or immersion of tail in hot water	Tail	Time latency of tail flick/withdrawal
	Hot Plate	Animal placed on heated metal plate	Hindpaw (forepaw)	Time latency of nociceptive behavior
	Hargreaves	Application of radiant heat on skin	Hindpaw	Time latency of paw withdrawal
Cold Stimuli	Cold Plate	Animal placed on cooled metal plate	Hindpaw	Time latency of nociceptive behavior
	Acetone Evaporation	Application of acetone on skin	Hindpaw	Duration/intensity of nociceptive behavior

*Adapted from (25)

a)

b)

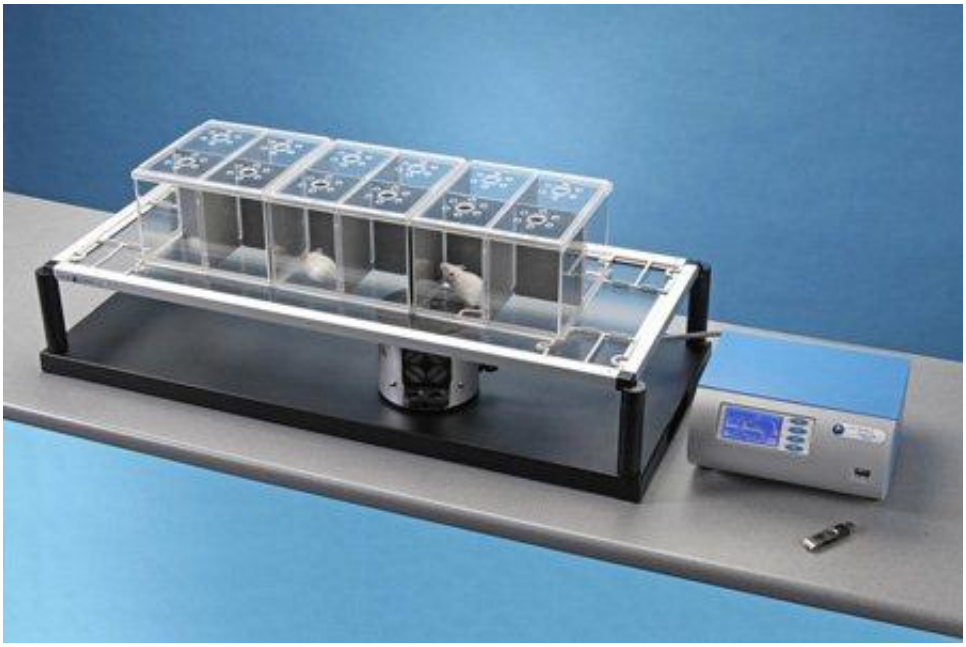

Figure 1.1 a) Electronic Von Frey apparatus used to measure animal response to mechanical stimuli (29) and **b)** Hargreaves test apparatus (30) used to measure animal response to thermal stimuli.

1.2 Chemotherapy Agents (Paclitaxel and Cisplatin)

1.2.1 Clinical Facts

CIPN is caused by many chemotherapeutic agents (31). In this work, paclitaxel and cisplatin were selected as model drugs because they demonstrated many similarities in their mechanism of action, related adverse effects, are often clinically used alone or in combination.

Paclitaxel is an effective therapeutic agent to treat many types of cancer, including ovarian, breast, lung, colon, bladder, esophagus, head and neck, multiple myeloma, and Kaposi's sarcoma (32, 33). Paclitaxel is a diterpenoid pseudo alkaloid having molecular formula $C_{47}H_{51}NO_{14}$ and a molecular weight of 853 Da (**Figure 1.2**). It is the first of a class of microtubule stabilizing agent (34). Paclitaxel is poorly soluble in aqueous medium (0.77-35 µM) and high lipophilic (logP ~ 4) (35-38). Therefore, the first approved formulation of paclitaxel, Taxol® (Bristol-Myers Squibb Company, Princeton, NJ), was developed in a vehicle composed of Cremophor EL® (polyoxyethylated castor oil) and ethanol (v:v, 1:1), which should be diluted subsequently with saline or dextrose solution (5%) to 0.3-1.2 mg/mL for administration (39). Common and often dose-liming adverse effects of Taxol® therapy includes peripheral neurotoxicity (42–70%), nephrotoxicity (18–34%) and hypersensitivity (31–45%), neutropenia (78-98%), leukopenia (90%), anemia (47-90%) (reported as percentages of patients after single-agent therapy) (40). Presence of Cremophor EL® is indicated to contribute to some of the side effects of Taxol® treatment, including hypersensitivity, hyperlipidaemia, aggregation of erythrocytes, and peripheral neuropathy (41). Taxol® is commonly given every 3 weeks intravenously (IV) over 3 h at a dose of 175 mg/m^2 or over 24 h at a dose of 135 mg/m^2 with cisplatin for non-small cell lung cancer. Other than being used with cisplatin, paclitaxel may be administered alone (for example, at 175 mg/m^2 over 3 h every 3 weeks for breast and ovarian cancer) (40). Reduction in dosage by 20% is required for patients experiencing severe CIPN. In a

recent study, 49 patients who received 80 mg/m^2 weekly of paclitaxel, 12 patients developed dose-limiting CIPN; and more than half (58.3%) of the 12 patients had their treatment discontinued (42).

Cisplatin (cis-diamminedichloroplatinum(II); CDDP) has been widely used since its approval in 1978 for treatment of metastatic testicular, metastatic ovarian, transitional cell bladder cancer, non-small cell lung cancer (in combination with gemcitabine) and cervical cancer (in combination with radiation). It is also commonly used off-label for head and neck, esophageal, gastric, colorectal, hepatocellular, metastatic melanoma, and as second-line to metastatic breast, prostate, etc. (43). Cisplatin is a platinum-based alkylating compound with the molecular formula $PtCl_2H_6N_2$ and a molecular weight of 300.1 Da **(Figure 1.2)**. The drug was first approved as Platinol® (Bristol-Myers Squibb Company, Princeton, NJ), which is formulated with sodium chloride and mannitol since its water solubility is up to 1 mg/mL (44). Pretreatment hydration with 1-2 L of fluid is recommended prior to cisplatin treatment for all cancers. Cisplatin is administered in cycles, for example, at 50-70 mg/m^2 every 3-4 weeks for bladder cancers and 100 mg/m^2 every 4 weeks for ovarian cancers (40). Cisplatin and its metabolites are mostly renally excreted and often causes nephrotoxicity because of the excessive accumulation in the renal proximal tubules. Patients with a creatine clearance less than 60 mL/min require dose adjustment (45). Other than nephrotoxicity (28-36%), common and often dose-liming adverse effects of cisplatin therapy includes peripheral neurotoxicity, leukopenia (90%), ototoxicity (40-60% in children and 10-31% in adults) (reported as percentages of patients after single-agent therapy) (40). Neurotoxicity developed in nearly 50% of patients who received cisplatin-containing regimen compared to 25% of patients treated with non-cisplatin-containing regimen. Additionally, the severity of neurotoxicity in cisplatin treated patients was more pronounced (46). Notably, almost 100% of patients who received a

cumulative dose of cisplatin at 500-600 mg/m^2 have an objective evidence of peripheral neuropathy (47-49).

1.2.2 Mechanisms of action of paclitaxel and cisplatin

The mechanisms of action of paclitaxel and cisplatin in cancer are well described **(Figure 1.3)**. Different from other microtubule agents, such as vinca alkaloids, paclitaxel is acting by inhibition of microtubule disaggregation from the microtubule polymer. The microtubule formed in the presence of paclitaxel is very stable, which causes cell cycle arrest in the G2-M phase junction (50). Cisplatin (similar to other platinum compounds) interferes with cancer cell proliferation by binding to the DNA. DNA bound cisplatin reacts with nitrogen in the purine rings and disrupt cell division and transcription to mRNA (51). Both agents alter function of the respiratory chain in mitochondria and subsequently increase production of reactive oxygen species. In addition, cisplatin result in damage to tumor cell by binding to the mitochondrial DNA and inhibition of mDNA replication and transcription (4). Both agents cause activation of immune cells by release of pro-inflammatory cytokines and activation of intrinsic and extrinsic apoptotic pathways, which may contribute to tumor cell death. Additionally, cisplatin causes cell death by altering calcium signaling pathways and function of protein kinases, such as protein kinase C and mitogen active protein kinases (51).

1.2.3 Mechanisms of CIPN induced by paclitaxel and cisplatin

The pathophysiology of CIPN development have been studied extensively. Even though paclitaxel and cisplatin have distinct neurotoxic and neuroinflammatory properties, several common pathologies have been proposed, including oxidative stress, activation of apoptotic pathways, axon degeneration, inflammatory processes, membrane remodeling, and ion channel alteration **(Figure 1.4)**. Several pathophysiology processes

that involves axon degeneration, oxidative stress, apoptotic mechanisms, altered calcium homeostasis as well as immune process and neuroinflammation will be discussed.

1.2.3.1 Axon degeneration

Long-term chemotherapy treatment causes axon degeneration, such as loss of large myelinated axons, small unmyelinated axons, and intraepidermal nerve fibers, which subsequently induces sensory-motoric peripheral neuropathy, (52-56). Since paclitaxel acts as a tubulin-stabilizer and prevents depolymerization, it disrupts axonal transport and leads to axonal degradation, axonopathy, and loss of epidermal innervation (57-59). Paclitaxel causes swelling and atypical morphology changes in mitochondrial C fibers and myelinated axons by opening the mitochondrial permeability transition pore (60, 61). Similarly, axonal degeneration of large myelinated fibers and secondary myelin breakdown have been observed in the peripheral nerves in cisplatin treated patients (62).

1.2.3.2 Oxidative stress and apoptotic pathways

Mitochondrial damage in neuronal and non-neuronal cells by chemotherapeutic agents leads to increased production of reactive oxygen species and increase oxidative stress (63-66). Since the mechanism of action of cisplatin is binding to DNA, it also forms mitochondrial DNA adducts and impair replication and transcription of mitochondrial DNA, leading to altered protein synthesis and respiratory chain disfunction (67). Unlike cisplatin, paclitaxel does not directly affect mitochondrial DNA, but it causes swollen and vacuolated mitochondria in myelinated and unmyelinated axons in saphenous nerves of the mid-thigh area in rats (60). These changes induce reactive oxygen species production in sensory neurons and spinal cord (68, 69).

1.2.3.3 Calcium homeostasis

Changes in intracellular calcium levels influence membrane excitability, neurotransmitter release and gene expression (70). Both paclitaxel and cisplatin have been shown to dysregulate calcium homeostasis, which contributes to CIPN development.

Paclitaxel induces rapid mitochondrial depolarization and calcium release in neuronal cells by activation of mitochondrial permeability transition pore (71, 72). Additionally, paclitaxel increases activity of both ligand-gated and voltage-gated ion channels in rodents, including voltage-gated sodium channel, voltage-gated potassium channel, transient receptor potential channel, and voltage-gated calcium channel (73). Similarly, cisplatin increases the activity of N-type voltage-gated calcium channels in sensory neurons (74, 75); but the contribution of calcium to cisplatin-induced neuropathy remains largely unknown.

Paclitaxel

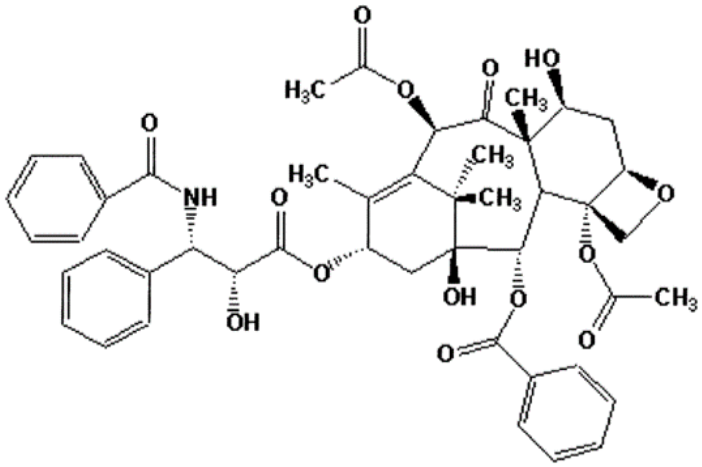

Cisplatin

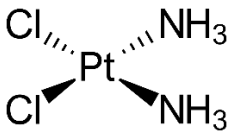

Figure 1.2 Chemical structure of paclitaxel (34) and cisplatin.

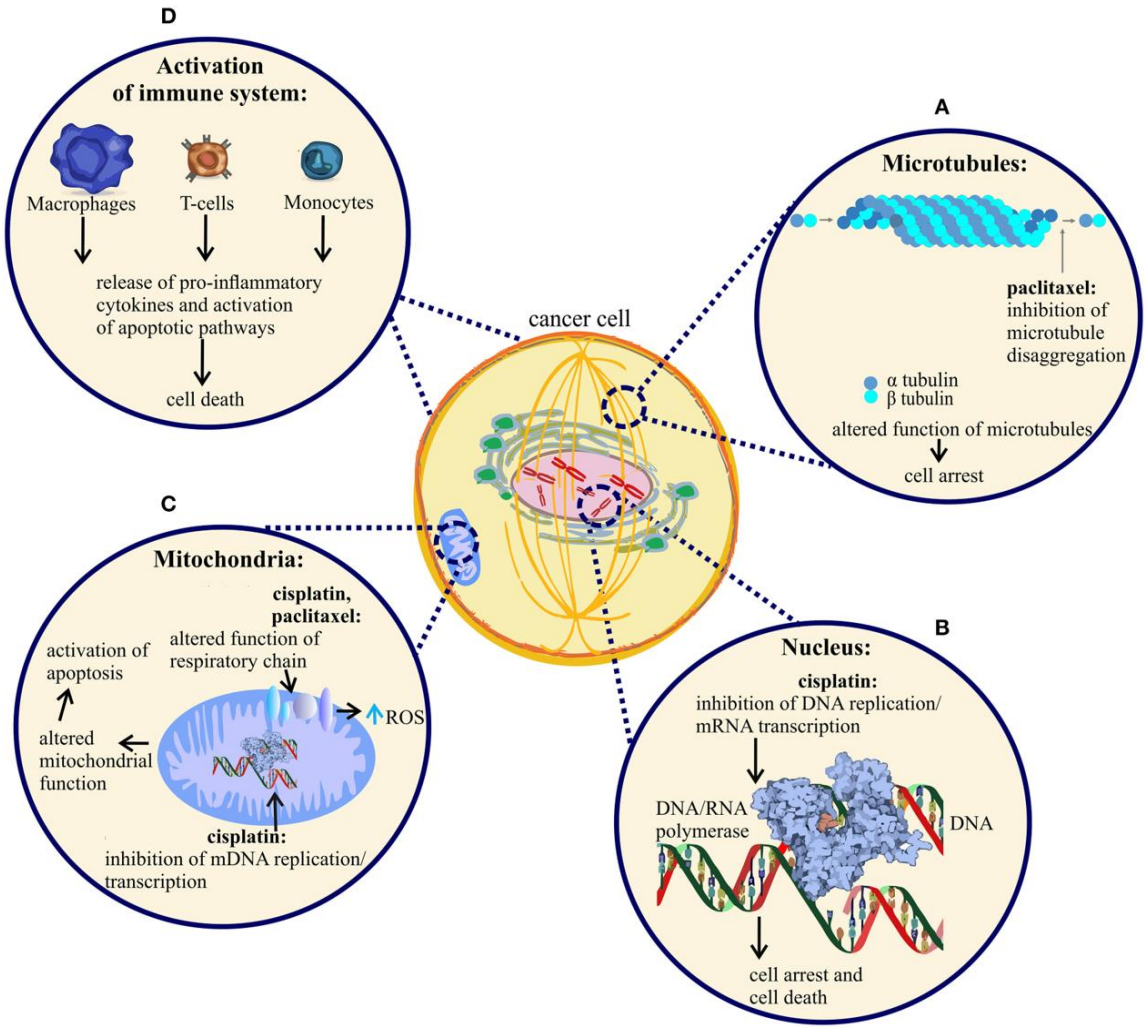

Figure 1.3 Anti-tumor mechanisms of action of paclitaxel and cisplatin. **A)** paclitaxel promotes microtubule aggregation, leading to arrest of cancer cell division and cell death. **B)** Cisplatin binds to nuclear DNA, affecting DNA replication and mRNA transcription, which subsequently cause cell division arrest and cell death. **C)** Both agents affect the mitochondrial function, followed by disruption of respiratory chain function and production of reactive oxygen species. **D)** Both agents activated the immune cells, which contribute to cancer cell degradation. Adapted from (4).

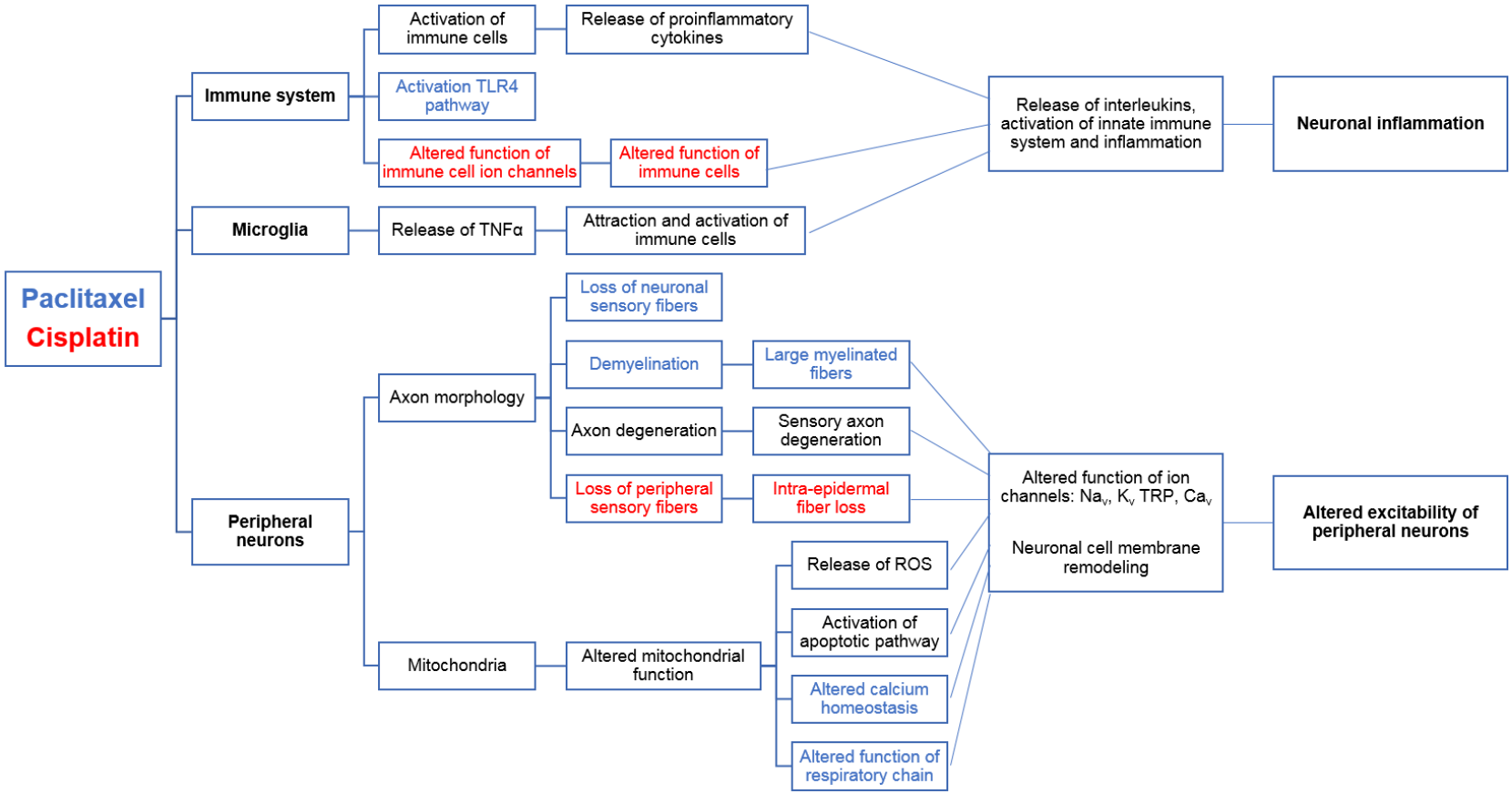

Figure 1.4 Putative mechanism involved in the development of paclitaxel and cisplatin-induced peripheral neuropathy. Overview of possible effect of paclitaxel and cisplatin on the immune system, microglia, and peripheral neurons leading to neuronal inflammation and altered excitability of peripheral neurons. Common mechanisms for paclitaxel and cisplatin are shown in black, paclitaxel specific mechanisms are shown in blue, and cisplatin specific mechanisms are show in red. TLR4, toll-like receptor 4; TNFα, tumor necrosis

factor alpha; ROS, reactive oxygen species; Na_v, voltage-gated sodium channel; K_v, voltage-gated potassium channel; TRP, transient receptor potential channel; Ca_v, voltage-gated calcium channel. Adapted from (4).

1.3 Nanoparticle formulations

1.3.1 Nanoparticle formulations

Chemotherapeutic agents provoke cytotoxic effects by inhibition of cell replication or induction of cell apoptosis (76). Although most cytotoxic agents are highly effective, one of the primary concerns of using chemotherapeutic drugs is the lack of ability to differentiate healthy cells from tumor cells (77). Chemotherapeutic drugs are most harmful to rapidly proliferating cells, such as hair follicle, intestinal epithelial cells, and bone marrow (76). One of the advantages of using nanoparticles for treatment of cancer is their potential to address the lack of specificity of anticancer drugs and narrow therapeutic window. Nanoparticles are colloidal carriers with dimensions between 1-100 nm (78). Various properties of nanoparticles can be manipulated to target and enhance interaction with tumor cells, including size, composition, surface functionalization, and stability (79, 80). Nanoparticles could significantly alter drug biodisposition (81), facilitate drug transport to intracellular organelles and induce greater cytotoxic effect (82). The most common nanoparticles are liposomes, micelles, dendrimers, nanospheres, and nanocapsules.

1.3.2 Liposomes

Liposomes is one of the most attractive drug delivery systems because its amphiphilic nature that is capable of encapsulating both polar and nonpolar compounds (83). They are spherical vesicles composed of one or more phospholipid bilayers surrounding an internal aqueous core. Due to this structure, hydrophilic molecules are encapsulated in the internal aqueous space, whereas hydrophobic molecules are incorporated into the lipid bilayer (84, 85). Liposomes are biodegradable, biocompatible, non-toxic and suitable both hydrophilic and hydrophobic molecules (86). Potential disadvantages of liposomes can be relatively low stability and rapid clearance from the bloodstream. To overcome this problem, functionalized liposomes (e.g., with

poly(ethylene glycol - PEG) were developed to shield the nanoparticles from opsonin adsorption and subsequently decrease their clearance by the mononuclear phagocyte system and reticuloendothelial system - system (87, 88). The shape, density, and length of the PEG chains can be modified to achieve different rates of clearance. It has been shown that PEG chains with molecular weight above 2000 Da increase the half-life of the nanoparticles (89). Based on a recent review, two drugs using PEGylated liposomes formulation have been approved for clinical use, and five PEGylated based liposome formulations are in clinical trial (90). Doxil® was the first PEGylated liposome formulation approved by the Food and Drug Administration in 1995. It is a formulation of doxorubicin to treat Kaposi's sarcoma, ovarian cancer, and multiple myeloma (91, 92). The formulation is very stable due to the presence of PEGylated liposomal surface, which improves the circulation half-life significantly to several days, and subsequently increases the likelihood of extravasating at sites with leaky vascular system causing hand-foot syndrome (93-95).

1.3.3 Liposomal Paclitaxel

Currently, one liposomal formulation of paclitaxel has been commercialized (Lipusu®) in China, and two formulations have reached to phase II clinical trials (LEP-ETU and EndoTAG-1). Lipusu® (Luye Pharma Group, Jiangsu, China) is approved for treatment of ovarian, breast, non-small cell lung cancer, gastric, head and neck cancers by IV administration. In a clinical trial of oxaliplatin (in combination with tegafur) in 58 patients with advanced gastric cancer, patients that received Lipusu had similar overall response rate, and no significant differences were observed in hematologic and neurologic toxicities similar to Taxol® at the same dose level. (96). The CIPN and hypersensitivity of LEP-ETU (NeoPharm) and EndoTAG-1 (Medigene) treatments have not been sufficiently investigated. In a phase I study of LEP-ETU, dose limiting toxicities occurred at 375 mg/m^2 and included febrile neutropenia and neuropathy (that appeared to be no worse than that

for Taxol®) (97). In another clinical study evaluating EndoTAG-1 treatment, fatigue and hypersensitivity reactions were reported (98).

1.3.4 Change of pharmacokinetics properties

The physicochemical properties of liposomes may affect the pharmacokinetics (PK) properties of the drug such as tissue distribution, drug elimination half-life, and drug release rate. Therefore, incorporation of a chemotherapeutic drug into liposome can potentially increase antitumor efficacy by providing more selective distribution into tumor tissues or reduce toxicity by avoiding of healthy tissues. Modulation of the PK of the drug improves the overall pharmacological properties. For example, drug distribution to healthy tissues may be reduced because of the particle size limitation for transport across healthy vascular endothelium; drug circulating half-life may be increased by reducing drug removal (clearance) from the blood (84, 99). Subsequently, the pharmacodynamic (PD) effects would manifest themselves following PK effects on drug distribution at tissue and cellular levels. The potency of a liposomal drug relative to the non-encapsulated drug often arises from alteration of PK of the encapsulated drug (100).

1.4 Physiologically-Based Pharmacokinetics (PBPK)

1.4.1 Pharmacokinetics (PK) of Paclitaxel and Cisplatin

Highly variable PK of paclitaxel has been reported in clinical studies. The PK of paclitaxel shows an initial rapid distribution to the peripheral compartments. In humans, the half-life elimination is about 13-20 h for a 3 h infusion and about 16-53 h for a 24 h infusion of Taxol® (32, 40). Paclitaxel is a substrate of cytochromes P450 2C8 and 3A4 and P-glycoprotein; and the protein binding rate is 89-98% (101-103). The fecal excretion is approximately 70% of the dose with one of the metabolites, 6a-hydroxypaclitaxel, being the major component (104); about 14% of the dose was excreted into urine as unchanged paclitaxel and metabolites (40, 104).

Unlike majority of drugs, cisplatin undergoes special metabolic transformation after administration into animals and humans. Cisplatin (parent drug) and its aquated species irreversibly bind to low molecular weight nucleophiles and nucleophilic sites on macromolecules to form mobile metabolites and fixed metabolites (105, 106). The tight and irreversible binding results in a slow elimination with a prolonged half-life (44). Most studies measured the total platinum concentration without differentiating between parent drug of cisplatin and its mobile or fixed metabolites. Plasma concentrations of cisplatin parent drug show a monoexponential decay with a half-life of about 0.5 h following intravenous (IV) bolus administration at a dose of 50 or 100 mg/m^2, or 2 h infusions at 100 mg/m^2 in clinical uses (44). In humans, cisplatin clearance and volume of distribution at steady state were reported as 15-16 L/h/m^2 and 11-12 L/m^2 respectively. Renal clearance is the major elimination pathway for cisplatin and its metabolites. Fecal excretion of platinum is insignificant because very minimal amount of platinum is present in the bile and large intestine (44).

1.4.2 PBPK

Classical PK analysis can be performed using compartmental or non-compartmental approaches (107, 108). Non-compartmental analysis (NCA) requires few assumptions compare to compartmental analysis where NCA can be applied practically to any PK data (109). The classical compartmental approach describes the body as a system of one-compartment (mono-exponential) or multiple-compartments (bi- or tri-exponential) that usually have no direct physiological or anatomical meaning. Rate constants describe drug movement between compartments and out of the compartments (elimination).

In the classical PK analysis, certain tissues of the body are lumped together to form hypothetical compartments, such as rapidly- or slowly-equilibrating compartments. The absorption and distribution process of a drug is dependent on multiple biochemical and physiological parameters, such as organ perfusion rate and tissue volume. Unlike the classical PK system, the physiologically-based approach separates the body into multiple anatomical compartments that are connected by the body fluid systems (**Figure 1.5**). Each compartment represents an organ or tissue which has anatomical significance. These models not only provide common PK parameters (e.g. clearance, volume of distribution) but also can be used to predict plasma, and importantly, tissue concentration-time profiles of drugs in human and other animals. PBPK model can also be used to extrapolate from healthy volunteers to diseased/special population if the related physiological properties of the targeting population are known. For example, a dose adjustment for patients with chronic liver disease can be easily done by incorporating data related to reduced cytochrome P450 expression into the PBPK model (110).

The use of PBPK modeling was initially limited to the pharmaceutical industry because of the mathematical complexity and the large number of parameters require extensive drug concentration measurement in multiple tissues. However, the application

of PBPK has increased significantly over the past decade in both academia and industry. One of the reasons is the ability to use *in vitro* and *in silico* data to predict one of the key drug-specific parameters, tissue to plasma partition coefficient (111-113). Application of PBPK modeling is often used during drug discovery where most of the preclinical ADME (absorption, distribution, metabolism, excretion) data *in vitro* and *in vivo* can be modeled. In addition, PBPK modeling approach demonstrates utility to assess drug-drug interaction in new drug application to regulatory agencies (114). There were 33 investigational new drug or new drug application to the FDA that included PBPK modeling between June 2012 and December 2012 (114). The guidance documents on drug-drug interaction assessment with drug candidate were issued by the FDA (115) and the European Medicines Agency (116) in the recent years.

1.4.2.1 PBPK model structure and assumptions

As mentioned previously, PBPK models are consist of multiple compartments which defined by tissue volume or weight and tissue blood flow rate. Each tissue is typically described as either perfusion rated limited kinetics (**Figure 1.6a**) or permeability rate limited kinetics (**Figure 1.6b**) (117). Perfusion rate limited model is common for small lipophilic molecules where the blood flow rate is the limiting step for disposition. The model assumes that the total drug concentration in tissue is in equilibrium with total drug concentration in the blood circulation at steady states, which can be described by the drug-specific tissue to plasma partition coefficient value (Kp). The time to reach steady state of each tissue is influenced by blood flow rate, Kp value, and tissue volume. Permeability rate limited kinetic model may be needed for larger hydrophilic molecules were the permeability across the cell membrane is the limiting step. The tissue is considered to have two sub-compartments, representing intravascular and extravascular space. The rate-limiting step is dependent on drug-specific permeability rate constant which drives the equilibrium across the membrane between intracellular and extracellular spaces. The

unbound drug concentration in intracellular space may be higher or lower than extracellular space when the active transport process is involved. Such process can be described by incorporating uptake parameters into the model.

In general, each tissue compartment follows the principle of “the rate of change of drug in the tissue is equal to the rate in minus the rate out”, which described as the following mass-balance differential equation $V \cdot {dC}/{dt} = Q \cdot C_A - Q \cdot C_T$, where Q is the blood flow, C is the drug concentration, V is the tissue volume, C_A is arterial blood concentration and C_T is venous blood concentration (118, 119).

The PBPK model is defined by physiological parameters and drug-specific input parameters. Physiological parameters include tissue volumes, blood flow rates, cardiac output, glomerular filtration rate, etc. PBPK models could be developed for many species, and the physiological parameters are different from one species to another, which are available in the literature (120-122) and routinely used by researchers (118, 119). It is also possible to incorporate physiological features to predict drug PK in special or disease populations. For example, hepatic flow, liver/renal function as a function of disease or age can be incorporated into PBPK models (3, 32,33).

Drug-specific input parameters are often estimated using the PBPK model or acquired from *in vitro* or *in vivo* experiments (e.g., clearance and tissue-specific partition coefficient). For example, the hepatic clearance can be scaled from *in vitro* system, using recombinant enzymes, hepatocytes, and microsomes (117). For renal or biliary excretion, the allometry scaling approach $CL = a \cdot BW^b$ (a is the allometric coefficient, b is the allometric power function, BW is body weight) is most frequently used where unbound clearance is scaled from one species to another or across multiple species (123, 124). Another important drug-specific parameter is Kp values, which defined as the ratio of total concentration of the drug in the tissue to plasma at steady state.

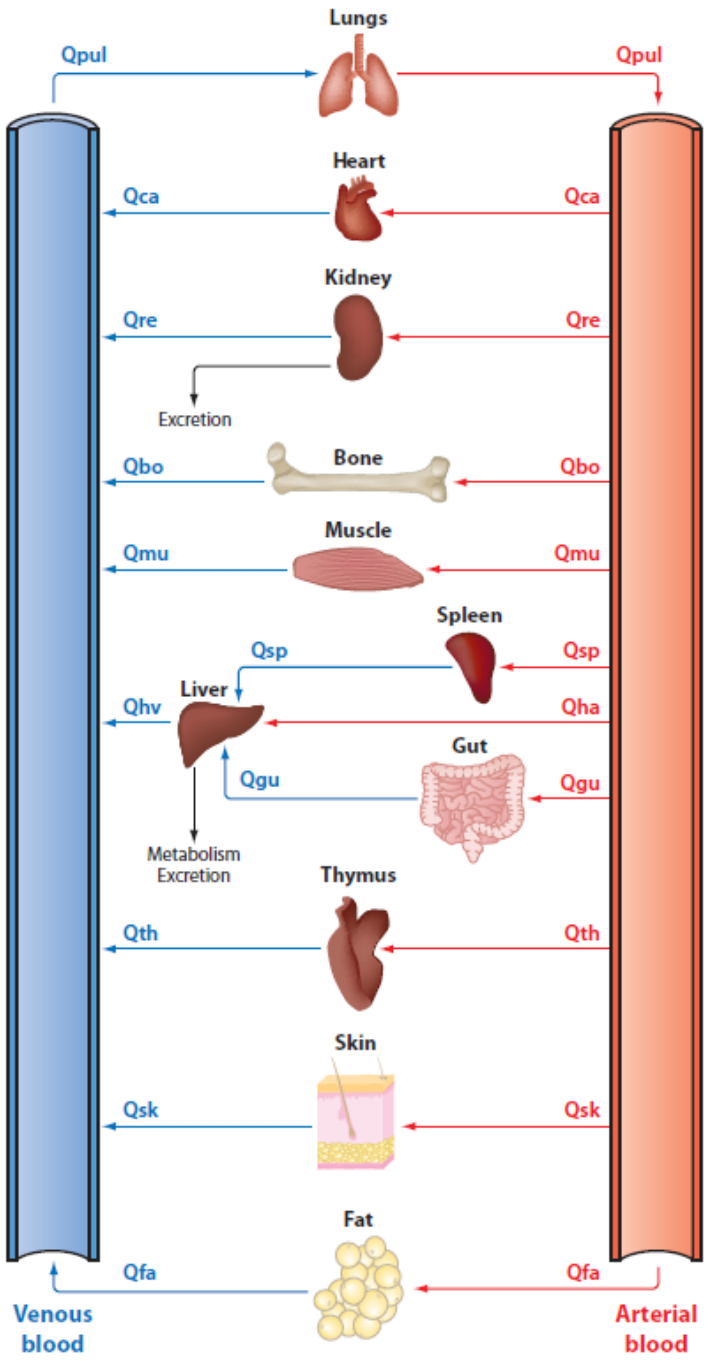

Figure 1.5 Schematic of a whole-body physiologically-based pharmacokinetic model (adapted from (125)). Elimination is depicted from liver and kidneys, where it can possibly happen at other sites for some drug. *Qi* blood flow of the tissues, *pul* lungs, *ca* heart, *re*

kidneys, *bo* bone, mu musles, *sp* spleen, *ha* liver, *gu* gut, *hv* hepatic vein, *th* thymus, *sk* skin, *fa* fat.

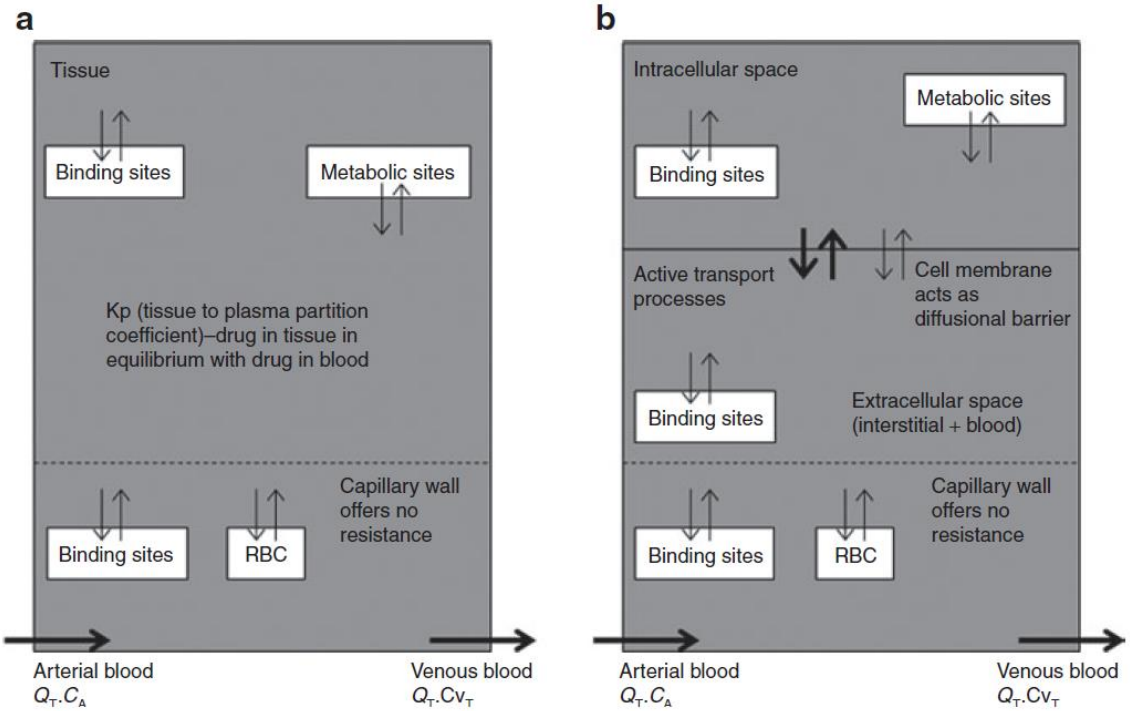

Figure 1.6 Examples of perfusion rate limited **(a)** and permeability rate limited **(b)** model structures. *Kp* tissue to plasma partition coefficient, *RBC* red blood cells (adapted from (117))

1.5 Mechanism-based Pharmacodynamic Models

Pharmacodynamics refers to the relationship between the substance concentration at the site of action, where the therapeutic targets are located, and the magnitude of the pharmacological response (126). The pharmacological effect produced by the compound includes the intensity of therapeutic and adverse effects, which is quantified by the PD analysis by linking the compound effect and concentration at the site of action (127). Mechanism-based models are very useful to estimate the inaccessible PD variables and parameters based on the mechanism of action of the drug and underlying mechanisms of biological systems. In general, there are irreversible effects and reversible effects, where the reversible effects can be broadly classified as direct and indirect responses.

Direct effect models are used if a drug immediately and directly produce a PD response being measured and is related to the drug concentration at the site of action. However, for compounds exhibiting a lag time between the peak in plasma concentration and peak of response, a biophase or indirect response models are commonly utilized depending on a reason for delayed response. When the delayed response is caused by equilibration delay between plasma compartment and the drug concentration at the site of action, the term “biophase” was proposed to link the plasma concentration and drug effect through a hypothetical effect compartment (**Figure 1.7**) (128). The biophase model is only appropriate for delayed response due to drug distribution. In contrast, if there is a lag time for development of a response even after the drug reaches the site of action, indirect response model or more complex PD relationship would be coupled with or without biophase to incorporate the changes.

Indirect response models (IDR) are considered to represent a mechanistic delay in the process of inhibition or stimulation of the production or dissipation of factors controlling the measured effect (129). IDR models may be suitable for many mechanisms

when a lag time exists between biophase drug concentrations and the time course of response. Four basic IDR models include inhibition of production of response (I), inhibition of dissipation of response (II), stimulation of production of response (III), and stimulation of dissipation of response (IV) with the corresponded differential equations (**Figure 1.8**).

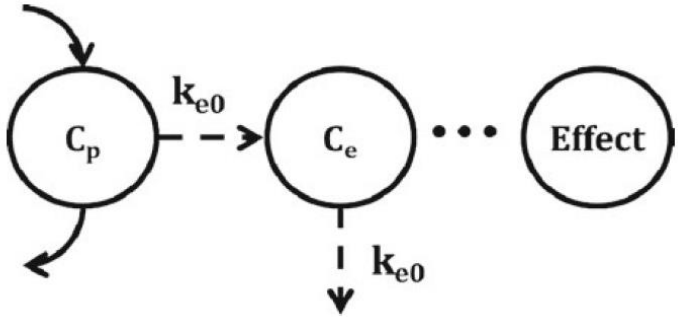

Figure 1.7 Biophase model structure (130). C_p, drug concentration in plasma; C_e, drug concentration in effect compartment, k_{eo}, first-order distribution rate constant

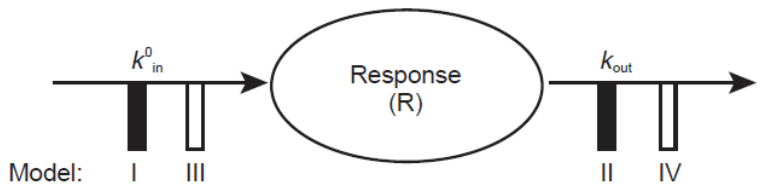

I. Inhibition – k^0_{in}

$$\frac{dR}{dt} = k^0_{in} \cdot \left(1 - \frac{I_{max} \cdot C_p}{IC_{50} + C_p}\right) - k_{out} \cdot R$$

$$0 < I_{max} \leq 1$$

III. Stimulation – k^0_{in}

$$\frac{dR}{dt} = k^0_{in} \cdot \left(1 + \frac{S_{max} \cdot C_p}{SC_{50} + C_p}\right) - k_{out} \cdot R$$

$$S_{max} > 0$$

II. Inhibition – k_{out}

$$\frac{dR}{dt} = k^0_{in} - k_{out} \left(1 - \frac{I_{max} \cdot C_p}{IC_{50} + C_p}\right) \cdot R$$

$$0 < I_{max} \leq 1$$

IV. Stimulation – k_{out}

$$\frac{dR}{dt} = k^0_{in} - k_{out} \left(1 + \frac{S_{max} \cdot C_p}{SC_{50} + C_p}\right) \cdot R$$

$$S_{max} > 0$$

Figure 1.8 Four basic indirect response model representing process that inhibit or stimulate the factors controlling the measured effect (129). k^0_{in}, a zero-order production rate constant; k_{out}, first-order elimination rate constant; I_{max}, maximum fractional factors of inhibition; S_{max}, maximum fractional factors of stimulation; IC_{50}, drug concentrations at 50% of the maximum inhibition effects; SC_{50}, drug concentrations at 50% of the maximum stimulation effects; C_p, plasma concentration; R, response.

1.6 Summary

Chemotherapeutic agents, such as paclitaxel and cisplatin, are a standard of care for many cancer treatments. Although they demonstrated superior efficacy, the associated side effects, especially CIPN, often lead to dose-reduction or discontinuation of the treatment.

The excipients of Taxol®, Cremophor EL, contribute to hypersensitivity and mechanical neuropathy in animal models as well as clinical trials (131, 132). Since significant number of patients experience hypersensitivity, premedication with corticosteroids, diphenhydramine, and H_2 antagonists is needed with Taxol® treatment. Therefore, researchers have been developing Cremophor EL-free formulations of paclitaxel for less toxicity. Multiple drug delivery systems have been investigated, such as albumin-bound nanoparticles, micelles, liposomes, nanogel polymers, solid lipid nanoparticles, and polymer-drug conjugates (78). Investigation of liposomal nanoparticles of paclitaxel has demonstrated similar or superior efficacy to Taxol® treatment because of the absence of Cremophor EL. Liposome paclitaxel has the potential of targeting delivery to tumors because of the enhanced permeability and retention effect. Additionally, PEGylated liposomes prolong the duration of pharmacological activities and decrease the adverse effects. However, none of the liposomal paclitaxel formulation have been tested clinically using PEGylation modification. There is an urgent need to investigate in the efficacy and toxicity profile of PEGylated liposomal paclitaxel.

The study of translational research from preclinical to clinical is critical to improve the understanding of pathophysiology of neuropathy and further apply to effective preventive and treatment approaches. Paclitaxel and cisplatin have been commercially available over decades but the PBPK mechanisms have not been fully understood. PBPK model development for chemotherapeutic drugs would advance the understanding of its pharmacokinetics and pharmacodynamics. Establishing such models could benefit

optimization for therapy with existing paclitaxel formulation and understand the potential correlation between the adverse effect (e.g. peripheral neuropathy) and tissue concentrations.

Similarly, the quantitative relationship between PK profiles of paclitaxel and its related CIPN has not been established in animals or clinically. Since CIPN is the dose-limiting toxicity of paclitaxel treatment, there is an urgent need to quantify the dose-CIPN relationship to assess the safety profiles. The PKPD model built up in animal models may ultimately be applied to clinical CIPN evaluation with paclitaxel treatment.

1.7 Specific Aims

1. **To characterize tissue disposition of paclitaxel after administration of Taxol® using PBPK modeling approach**.

PBPK model of paclitaxel disposition was developed based on published data. Animal data from several publications was used for model development, and pertinent model parameters were successfully estimated. The model was used to predict paclitaxel tissue disposition in other species, including humans.

2. **To evaluate the effect of encapsulation of paclitaxel in liposomes on tissue disposition and neurotoxicity in an animal model of neuropathic pain.**

Pegylated liposomes containing paclitaxel were successfully developed and demonstrated reduced neurotoxicity *in-vitro*. Furthermore, in an animal study liposomal formulation did not produce neuropathic symptoms, in contrast to Taxol® that was neurotoxic.

3. **To develop quantitative model to capture the time-course of development of neuropathy in rats following administration of Taxol®.**

PK-PD (a combination of a biophase and indirect response) model was successfully developed and captured induction of neuropathy in rats and recovery using several data sets (experimentally obtained and collected from the literature).

4. **To characterize tissue disposition of cisplatin using PBPK modeling approach**.

PBPK model of cisplatin disposition was developed based on multiple animal data sets from published literature. The model included conversion of cisplatin to mobile and fixed metabolites. The PBPK in combination with interspecies scaling based on protein turnover successfully predicted tissue disposition of platinum in humans.

Chapter 2. Physiologically-Based Modeling and Interspecies Prediction of Paclitaxel Pharmacokinetics[1]

2.1 INTRODUCTION

Paclitaxel is a standard therapy for various types of cancer, including ovarian, breast, lung, colon, bladder, esophagus, head and neck, multiple myeloma, and Kaposi's sarcoma (32, 33). First discovered in the early 1960s (33), paclitaxel was approved by the Food and Drug Administration for drug-resistant ovarian cancer in 1992 and breast cancer in 1994. This diterpenoid pseudoalkaloid has a molecular weight of 853 Da, and was the first in a new class of microtubule stabilizing drugs. Different from vinca alkaloids, which promote the disassembling of microtubules, paclitaxel stimulates the polymerization of tubulin (102, 133-135). The disruption of cytoskeletal microtubule homeostasis leads to termination of the cell cycle at interphase and metaphase and inhibition of cell division (136).

Paclitaxel poses a significant pharmaceutical development challenge due to is high lipophilicity (logP~4) and poor aqueous solubility (0.77-35 μM) (35-38). Taxol® (Bristol-Myers Squibb Company, Princeton, NJ), the first approved formulation of paclitaxel is based on dissolving the drug in polyoxyethylated castor oil (Cremophor EL) and ethanol (1:1, v/v). Taxol® is commonly administrated in cycles. For example, treatment for breast and ovarian cancer is 175 mg/m^2 intravenous infusion over 3 h every 3 weeks for 4 cycles or 135 mg/m^2 over 24 h every 3 weeks for non-small cell lung cancer in combination with cisplatin (40). Although highly efficacious, Taxol® therapy is associated with serious (and often dose-limiting) adverse effects, including peripheral neurotoxicity (42-70%), nephrotoxicity (18-34%) and hypersensitivity (31-45%) (reported as percentages of patients after single-agent therapy) (40). Some of the adverse reactions, including the

[1] Part of the chapter has been published by Zang and Kagan in J Pharmacokinet Pharmacodyn. 2018 Aug; 45(4):577-592

hypersensitivity, have been partly attributed to Cremophor EL (137); and significant effort was invested into developing alternative formulations of paclitaxel. Abraxane®, a Cremophor EL-free albumin-bound paclitaxel formulation, became available in the US in 2005. Later, polymeric micelle (Genexol®-PM) and liposome (Lipusu®) formulations were approved in Korea and China, respectively. A variety of particulate formulations has been developed mostly focusing on enhanced tumor penetration and improved efficacy (78, 138, 139).

Highly variable pharmacokinetics of paclitaxel has been reported in clinical studies. In humans, the terminal half-life ranges from 13 to 20 h with a 3 h infusion of Taxol® and up to 53 h after a 24 h infusion in adults (32, 40). Paclitaxel is extensively metabolized by cytochromes P450 2C8 and 3A4 in the liver, and >90% is bound to plasma proteins (101-103). The fecal excretion was approximately 70% of the dose with 6α-hydroxypaclitaxel metabolite being the major component (104), and about 14% of the drug is excreted in urine as unchanged paclitaxel and metabolites (40, 104). Paclitaxel plasma pharmacokinetic profiles follow multiphase decline, and variety of pharmacokinetic models have been proposed to capture this behavior (140-142); however, a model of whole-body biodisposition of paclitaxel has not been reported before. Development of physiologically-based pharmacokinetic (PBPK) models can provide important insights into the mechanisms of biodisposition, allow for predicting drug exposure profiles in human tissues, and establishing pharmacokinetic-pharmacodynamic relationships (125).

Establishing a PBPK model for paclitaxel can advance the understanding of its pharmacokinetics and pharmacodynamics, will be beneficial for optimization of therapy with existing paclitaxel formulations, and will inform development of novel formulation with improved efficacy and safety profiles. The primary goal of this work was to develop a PBPK model to characterize the disposition of paclitaxel in mice. The second goal was to

evaluate the utility of the PBPK model for predicting paclitaxel pharmacokinetic in other species including humans.

2.2 MATERIALS AND METHODS

2.2.1 Data sources

To investigate whole-body biodisposition of paclitaxel, pharmacokinetic data were collected from the literature. Only studies that evaluated the Taxol® formulation administered by the intravenous route were included in the analysis in order to minimize formulation-dependent or absorption-dependent variability. Mean data (total paclitaxel concentration in plasma and tissues) in each publication were captured by Plot Digitizer (version 2.6.8). Twelve publications reporting paclitaxel pharmacokinetic profiles in plasma and tissues after a single intravenous (IV) bolus administration to mice were identified after initial screening. Only four of these publications were selected for the subsequent PBPK model construction, and others were excluded from the analysis based on one or combination of the following reasons: 1) insufficient data (no plasma profiles or too few tissue samples); 2) reported concentration was a thousand times higher than in any other sources, 3) did not use a commercially available Cremophor EL/ethanol formulation. The selected studies (six dose levels) were used to construct a PBPK model of paclitaxel disposition in mice (**Table 2.1**) (143-146). Shin and colleagues reported plasma pharmacokinetic profiles and tissue concentrations (stomach, small intestine, large intestine, liver, kidney, spleen, and lung) up to 24 h following IV injection of Taxol® at three different dose levels of 5, 10, and 20 mg/kg to female ICR mice. For the data sets derived from Shin et al., the concentration in the gastrointestinal (GI) tract compartment was calculated by taking the mean of concentrations reported for small intestine, large intestine, and stomach. Gong and colleagues reported plasma and tissue biodistribution (liver, kidney, spleen, lung, and heart) up to 24 h following IV injection of Taxol® at 4 mg/kg to C57BL/6 mice. Li et al. and Yang et al. reported plasma and tissue distribution (liver, kidney, spleen, lung, and heart) up to 12 h and 6 h respectively, following IV administration of 15 mg/kg and 3 mg/kg of Taxol® to Kunming mice.

Rat and human data were used for evaluating interspecies prediction using the PBPK approach. Thirteen studies were identified that reported plasma pharmacokinetic data of Taxol® following single IV administration to rats (147-159), and four of them reported tissue concentrations, including liver, kidney, spleen, lung, heart, and muscle. The doses ranged from 2.5 to 10 mg/kg. Five studies that reported plasma profiles of Taxol® following IV infusion administration in cancer patients were used. The drug was administered as an IV infusion of 175 mg/m^2 over 3 h (160-162), and 125 mg/m^2 as an IV infusion over 3 h (163), and 160 mg as an IV infusion over 3 h (164). No information on concentration of paclitaxel in human tissues could be identified in the literature.

2.2.2 Physiological parameters

Physiological parameters, including tissue weights, fractions of vascular space in tissues, and plasma flow rates to organs, were fixed to literature values (120-122). Plasma cardiac output (CO) for rats and mice was calculated using allometric relationships: $CO_{rat}(L/h) = 14.1 \cdot (1 - Hematocrit) \cdot (body\ weight\ in\ kilograms)^{0.75}$ and $CO_{mouse}(L/h) = 16.5 \cdot (1 - Hematocrit) \cdot (body\ weight\ in\ kilograms)^{0.75}$ (120). Cardiac output for humans was fixed to 312 L/h (120). All tissues that were not reported in the publications were lumped into a remainder compartment (107). The densities of all tissues were assumed to be 1.

2.2.3 Drug-specific parameters

For model development, the fraction unbound of paclitaxel (${f_u}^{pl}$) was fixed to 0.1 for all species since paclitaxel was reported to be 89-98% bound to plasma protein in humans (40), 89-95% bound in mice (165, 166), and approximately 90% bound in rats (167). Paclitaxel is extensively metabolized by cytochrome P450 enzymes (CYP2C8 and CYP3A4) in humans, rats, and mice (168). Major biliary metabolites identified includes 6α-hydroxypaclitaxel (humans and mice), *3'-p*-hydroxypaclitaxel (humans, rats, and mice), *2-m*-hydroxypaclitaxel (rats), and 6α,3'-p-dihydroxypaclitaxel (humans) (40, 169-171).

Metabolites of paclitaxel are mostly recovered in feces in mice, rats, and humans, with minimal contribution of urinary excretion (40, 104, 169, 172). A total of 90 ± 6% of radioactivity was recovered in feces by labeling ^{3}[H]-paclitaxel in mice, and the amount of unchanged drug recovered in urine were very limited (1%) (172). In a clinical study, the amount of unchanged drug collected in urine was 4.5% of the total dose (up to 12 h after dosing) (104). Because only a minor fraction of the dose is recovered in the urine as an unchanged drug, renal clearance was fixed to zero and only hepatic clearance was estimated in the final PBPK model.

2.2.4 Initial data assessment and modeling strategy

Multiple publications reported plasma concentration-time profiles of paclitaxel (and some included tissue data) in mice and rats. Initial data evaluation using visual inspection and noncompartmental analysis revealed a very high between-study variability. For the same formulation and the same dose level, the reported concentrations often differed more than 10-fold (representative plasma concentration-time profiles following Taxol® injection to mice are shown in **Figure 2.1**). In our previous works, a common PBPK model of amphotericin B disposition was developed by combining data from multiple publications (173, 174). However, in case of paclitaxel, initial attempts to fit multiple data sets using the proposed PBPK model structure (as described below) and a single set of parameters demonstrated that this approach was not feasible. While nonlinear pharmacokinetics has been reported for paclitaxel before (140-142), visual inspection of dose-normalized profiles pooled from multiple sources did not reveal any trends. To allow for development of a useful PBPK model, it was assumed that paclitaxel disposition in mice follows the same model irrespective the specific study design. Each of the murine data sets was fitted separately using the same structural model and separate sets of parameters were estimated and compared. Available rat data sets contained only limited number of sampled tissues or time points and could not be reliably used for parameter estimation.

Therefore, rat and human data were used for assessment of interspecies scaling approaches using the PBPK model as described below.

2.2.5 Construction of the PBPK model using murine data

The PBPK model was developed using murine data, and only organs that were sampled in more than two studies were incorporated. The final structural model included plasma, gastrointestinal (GI) tract (gi), spleen (sp), liver (li), kidneys (kd), lungs (lu), heart (hr), and remainder (rm) (lumped all non-sampled tissues) compartments (**Figure 2.2**). Initially, each tissue was represented by a single "well-stirred" compartment, where the venous plasma is considered to be in instant equilibrium with the tissue concentration; and tissue-specific partition coefficients ($K_p{}^{tissue} = f_u{}^{pl}/f_u{}^{tissue}$) were used to describe these compartments. However, this structural model could not satisfactory describe some of the data sets. In the final model, the structure of the remainder compartment was changed to include two sub-compartments (vascular and extravascular spaces) that were described using two parameters: permeability-surface area term (PS_{rm}) and tissue-specific unbound fraction ($f_u{}^{rm}$). The differential equations used to describe the model were similar to our previous publication (173), as shown in the Appendix. Because drug concentration in the GI tract were unavailable in the data sets derived from Li et al. and Yang et al. studies, and concentration in the heart were unavailable in the data sets derived from Shin et al., the corresponding parameters could not be estimated with sufficient precision. To overcome this difficulty, $K_p{}^{gi}$ for Li et al. and Yang et al. data sets and $K_p{}^{hr}$ for Shin et al. were set to be equal to $K_p{}^{rm}$ (which was calculated from $f_u{}^{rm}$ as $K_p{}^{rm} = f_u{}^{pl}/f_u{}^{rm}$).

2.2.6 Interspecies scaling and PBPK simulations for rats and humans

To evaluate predictive performance of the PBPK model, pharmacokinetic profiles of paclitaxel in rats and humans were simulated and compared to published results. Body weights of 213 g and 66 kg were assumed for rats and humans, respectively, by taking

the mean of the reported body weight values from used publications. Rat and human physiological parameters, including organ volumes, blood flows, and fraction of vascular space in the tissues, were reported previously (120-122, 173). Unbound fraction of plasma ($f_u{}^{pl}$) was fixed to 0.1 for rats and human as previous stated, and $K_p{}^{tissue}$ and $f_u{}^{tissue}$ were assumed to be identical among different species. CL_{li} and PS_{rm} were scaled from the values estimated for mice using an allometric equation: $P = P_{mouse} \cdot (\frac{BW}{BW_{mouse}})^B$, where P is the parameter of interest, BW is species body weight, and B is an allometric exponent. Based on the assumptions that permeability of tissues for paclitaxel among species is similar and that the surface area is proportional to the $BW^{2/3}$, the allometric exponent B was fixed to 0.67 for PS_{rm} (173, 175). To determine the allometric exponent for clearance, regression analysis of total clearance vs. body weights across different species was performed. Plasma concentration-time profiles from 6 mouse (143-146), 12 rat (147-150, 152-159), 1 rabbit (176), and 5 human (160-164) studies were used to calculate the systemic clearance using noncompartmental analysis in Phoenix WinNonlin (64-bit version 7.0, Pharsight, a Certara Company). Clearance values were plotted against species body weights on a log-log scale, and a power-based regression was generated based on simple allometry equation $CL = a \cdot BW^b$.

Plasma and tissue distribution profiles of paclitaxel following IV bolus administration of Taxol® to rats and IV infusion of Taxol® to humans were simulated using the final PBPK model structure and six separate parameters sets. The resulting profiles were overlaid with and compared to data obtained from the literature. Because the final PBPK model did not contain non-linear mechanisms, for simplicity the simulations were performed for a single dose level: 1 mg/kg (for rats) and 175 mg/m^2 (for humans). Sensitivity analysis was performed to evaluate the effect of allometric exponent (B) for clearance term and the effect of protein binding on human predictions.

2.2.7 Data analysis

Modeling and simulation were conducted using MATLAB R2015b software (The MathWorks, Natick, MA). All pharmacokinetic parameters were estimated using the maximum likelihood method. The variance model was defined as $VAR_i = (\sigma_1 + \sigma_2 \cdot Y(\theta, t_i))^2$, where VAR_i is the variance of the ith data point, σ_1 and σ_2 are the variance model parameters, and $Y(\theta, t_i)$ is the ith predicted value from the pharmacokinetic model. The goodness of fit was assessed by system convergence, Akaike Information Criterion, estimator criterion value for the maximum likelihood estimation method, and visual inspection of residuals and fitted curves.

2.3 RESULTS

Initial evaluation of paclitaxel pharmacokinetic data in published literature revealed large variability. Some reported plasma concentration profiles differed by several orders of magnitude for the same dose level. Therefore, to overcome the uncertainty and allow for a meaningful comparison of the results, each of the murine datasets was fitted separately to the same structural model. Then, each separate parameter set was used to provide the simulation for other species generating a range of predicted concentration-time profiles.

2.3.1 Whole-body PBPK model in mice

A whole-body PBPK model was constructed according to the schematic presented in Figure 2. Initial model structure, in which all tissues were represented using a single compartment, could not capture the data. The modified PBPK model (that included two sub-compartments for the remainder) provided a good description of the experimental plasma and tissues data (representative fits are shown in **Figure 2.3**), and all parameters were estimated with sufficient precision (**Table 2.2**). For some of the parameters the estimates differed by 10-fold; however, no dose-dependence could be identified across all data sets. Additional model modification (e.g., using two sub-compartments for other organs) did not improve model fits and resulted in decreased precision in parameter estimation.

2.3.2 Interspecies scaling and PBPK simulations for rats and humans

To evaluate the performance of the PBPK model in predicting paclitaxel biodisposition in other species, pharmacokinetic profiles of paclitaxel in rats and humans were simulated and compared to published results. The allometric relationships between species body weights (mice, rats, rabbits, and humans) and paclitaxel clearance is shown in Figure 4. Data were fitted well by power-based regression and the resulting allometric equation was $CL = 0.5514 \cdot BW^{0.8634}$ (R^2=0.9, and the standard errors were 0.0587 and

0.001 for the allometric exponent and allometric coefficient). Therefore, the allometric exponent of 0.86 was used for interspecies scaling of the hepatic clearance in the PBPK model for simulating pharmacokinetics of paclitaxel in rat and human studies.

Figure 2.5 shows simulated paclitaxel plasma and tissue concentration-time profiles following administration of 1 mg/kg IV bolus dose of Taxol® to rats. A range of predictions was generated using six mice parameter sets (**Table 2.2**) and overlaid onto 12 observed plasma profiles and a limited number of tissue concentration-time data from rats. To facilitate the comparison, the observed data were normalized to 1 mg/kg dose level. In general, reasonable predictions of paclitaxel concentrations were obtained for plasma, spleen, liver, lung, heart, kidney, and muscle (**Figure 2.5**). Concentration of paclitaxel in the muscle tissue was not evaluated in mice studies, and muscle was incorporated into the remainder compartment of the model. Muscle accounts for approximately 50% of the mass of the remainder compartment; and the model was able to reasonably predict the concentration of paclitaxel in muscle using the simulated curves for the remainder compartment. The simulations showed that predictive performance of each separate parameter set varied among different tissues. For example, pharmacokinetic estimates from Shin et al. at the dose level of 20 mg/kg resulted in an underestimation of paclitaxel concentrations in the spleen, liver, lung, and kidney; and overestimation in the heart.

At the next stage, the ability of the PBPK model to predict paclitaxel pharmacokinetics in humans was evaluated. Plasma and tissue concentration-time profiles in humans were simulated using the model structure and six parameter sets estimated in mice **(Figures 2.6a and 2.7**). Simulations were performed for 175 mg/m^2 dose level and the observed plasma data from human studies were normalized accordingly (paclitaxel tissue disposition in humans were not available in the literature). The allometric exponent of 0.86 was applied for hepatic clearance parameter as described above. The model predicted profiles are in good agreement with the experimental data

except for the simulation resulting from the use of parameters estimated for Shin et al. at the dose level of 20 mg/kg (**Figure 2.6a**).

Allometric exponent of 0.75 is frequently used for interspecies scaling of clearance of compounds that are eliminated through a physical process, such as biliary or renal excretion. However, the appropriate approach for scaling of metabolic clearance among species is less defined. Sensitivity of the model predictions to the allometric exponent for the hepatic clearance term was conducted, and a range of exponents was evaluated. Figure 6b shows representative simulation results of the human pharmacokinetic profiles obtained using allometric exponents (B) of 0.75, 0.86, and 0.95 and the parameter set estimated for Shin et al. at the dose level of 5 mg/kg murine data set. The observed data were reasonably predicted using allometric exponents of 0.86 and 0.95. A range of paclitaxel plasma protein binding values has been reported in human, (89%-98%) (40). Therefore, sensitivity analysis was also performed using different fraction unbound values, including 0.02, 0.06, and 0.1 (**Figure 2.6c**); the parameter set estimated for Shin et al. at the dose level of 5 mg/kg was used. The observed data were better described using the value of 0.1.

2.4 DISCUSSION

A better understanding of PKPD relationships for paclitaxel is required for improving efficacy and minimizing the toxicity of therapy. Multiple preclinical and clinical pharmacokinetic studies with paclitaxel have been conducted mostly focusing on the time-course of plasma concentrations of the drug. Recently, a model-based population meta-analysis has evaluated the variability in plasma pharmacokinetics of paclitaxel and associated neutropenia using data from 20 clinical studies (177). Severe neutropenia and peripheral neuropathy might limit the dose and affect the frequency of paclitaxel administration (39). However, definitive quantitative relationships between the exposure to paclitaxel *in-vivo* and the efficacy and toxicity have not been established. For example, no relationship between the steady-state concentration of paclitaxel in plasma and the response rate to treatment, time to treatment failure, survival, or development of neurotoxicity was found in non-small cell lung cancer patients (treated with 135 or 250 mg/m^2 of paclitaxel in combination with cisplatin and granulocyte colony-stimulating factor) (178). In another clinical study, the incidence of grade 3 or 4 neutropenia was not correlated with plasma C_{max}, AUC, or dose in advanced breast or ovarian cancer patients (140). In an *in-vitro* study using eight human tumor cell lines, the IC50 of paclitaxel was found to be 2.5-7.5 nM, and no additional cytotoxicity was observed with concentrations above 50 nM (42.7 ng/mL) (179). In thyroid cancer cells, paclitaxel concentrations below 10 nM led to cell cycle changes typical for apoptosis without cell cycle arrest; however, exposure above 50 nM arrested cell cycle in G2/M phase (180). Previously, it has been demonstrated that the duration of exposure to paclitaxel when the plasma concentration exceeds 50 nM may be predictive of the severity of haematologic toxicity (neutropenia) (140, 181). Our simulations of human data show that total plasma and tissue concentrations are higher than 115 nM (100 ng/mL) for at least first 24 hour after IV infusion of 175 mg/m^2 over 3 h of Taxol® (**Figures 2.6 and 2.7**). The extent of neurotoxicity

in humans has not been directly connected with a concentration but shown to increase with cumulative dose (182). On the other hand, in an animal model of paclitaxel-induced neuropathy, no correlation was found between paclitaxel dose (0.5-2 mg/kg) and the mechanical and thermal sensitivity (183), which may be related to a similar exposure of the central or peripheral nervous system to the drug at tested dose levels. Therefore, a better understanding of the time-course of paclitaxel disposition to various tissues (both tumors and sites of toxicities) may be required for establishing a link between pharmacokinetics and pharmacodynamics and optimization of paclitaxel therapy. Since comprehensive evaluation of drug disposition to tissues in humans is usually not feasible, a combination of animal whole-body disposition studies, PBPK modeling, and interspecies scaling is a valuable approach for achieving this goal.

Despite development of alternative formulations and the fact that Cremophor EL can contribute to toxicity, modulate efficacy and the pharmacokinetics (137, 177, 179), Taxol® remains the standard paclitaxel formulation in clinical practice. Taxol® is also commonly used as a control arm in *in-vitro* activity studies and preclinical disposition studies for novel paclitaxel delivery systems. Therefore, it was essential to characterize the whole-body distribution of paclitaxel after administration of Taxol®. It should be noted that only total paclitaxel concentrations in animal plasma and tissues were available in the literature; and pharmacokinetic behavior of the formulation entrapped drug and the released drug could not be separately characterized (as we have reported before for liposomal amphotericin B) (174). Therefore, pharmacokinetic parameters of paclitaxel reported in this work should be viewed as formulation-dependent.

A certain degree of lab-to-lab (or between study) variability is an expected challenge in meta-analyses. For example, Caco-2 cell permeability assay results of drug candidates are always interpreted relative to the permeability of standards, as substantial differences in permeability of the same compounds has been demonstrated among

various laboratories (184). In this study, an exceptional extent of variability in reported preclinical paclitaxel pharmacokinetic data was found, which made it unfeasible to estimate a single set of parameters for multiple data sets. The use of nonlinear mixed effect modeling approach has been considered for data analysis with a purpose of linking some of variability to know factors. However, this approach was not feasible due to a large number of parameters in the PBPK, limited data, and lack of some pertinent details on experimental design in the utilized publications. Several plausible sources for such variability can be proposed (in addition to commonly mentioned inter-animal and bioassay-related variability). Due to physicochemical properties of paclitaxel, preparation of the dosing formulation can be difficult (185). For clinical use, commercially available Taxol® (6 mg/mL) is supposed to be diluted 5- to 20-fold with normal saline or 5% dextrose to achieve an infusion solution of 0.3 – 1.2 mg/ml, which is stable for 12 h (185). However, the details of the preparation (and dilution) of paclitaxel dosing solution are commonly not reported in animal studies and the drug is commonly given as an IV bolus (rather than infusion in clinical studies). In one of the analyzed studies, the working solution was used at concentrations of 2 and 4 mg/mL, which potentially supersaturated the solution (143). The dosing container and tubing may be incompatible with Taxol® formulation; and it was recommended to prepare working solution in glass or polyolefin containers and polyethylene-lined tubing to avoid the complication (186, 187). Furthermore, binding of paclitaxel to plastic and glass was reported during sample storage which might have significantly affected the performance of the bioanalytical assay (188). It can be speculated that precipitation of paclitaxel and binding might have largely contributed to the reported variability of pharmacokinetic profiles.

As described above, an estimation of a single set of parameters for all murine data was not feasible; therefore, each murine data set was fitted separately using the same structural model. Reasonable fits of tissue-disposition profiles were obtained and

parameters were estimated with good precision (**Table 2.2**). The estimated parameters were generally within a 10-fold range among various data sets; however, no dose dependence could be identified. It should be noted that in all evaluated studies distribution profiles to the largest organs (muscle, fat, bone, and skin) were not available.

Some previous studies in humans and mice reported nonlinear pharmacokinetic behavior of paclitaxel in plasma. Plasma concentrations of paclitaxel were described by a two-compartment model with saturable elimination and saturable tissue distribution after a 24 h infusion to pediatric patients with refractory solid tumor (189); and similarly, a three-compartment model with saturable distribution to one of the peripheral compartments and saturable elimination was used to capture paclitaxel kinetics after a 3 h or 24 h infusion to patients with advanced ovarian or breast cancer (140). Saturable tissue transport or saturable binding was also used to describe the plasma concentration-time course of paclitaxel in mice (141). Cremophor EL was shown to affect the pharmacokinetics of paclitaxel in mice (190); and nonlinear pharmacokinetics was attributed to entrapment of paclitaxel in plasma by Cremophor EL in the form of micelles (191). It was suggested that nonlinear distribution could be explained by Cremophor EL binding and that the unbound drug displayed linear pharmacokinetics (142). A combination of “carrier-mediated drug disposition” and saturable protein binding was recently used in the model-based meta-analysis of paclitaxel kinetics in humans (177). Although saturable protein binding has been reported for paclitaxel (140-142, 189, 190), such data (or free drug concentration) were not available in the publications used for building the model. Sensitivity analysis was performed to evaluate the effect of unbound fraction in the plasma on model performance (as described in the Methods). Similarly, blood-to-plasma partition data were not available in the publications used for building the model; and therefore, this process could not be included into the PBPK model. In this study, published data from different mice xenograft models and healthy mice studies were included. While uptake of the drug to a tumor could

have potentially contributed to elimination of paclitaxel, no correlation between changes in paclitaxel exposure and animal strain or presence of tumor could be identified. It can be potentially attributed to the fact that only animals with very small tumors (200 mm^3) were used.

During the initial data evaluation in this study, nonlinear pharmacokinetic behavior was observed in Shin et al. publication and these data could be captured by adding a Michaelis-Menten elimination mechanism (data not shown). However, no trends were identified by combining Shin et al. data sets with other references. Due to high between-study variability and limited data in each separate study, nonlinear disposition mechanisms were not included into the final PBPK model. Furthermore, no relationships could be identified between the dose levels and the pharmacokinetic parameters (that were estimated separately for each data set).

An important advantage of the PBPK modeling is the ability to predict distribution to human tissues, which can be rarely tested experimentally. However, approaches for combining PBPK with interspecies scaling approaches are not fully developed. Recently, the plasma pharmacokinetics of moxifloxacin in five species was simultaneously fitted using a minimal PBPK model (192), and the allometric exponent for the clearance term was estimated to be 0.59. For amphotericin B, renal and biliary clearances were scaled among species using an exponent of 0.75 (173, 174). Docetaxel hepatic and intestinal clearances were scaled using as an allometric exponent of 0.67 (193). The use of an exponent of 0.67 or 1 has been proposed for scaling of the PS terms for “permeability-limited” tissues in the PBPK models (173, 174, 194). Determining species differences in clearance for compounds eliminated through metabolism can be challenging (195). In their analysis of published data for multiple compounds, Hu and colleagues suggested using an allometric exponent of 0.67 for clearance of compounds eliminated mainly by renal

excretion, and 0.75 when substances are mostly eliminated by metabolism or by metabolism and excretion combined (196); and they further noticed that often the exponent values of 0.67 and 0.75 cannot be differentiated statistically. In this study, the allometric exponent for the clearance term was determined using noncompartmental analysis of plasma paclitaxel concentration-time profiles from four species; and the exponent estimated using the regression analysis (**Figure 2.4**) was incorporated into the PBPK model for interspecies simulations. A range of predicted paclitaxel concentration-time profiles in human plasma and in rat plasma and tissues was generated and visually compared to observed data. In general, a reasonable prediction of paclitaxel pharmacokinetics was achieved (**Figures 2.5 and 2.6a**); however, the performance of each separate set of parameters was different. The parameters estimated from Shin et al. 20 mg/kg data set demonstrated the worst prediction performance. To further evaluate the effect of the allometric exponent on interspecies predictions a sensitivity analysis using a range of values of for the clearance term was performed; exponent values of 0.86 and 0.95 provided reasonable predictions of plasma paclitaxel profiles in humans (**Figure 2.6b**). It is proposed that the use of multiple values for allometric relationships to generate a range of predictions can be beneficial for enhancing the interspecies predictive performance of PBPK models. To further understanding the source of variability in plasma and tissue concentrations, an additional sensitivity analysis using a range of f_u^{pl} values in human was conducted; protein binding of 90% provided a better prediction of the plasma paclitaxel profiles in humans (**Figure 2.6c**).

2.5 CONCLUSION

In conclusion, a PBPK model for paclitaxel administered as Cremophor EL and ethanol formulation (Taxol®) was developed using mice data and provided reasonable prediction of paclitaxel pharmacokinetics in other species. Given the variability of the observed data especially in preclinical studies the use of multiple separate data sets for creating a range of predictions of drug pharmacokinetics in humans, rather than generating a single profile, appears to be a valuable approach for translational research. Formulation (Taxol®)-dependent PBPK parameters has been determined and can be further utilized for development of novel formulations of paclitaxel. Future studies, that measure free, released, and formulation-associated drug concentrations in multiple tissues after administration of a range of dose levels are needed to fully resolve the complexities associated with paclitaxel pharmacokinetics.

Table 2.1 Sources of paclitaxel pharmacokinetic data in mice used for model development.

Author	Route of Administration	Dose (mg/kg)	Strain	Tumor	Tumor Size (mm^3)	Sex	Weight (g)	Formulation [a]	Analysis Method
Shin et al., 2009 (143)	IV Bolus	5, 10, 20	ICR	None	-	F	28-35	Taxol®	HPLC-UV
Gong et al., 2012 (144)	IV Bolus	4	C57BL/6	Pulmonary carcinoma	200	M	16-20	Taxol®	HPLC
Li et al., 2012 (145)	IV Bolus	15	Kunming	Armpit tumor	200	M	NA	Taxol®	HPLC
Yang et al., 2013 (146)	IV Bolus	3	Kunming	Right axillary tumor	200	NA	18-22	Taxol®	HPLC-UV

ICR, Institute for Cancer Research; IV, intravenous; NA, Not Applicable;

[a] In Li et al. and Yang et al. the manufacturer of Taxol® was not specified.

Table 2.2 Estimated pharmacokinetic parameters of paclitaxel in mice using the PBPK model

		Shin et al., 2009 (143)		**Shin et al., 2009 (143)**		**Shin et al., 2009 (143)**		**Gong et al., 2012 (144)**		**Li et al., 2012 (145)**		**Yang et al., 2013 (146)**	
Dose		5 mg/kg		10 mg/kg		20 mg/kg		4 mg/kg		15 mg/kg		3 mg/kg	
Parameter, units	Definition	Estimate	%CV	Estimate	%CV	Estimate	%CV	Estimate	%CV	Estimate	%CV	Estimate	%CV
CL_{li}, L/h	Hepatic Clearance	0.214	11	0.133	12	0.0465	12	0.0772	11	0.106	13	0.358	11
Kp_{gi}	Partition coefficients	3.33	13	3.27	15	2.18	16	7.48	29	1.90[a]	-	1.94[a]	-
Kp_{sp}		3.61	13	2.14	15	0.913	16	0.728	13	2.98	14	2.38	11
Kp_{li}		11.1	14	8.75	15	3.62	16	1.44	13	9.71	15	4.68	13
Kp_{kd}		3.35	13	2.26	15	1.05	16	1.67	14	3.25	15	2.69	11
Kp_{lu}		3.26	14	3.08	16	1.28	16	0.403	14	2.58	15	2.80	11
Kp_{hr}		1.50[a]	-	1.25[a]	-	9.01[a]	-	1.18	13	2.62	15	4.05	11
f_u^{rm}	Unbound fraction	0.0665	12	0.0798	13	0.0111	24	0.0253	16	0.0525	24	0.0516	11
PS_{rm}, L/h	Permeability -surface area term	0.317	23	0.0862	19	0.0220	18	0.121	13	0.0887	17	0.209	13
f_u^{pl}	Unbound fraction in plasma	0.100[b]	-	0.100[b]	-	0.100[b]	-	0.100[b]	-	0.100[b]	-	0.100[b]	-

%CV estimator criterion value for the maximum likelihood method.

[a] Calculated from $K_p^{tissue} = f_u^{pl}/f_u^{tissue}$ because tissue pharmacokinetic profile was not reported in the publication. The parameter was not estimated.

[b] Fixed to match previously reported values.

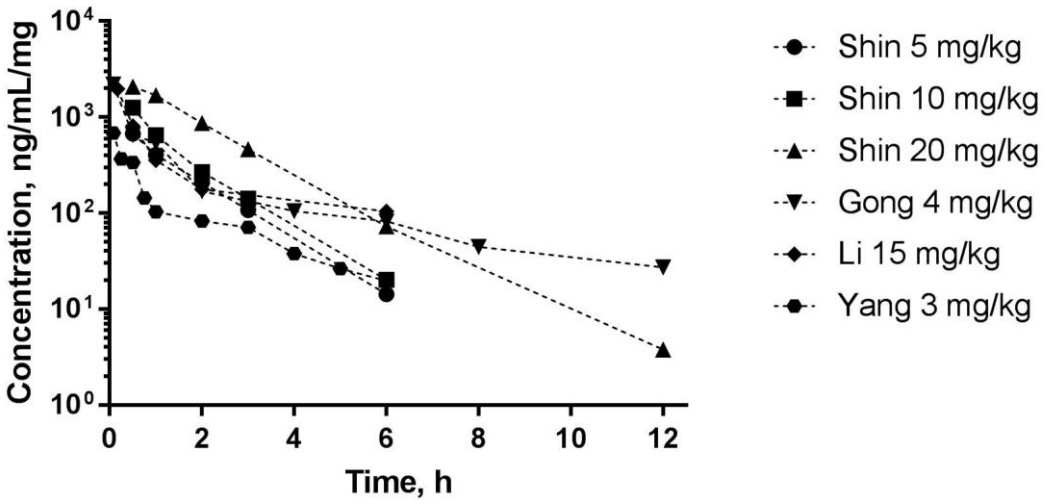

Figure 2.1 Variability in reported paclitaxel plasma concentration-time profiles following IV bolus administration of Taxol® to mice. Six datasets obtained from four different laboratories were used for model development (143-146). The legend identifies the first author of the study and the dose level; for illustration, the concentrations were normalized by the dose.

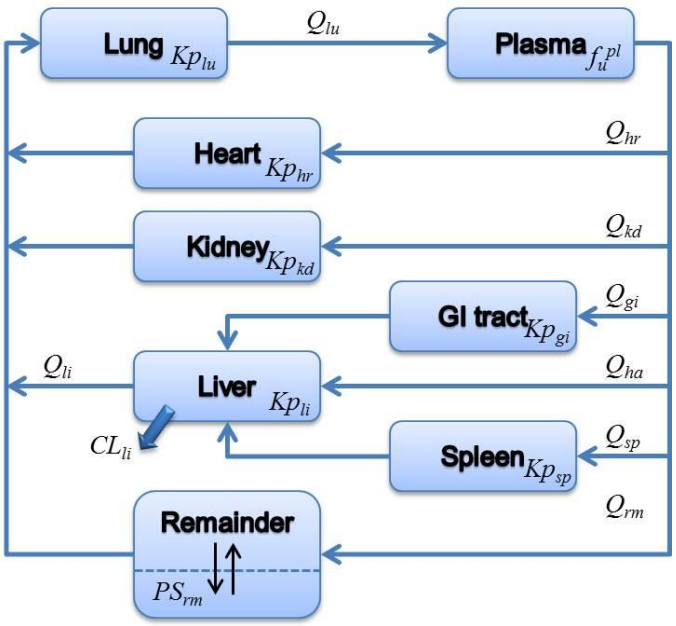

Figure 2.2 Schematic of the whole-body PBPK model used to describe the disposition of paclitaxel in mice, rats, and humans following intravenous dose of Taxol®. Q_{ti} - plasma flow rate to different organs; CL_{li} – hepatic clearance; f_u^{pl}– fraction unbound in plasma; gi – gastrointestinal; hr – heart; kd – kidneys; kp – partition coefficient; li – liver; lu – lungs; PS – permeability-surface area term; pl – plasma; rm – remainder; sp – spleen.

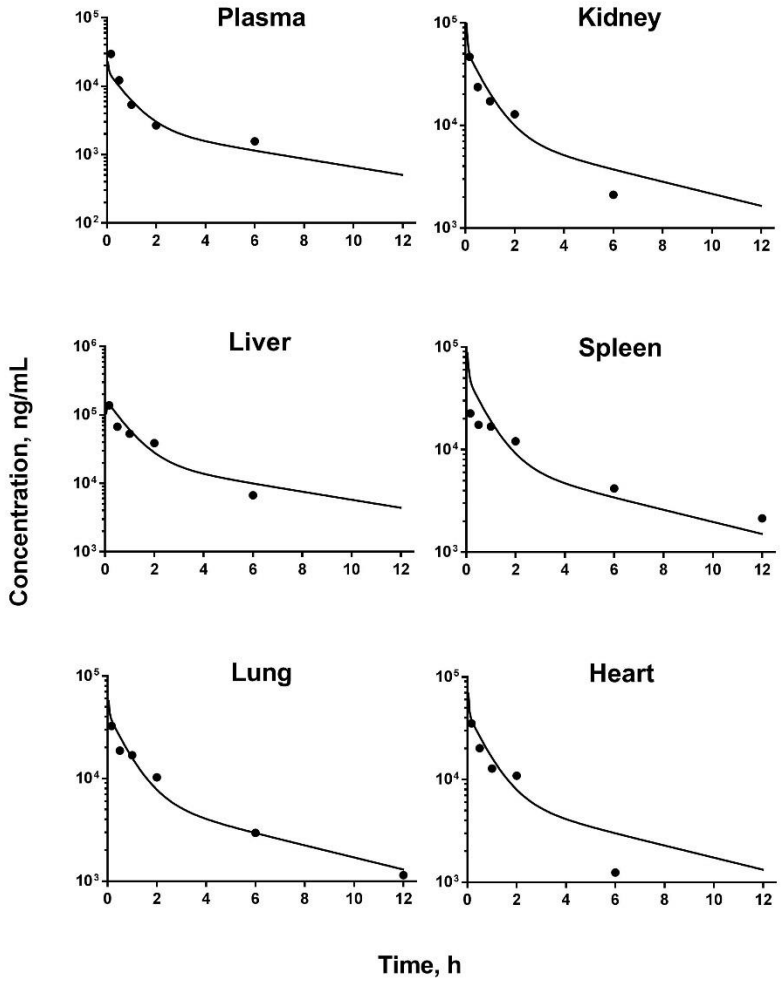

Figure 2.3 Representative observed (symbols) and the PBPK model fitted (lines) pharmacokinetic profiles of paclitaxel in plasma and tissues of mice following single IV bolus administration of 15 mg/kg of Taxol®. Observed data extracted from Li et al. (145).

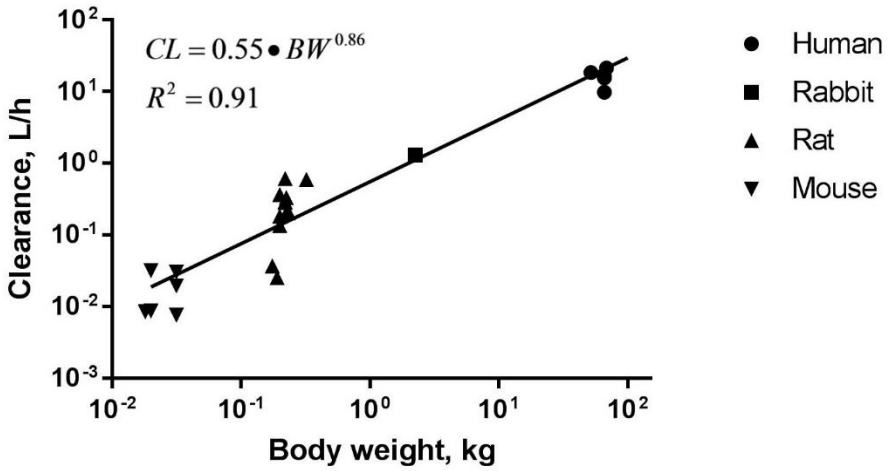

Figure 2.4 Allometric scaling plot of paclitaxel plasma clearance calculated using the noncompartmental approach. Data were obtained in mice (143-146), rats (147-150, 152-159), rabbit (176), and humans (160-164) as described in the Methods.

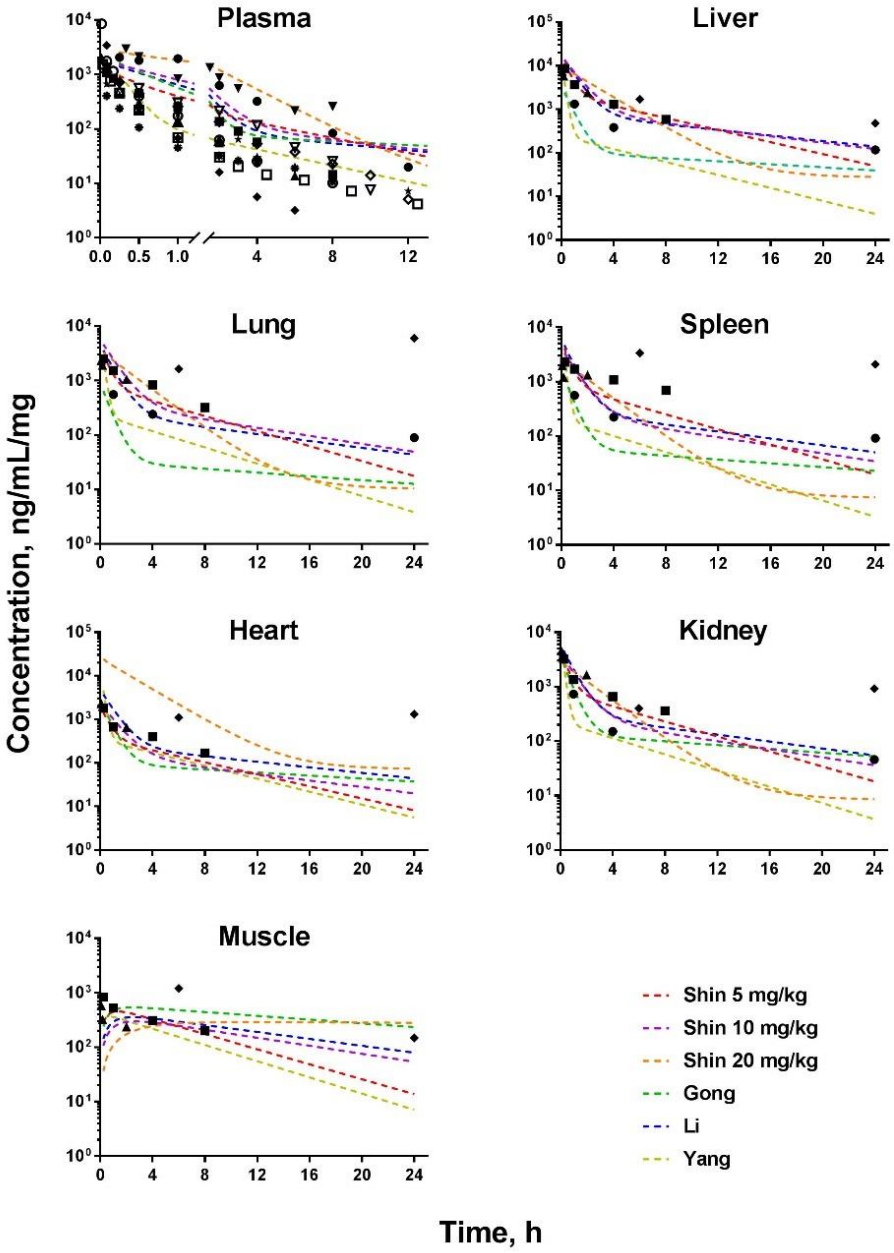

Figure 2.5 Time-course of paclitaxel in plasma and tissues of rats following single IV bolus administration. Symbols represent data extracted from 12 different references (147-159). Lines represent PBPK model predicted profiles using six different parameters sets (see Methods for detail). The data were dose-normalized and simulation performed for 1 mg/kg

dose level. For the muscle tissue, the lines represent predicted concentrations in the remainder compartment.

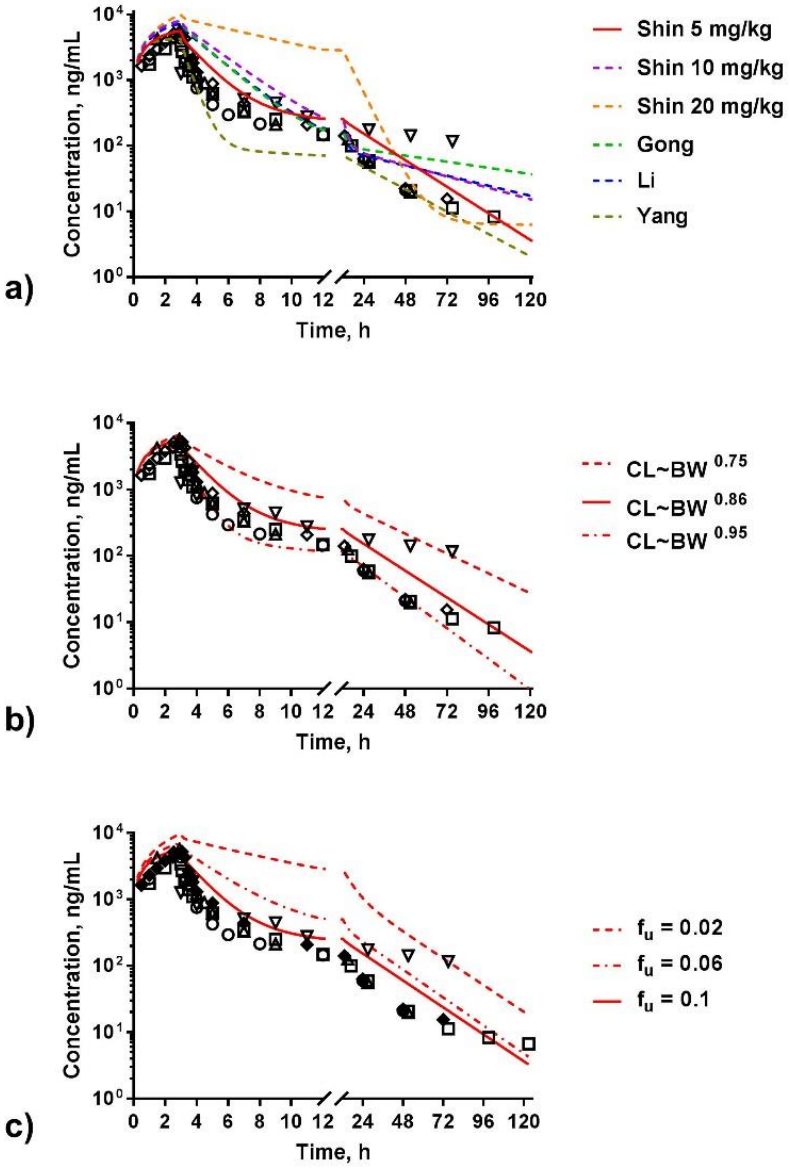

Figure 2.6 Time-course of paclitaxel in human plasma following IV infusion administration of Taxol® at the dose level of 175 mg/m^2. Symbols represent data extracted from references (160-164) (all observed data were normalized to 175 mg/m^2)**.** Lines represent PBPK model predicted profiles after: a) simulation using six different parameters sets and clearance scaled with body weight using exponent of 0.86 (see Methods for detail), b) sensitivity analysis - simulation using parameters estimated from Shin et al. at the dose

level of 5 mg/kg with different allometric exponents for clearance, and c) sensitivity analysis - simulation using parameters estimated from Shin et al. at the dose level of 5 mg/kg with different fraction unbound values in humans.

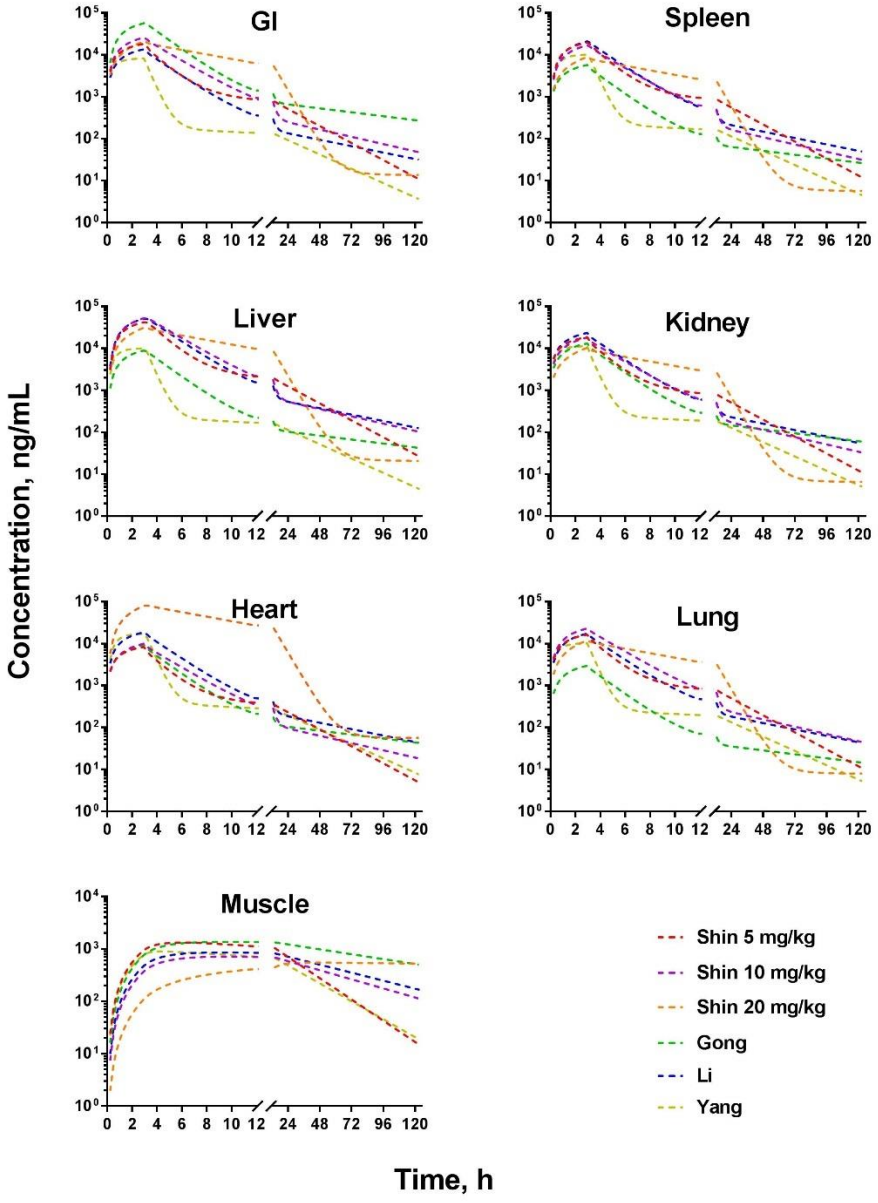

Figure 2.7 Predicted time-course of paclitaxel in human tissues following single IV infusion administration of Taxol® at the dose level of 175 mg/m^2. Lines represent PBPK model predicted profiles using six different parameters sets (see Methods for detail). For the muscle tissue, the lines represent predicted concentrations in the remainder compartment.

Chapter 3. Prevention of Paclitaxel-Induced Neuropathy by Formulation Approach

3.1 INTRODUCTION

In 2014, it was estimated that more than 14.5 million cancer survivors were living in the US, and this number was estimated to increase to 19 million by 2024 (197). Based on recent data from the Center of Disease Control and Prevention, about 650,000 cancer patients receive chemotherapy in an outpatient oncology clinic in the US. Highly effective treatments have been developed, and the increase in survival demands more attention to patients' quality of life and management of adverse effects.

Chemotherapy-induced peripheral neuropathy (CIPN) is a major, often dose-limiting adverse effect of various cancer therapies (198). Taxanes (paclitaxel, docetaxel) is one out of the six main classes of agents that induce toxicity to peripheral sensory and motor neurons that leads to CIPN. Other drugs associated with CIPN include platinum-based chemotherapeutics (cisplatin, carboplatin, oxaliplatin), proteasome inhibitor (bortezomib), immunomodulator (thalidomide), epothilones (ixabepilone), and vinca alkaloid (vincristine and vinblastine). Up to 40-90% of patients treated with neurotoxic chemotherapy will develop CIPN, which may lead to long-term morbidity and reduced quality of life. CIPN can be particularly severe and long-lasting (199), symptoms have been reported for up to 11 years after completion of therapy (200). Neuropathic pain is one of the most challenging pain conditions with poor response to pharmacotherapy (201). Therefore, discontinuation of chemotherapy or dose reduction often remains the only clinical solution (202).

Paclitaxel is used for treatment of various cancers, including ovarian, breast, small and non-small-cell lung, colon, bladder, esophagus, head and neck, multiple myeloma, and advanced forms of Kaposi's sarcoma (32, 33). It was the first in a new class of

microtubule stabilizing drugs that inhibit mitosis and normal cell division by stimulating the polymerization of tubulin (102, 133-135). Paclitaxel is a Biopharmaceutics Classification System class IV drug with high lipophilicity (logP~4) and poor aqueous solubility (0.77 - 35 μM) (35-38). Taxol® (the first approved formulation of paclitaxel by Bristol-Myers Squibb Company) is formulated with polyoxyethylated castor oil (Cremophor EL) and ethanol (1:1, v/v) due to the poor solubility of the drug. Although highly efficacious, several severe (and often dose-limiting) adverse events were reported with Taxol® treatment, including peripheral neurotoxicity (42-70%), nephrotoxicity (18-34%) and hypersensitivity (31-45%) (reported as percentages of patients after single-agent therapy) (40). Presence of Cremophor EL in the formulation was reported to contribute to mechanical hyperalgesia after five weekly intravenous (IV) doses in rodents (137), and it is a major cause of hypersensitivity reactions. While some other formulations of paclitaxel became available, Taxol® remains the standard of care for many cancers.

For successful clinical use, efficacy of a drug should be balanced with an acceptable level of adverse reactions. Several liposome-based products have been approved and demonstrated superior efficacy and safety profiles. For example, Doxil® (PEGylated liposomal doxorubicin) that is used for Kaposi's sarcoma and recurrent ovarian cancer enhanced the bioavailability at the tumor site and reduced side effects (203-205). AmBisome® (liposomal amphotericin B) significantly improved toxicity profile compared to conventional amphotericin B while retaining the antifungal effect (206). Although multiple groups developed various particulate formulations of paclitaxel, the majority of efforts was focused on enhancing delivery to the tumor and improving efficacy. Reducing toxicity, and especially neurotoxicity, of these formulations was not a primary objective and was rarely tested. Only one liposomal paclitaxel formulation, Lipusu®, was approved for clinical use by Chinese Food and Drug Administration (207); no liposomal paclitaxel formulation is available in the US yet.

The first aim of this work was to evaluate the effect of liposome formulation of paclitaxel (L-PTX) on neurotoxicity *in-vitro* and *in-vivo* in comparison to the standard Taxol® formulation. The second aim was to investigate the effect of formulation on paclitaxel biodistribution following IV administration in a preclinical model.

3.2 MATERIALS AND METHODS

3.2.1 Materials

Taxol® (6 mg/mL, Teva, North Wales, PA) was generously provided by Rutgers Cancer Institute of New Jersey (New Brunswick, NJ). Paclitaxel was purchased from Sigma Aldrich (St. Louis, MO). A549 human non-small-cell lung adenocarcionoma epithelial cells were purchased from American Type Culture Collection (ATCC, Manassas, VA) and human neuroblastoma SH-SY5Y cells were generously provided by Dr. Kiledjian's laboratory at Rutgers University. Egg phosphatidylcholine (egg PC), cholesterol, and 1,2-distearoyl-*sn*-glycero-3-phosphoethanolamine-N-[methoxy(polyethylene glycol)-2000] (ammonium salt) (mPEG 2000) were purchased from Avanti Polar Lipids (Alabaster, AL). All other chemicals were of analytical grade, and solvents were of HPLC grade.

3.2.2 Synthesis and Characterization of Liposomes Containing Paclitaxel

Drug-loaded liposomes were prepared with three lipids as described previously (208). Briefly, PEGylated liposomes were formulated from egg PC:cholesterol:mPEG 2000 in mole ratio 55:40:5 by dissolving in 100% ethanol and loading with paclitaxel. The solution was subsequently evaporated to a thin film layer using a rotary evaporator Rotavapor® R-210/R-215 (BUCHI Corp., New Castle, DE) and rehydrated with 0.9% NaCl to final lipid concentration 20 mM. The suspension was aliquoted to 5 mL in a small glass vial for probe sonication to obtain a more homogenous population of nano-sized liposomes (Fisher Scientific Model 120 Sonic, Waltham, MA, 50 constant output for 4 min with 15 sec/cycle and 5 sec pauses to avoid overheating). The probe was immersed to a depth of 15 mm above the bottom of the glass vial. The time for sonication was optimized to obtain a mean diameter of 50-60 nm. Free paclitaxel was separated from liposomes by dialysis using dialysis membrane with pore size 50 kDa (Spectrum Labs, New Brunswick, NJ) against 100 volumes of 0.9% NaCl three times (0.5 h, 3 h, and overnight) at 4°C.

The particle size distribution was measured by Malvern ZetaSizer NanoSeries (Malvern Instruments Enigma Business Park, UK) according to the manufacturer's instruction. All measurements were carried out at room temperature. The stability of liposome was monitored up to 4 weeks at 4 °C. The free drug was removed by dialysis as described above. Encapsulation efficiency of paclitaxel was determined (after free drug was separated from the liposomes) using the following formula, $Percent\ encapsulated = \frac{[Total\ paclitaxel]-[Free\ paclitaxel]}{[Total\ paclitaxel]} \times 100\%$. The concentration of paclitaxel encapsulated in liposomes was further determined by the HPLC. Each parameter was measured three times for each batch, and average and standard deviations were calculated.

3.2.3 Cell Culture and Cell Viability Study

The experiments were carried out using two cell lines. A549 human lung carcinoma cells were cultured in RPMI 1640 medium (Corning, Manassas, VA) supplemented with 10% fetal bovine serum (Corning, Manassas, VA). SH-SY5Y human neuroblastoma cells were cultured in Dulbecco's modified Eagle's medium / Ham's F-12 50/50 mix (Corning, Manassa, VA) supplemented with 10% fetal bovine serum. Both cell lines were maintained in tissue culture-treated dish (Falcon, Catalog No. 353003, Durham, NC). All cells were grown at 37°C in a humidified atmosphere of 5% CO_2 (v/v) in air and passed every 3-4 days. The experiments were performed on cells in the exponential growth phase.

Cell viability was assessed using CellTiter-Fluor™ assays (Promega Corporation, Madison, WI) that was performed according to the manufacture's protocol. Briefly, 50,000 cells/well of SH-SY5Y cells and 20,000 cells/well of A549 cells were plated in the 96-well plate with the complete medium. After 24 hours, the cells were treated with either paclitaxel or liposomal paclitaxel at 0.1, 0.2, 0.39, 0.78, 1.56, 3.13, 6.25, 12.5, 25, 50, 100 µg/mL for another 24 h with 0.1% DMSO in all wells. On the third day, cell viability was assessed by

CellTiter-Fluor™ assay using a microplate reader Spectra Max M3 (Molecular Devices, San Jose, CA) with excitation and emission wavelengths of 390 and 505 nm. Untreated cells (medium only) served as a negative control (100% viability), and cells treated with 0.1% Triton X-100 in medium served as a positive control for maximal cytotoxicity. Cell viability tests were performed in triplicate.

3.2.4 *In-Vivo* Neurotoxicity Study

Veterinary care followed the guidelines of the Association for Assessment and Accreditation of Laboratory Animal Care (AAALAC), and all procedures were approved by the Rutgers Institutional Animal Care and Use Committee (IACUC). Adult (140-160 g) male Sprague-Dawley rats (Envigo, Somerset, NJ) were used for all experiments. Rats were housed two per cage in a temperature- and humidity-controlled room on a 12:12 h light:dark cycle with free access to food (Catalog No. 5001, LabDiet, St. Louis, MO) and water. All experiments were performed during the same period of the day (8:30 am to 12:00 pm) to avoid diurnal variations in animal responses.

The animal study was conducted to evaluate the difference in paclitaxel-induced peripheral neuropathy in rats following administration of L-PTX and the control formulation (Taxol®). A previously reported *in-vivo* model of Taxol®-induce peripheral neurotoxicity (increased sensitivity of hind paws to mechanical and thermal stimuli) was used (209). In this model, development of neurotoxicity is observed after a few days following a series of IV injections of Taxol® with animal recovery after approximately 4-5 weeks.

Baseline sensitivity of animals to mechanical and thermal stimuli was measured for 3-4 times before drug administration (as described below). The investigator collecting behavioral data was blinded to the treatment groups. Rats were randomly assigned to two treatment groups. Neuropathy was induced by repeated IV dosing of paclitaxel at a cumulative dose of 8 mg/kg (2 mg/kg, every other day for a total of 4 doses) (183, 209).

Prior to administration, Taxol® was freshly diluted in sterile normal saline and injected at a concentration of 1 mg/mL. Liposomal paclitaxel (L-PTX) formulation was freshly prepared two days before injection at a concentration of 1 mg/mL. Rats were administered dosing solutions via tail vein (under isoflurane anesthesia) on days 0, 2, 4, and 6. Drug administration was performed after animal sensitivity thresholds were measured.

Assessment of sensitivity of rats to mechanical stimuli was performed using the dynamic plantar aesthesiometer (Ugo Basile, Italy), as previously described (210). Rats were habituated to the testing procedure, equipment, and the investigator for two or three days before the collection of baseline data. To obtain a reliable baseline, rats' sensitivity was measured on at least 3 consecutive days. Briefly, rats were left to habituate inside plastic enclosures on top of a perforated platform before starting the measurement for approximately 30 min. A linearly increasing force was applied on the plantar surface of hind paws using a metal filament which was programmed with the microprocessor (2.5 g/s, with a cut-off of 50g). A "positive response" signal was automatically recorded when the animal withdrew the paw. Withdrawal thresholds in response to the mechanical stimuli was recorded in grams. Each animal was tested 3 times with a 5-min interval, and the average of the 3 measurements for each paw was considered the withdrawal threshold.

Assessment of sensitivity of rats to thermal stimuli was performed using the Hargreaves apparatus (plantar test) (Ugo Basile, Italy), as previously described (211). Similar to the assessment of mechanical sensitivity, rats were habituated before the study and a reliable baseline was established before drug administration. Briefly, rats were left to habituate inside plastic enclosures on top of a glass surface for approximately 30 min. A radiant heat source was located below the glass platform. The paw withdrawal reaction time of rats exposed to a radiant heat on their plantar surface of hind paws was recorded with a precision margin of 0.1 s. The response of the animal was calculated by taking the

average of 3 measurements with a 5-min interval. The maximum time was set to 20 s to prevent damage to the plantar surfaces.

3.2.5 Paclitaxel Tissue Disposition Study

Sprague-Dawley rats were used to investigate the effect of formulation on the biodistribution of paclitaxel after IV administration. Rats were randomly divided to receive a single dose of 6 mg/kg of Taxol® or L-PTX via the tail vein. Animals were sacrificed under isoflurane anesthesia (n=3-4 for each time point). Blood and tissue (liver, lung, brain, spinal cord, skin, and muscle) samples were collected at 0.5, 1, 2, 4, and 6 h after drug injection. Blood samples were collected into heparinized tubes and immediately processed for plasma by centrifugation at 1300 x g for 10 min. Tissue samples were washed with saline and blotted dry with Kimwipes to remove excess fluid. Samples were stored at -80°C until analysis.

3.2.6 Bioanalytical procedure

The analysis of paclitaxel was carried out using an HPLC-UV system (Agilent 1260 Infinity, Santa Clara, USA). A reverse phase column EC-C18 (4.6 x 100 mm, 2.7 µm) (Agilent, Santa Clara, USA) was used at 45 °C. The mobile phase consisted of a mixture of (A) acetonitrile and (B) water with the following gradient scheme: 0 – 1 min, A – 30%; 1 – 8 min, A increased to 85%; 8 – 8.5 min, A – 85%; 8.5 – 8.7 min, A decreased to 30%; 8.7 – 10 min, A – 30%. The run time was 10 min with flow rate of 1.0 mL/min. The detector wavelength was set at 225 nm. Retention times for paclitaxel and internal standard (N-benzylbenzamide) were 7.0 and 5.0 min. The lower limit of quantification for paclitaxel was 50 ng/mL, and the method was linear between 50 and 20,000 ng/mL.

Paclitaxel was extracted from plasma samples using a liquid-liquid extraction method. Briefly, 100 µL of plasma was mixed with 10 µL of N-benzylbenzamide (100

µg/mL in acetonitrile, internal standard), 300 µL of acetonitrile, and 3 mL of methyl tert-butyl ether by vortexing for 10 min and followed by centrifugation for 5 min at 3000 rpm. The supernatant was transferred to new glass tubes and evaporated under a light stream of nitrogen at 40°C. The residue was reconstituted with 100 µL of 50% acetonitrile in water and filtered through a 0.2 µM nylon filter (Thermo scientific, Rockwood, TN). The injection volume was 40 µL.

Liver, lungs, brain, and spinal cord were sliced into strips and weighted. The density of all tissues was assumed to be 1 mg/mL. Each tissue was mixed with PBS (a double volume of the sample) and 0.5 mm zirconium oxide beads or 3.2 mm stainless steel round beads followed by 3-4 min of homogenization at speed 8, 12, or 20 (Bullet Gold Blender®, Next Advance, Troy, NY). Skin and muscle were sliced into strips and mixed with PBS (a quadruple volume of the sample) followed by homogenization. Paclitaxel was extracted from tissue homogenates using a solid phase extraction method. Briefly, tissue homogenate (100 µL for liver, lungs, brain, and spinal cord or 200 µL for skin and muscle) were combined with an equal amount of methanol and the internal standard (10 or 20 µL, respectively). The samples were then vortexed for 20 s and centrifuged at 13,000 rpm for 5 min. The supernatant was transferred to the preconditioned cartridges (Bond Elut Plexa 30mg, Agilent, Santa Clara, CA) followed by washing with 5% methanol in water, then eluted by applying 400 µL of methanol twice. The eluent was evaporated and reconstituted as described for plasma extraction. For each tissue a separate calibration curve was used using the corresponding blank tissue matrix.

3.2.7 Data Analysis

Mean plasma and tissue concentrations of paclitaxel at each time point were calculated for both formulations. Noncompartmental analysis was completed using a Phoenix WinNonlin version 7.0 (Pharsight Corp., California, USA). Logarithmic trapezoidal

method was used to calculate the area under curve (AUC) to the last available timepoint (AUC_{last}).

Data from different experiments are presented as mean ± SD. For statistical analysis of the differences in mechanical and thermal sensitivity between two administration groups, Student's t-test of independent means was used. A value of $P < 0.05$ was considered statistically significant. Cell viability analysis and determination of IC50 values were conducted using GraphPad Prism 7 software.

3.3 RESULTS

Liposomal formulation of paclitaxel was developed and characterized. The size of the liposomes was 55.1 ± 8.9 nm (n=5), and the encapsulation efficiency was 99.6% ± 3.6% (n=3). The formulation stability in the 4 °C was evaluated for up to 4 weeks. After a week of storage in the 4 °C, 79% of the drug were encapsulated in the liposome after a second round of dialysis; the particle size changed from 55.1 nm to 54.1 nm. After 4 weeks, 67% of the drug was encapsulated in the liposomes after dialysis, the particle size increased to 121.7 nm.

The cytotoxicity of L-PTX formulation was compared with paclitaxel with human lung carcinoma A549 **(Figure 3.1a)** and human neuroblastoma SH-SY5Y **(Figure 3.1b)** cell lines. The IC50 value for A549 cells for paclitaxel solution and L-PTX were 59.1 and 33.7 µg/mL. The IC50 value for SH-SY5Y cells for paclitaxel solution and L-PTX were 18.4 and 31.8 µg/mL. The study showed that free paclitaxel was toxic to cell of neuronal origin at a lower concentration than to lung cancer cells, and liposomal formulation demonstrated a comparable toxicity to both cell lines.

To evaluate the effect of pharmaceutical formulation on paclitaxel-induced neurotoxicity, changes in rat sensitivity to mechanical and thermal stimulation of hind paws was tested after administration of Taxol® and L-PTX formulations by IV route at 2 mg/kg per dose for a total of 4 doses on day 0, 2, 4, and 6 **(Figure 3.2a)**. The study was initiated when the animals were at 6 weeks of age. The baseline response to mechanical stimulation before drug administration was similar between the groups (30.17 ± 1.15 g for Taxol® group, and 29.62 ± 0.77 g for L-PTX group). Administration of Taxol® resulted in a significant reduction of withdrawal threshold in response to mechanical stimuli from day 9 to day 26 after the first drug injection (as compared to the baseline threshold). In comparison, administration of L-PTX did not result in increased sensitivity to mechanical stimulation. From day 4 till day 34, a statistically significant difference was observed

between the groups. The nadir of reduction (24.64 ± 2.17 g) for Taxol® treated rats was achieved on day 11 as compared to 38.04 ± 3.55g for L-PTX treated rats.

Animals in both groups returned to a similar withdrawal threshold after day 36, at which time Taxol® group had a withdrawal threshold of 40.11 ± 4.82 g compared to 40.71 ± 5.32 g for L-PTX treated rats. The withdrawal threshold by the end of the study was higher than the baseline before paclitaxel injections. An increase in withdrawal threshold with age (and body weight) was previously observed in a separate animal cohort without paclitaxel administration **(Figure 3.2b)**, from 30.2 ± 3.6 g on week 6 to 45.4 ± 2.0 g on week 10.

In addition, animal sensitivity to thermal stimuli was investigated in animals receiving Taxol® or L-PTX formulations at 2 mg/kg every other day for a total of 4 doses **(Figure 3.3)**. The baseline sensitivity before drug administration was similar between two groups, 12.99 ± 2.48 s for Taxol® and 14.32 ± 3.60 s for L-PTX treated group. Taxol® treatment produced a significant reduction in reaction time to heat stimulation, from day 9 to day 26 after the first drug dose administration compared to the L-PTX treatment group. The nadir of reduction of the response time was on day 18, when Taxol®-treated rats had a reaction time of 10.80 ± 1.61 s compared to 17.87 ± 3.00 s for L-PTX-treated rats. For technical reasons thermal thresholds were not measured beyond day 26.

To investigate the effect of formulation of paclitaxel biodisposition, Sprague-Dawley rats were given a single IV injection of Taxol® or L-PTX at 6 mg/kg dose level. The time-course of drug concentrations in the plasma and tissues was determined **(Figure 3.4** and **Table 3.1)**. The disappearance of paclitaxel from plasma was much faster for L-PTX than for Taxol® group. Plasma concentration extrapolated to time zero (C_0) and the area under the plasma concentration-time curve (AUC to the last measured concentration) for Taxol® group were 3.5-fold and 6.2-fold higher than for L-PTX, respectively. Furthermore, plasma half-life of paclitaxel was 3.2 times longer for Taxol® than for L-PTX group.

Biodistribution of paclitaxel to liver and lungs was studied because the reticuloendothelial system represents a major mechanism for clearance of circulating liposomes. L-PTX was taken up by the liver to a greater extent than was Taxol®; the concentration of paclitaxel at 0.5 h was 112.7 ± 11.4 µg/mL for L-PTX and 30.6 ± 2.7 µg/mL for Taxol®. In the lungs, the drug concentration at 0.5 h was 46.2 ± 7.7 µg/mL for L-PTX and 12.2 ± 1.2 µg/mL for Taxol®. As neurotoxicity was the main focus of the study, exposure to paclitaxel in the nervous system (brain and spinal cord) and in the skin and muscle (location of sensory axons) was evaluated. The exposure to paclitaxel in the skin, muscle, brain, and spinal cord was lower in the L-PTX group compared to Taxol® group. In the brain and spinal cord, the concentration of paclitaxel at 0.5 h was 138.0 ± 26.1 ng/mL and 111.8 ± 20.4 ng/mL for L-PTX group; and 220.6 ± 34.3 ng/mL and 134.1 ± 28.5 ng/mL for Taxol® group. In the skin and muscle, the concentration of paclitaxel at 0.5 h was 462.9 ± 187.3 ng/mL and 289.3 ± 87.3 ng/mL for L-PTX group; and 1973.9 ± 373.2 ng/mL and 2236.5 ± 460.2 ng/mL for Taxol® group. Drug concentration for plasma, brain and spinal cord after 2 h time points was below the lower limit of quantification.

To further highlight the difference between paclitaxel exposure between two formulations, the ratio of paclitaxel concentrations in various tissues between Taxol®- and L-PTX-treated groups was calculated **(Figure 3.5)**.

3.4 DISCUSSION

Chemotherapy-induced neuropathy is a very common, serious, and debilitating adverse effect of paclitaxel and many other anticancer drugs. Common neuropathic symptoms include numbness, tingling, pain or impaired sensory function in hands and/or feet, hypersensitivity to mechanical and cold stimuli, clumsiness in fingers, peripheral muscular weakness or difficulties in walking (2). CIPN is often presents in a “stocking and glove” pattern in feet and hands because longer axons are affected first (10). Variable statistics exists regarding the prevalence of CIPN, depending on the study design and assessment period. A recent systematic review (31 studies, 4179 patients) reported CIPN prevalence of 68% when measured in the first month after chemotherapy, 60% at 3 months and 30% at 6 months or more (6). Prevalence as high as 80-90% has been reported (7, 212). Different drugs may result in a different clinical presentation of neuropathy symptoms; the underlying mechanism of development of CIPN are complex (212, 213) and not fully understood. The pathophysiological changes caused by paclitaxel include immune-mediated processes, loss of peripheral fibers, demyelination and axon degradation, and mitochondrial dysfunction (4). Treatment of CIPN is mostly symptomatic (using anticonvulsants, gabapentin, opioids (202)) and remains largely ineffective (201). Some prevention treatments using vitamin E, amifostine, and glutathione were reported (202); however, discontinuation of chemotherapy or dose reduction remains the only clinical solution (202). Therefore, there is an urgent need to develop approaches for prevention of CIPN.

Taxol® remains the standard therapy for many cancers, although some other formulations are available. Abraxane®, a nanoparticle albumin-bound paclitaxel formulation (Cremophor EL-free), was approved in the US in 2005. However, this formulation also resulted in dose-dependent mechanical and cold allodynia in rats, which tended to be even stronger (in degree of sensitivity) than that of Taxol® at the doses used

clinically (214). Later, polymeric micelle (Genexol®-PM) and liposome formulations (Lipusu®) of paclitaxel were approved in Korea and China, respectively. The incidence for peripheral neurotoxicity did not differ significantly between Genexol®-PM and Taxol® treatments in recurrent or metastatic HER2-negative breast cancer patients (215). Limited information could be found for Lipusu® treatment, and the incidence of peripheral neurotoxicity was reported as 62% in the package insert (216).

Preclinical formulation development for paclitaxel and other cancer drugs is often primarily focused on tumor targeting and overall efficacy, without specifically considering adverse effects and especially neurotoxicity. Only two groups reported assessment of neurotoxicity as a part of formulation development for paclitaxel. A phase I study with a polymer-conjugated prodrug of paclitaxel in refractory solid tumors patients was discontinued prematurely because of severe neurotoxicity - 4 out of 12 patients developed grade 2-3 peripheral neuropathy (217). Another micellar nanoparticle formulation was found to be less neurotoxic than free paclitaxel; however, only *in-vitro* studies were completed (131).

In this study, the liposomal formulation of paclitaxel was less toxic to neuronal cells than paclitaxel solution and prevented development of neurotoxicity *in-vivo* as compared to Taxol® administration (that resulted in a significant increase in sensitivity of rats to mechanical and thermal stimuli). In the animal study, rats were randomly assigned to treatment groups and the investigator that measured sensitivity thresholds was blinded to the treatment group assignment. Moreover, the results closely resembled our pilot study with 5 animals in each group (L-PTX vs. Taxol®, data not shown). The time-course of dynamics of animal responses (increased sensitivity followed by a recovery phase) after administration of Taxol® in our study was also similar to previous result by other investigators (209). Increased sensitivity to mechanical stimuli developed on day 4 after first injection of Taxol®, and animals recovered on day 37.

In this study, L-PTX showed lower IC50 in lung cancer cells compared to paclitaxel solution. We have previously showed that nontargeted and targeted liposomal formulations of paclitaxel are effective in suppression of tumor growth in nude mice bearing human A549 lung carcinoma xenografts (208). Future studies in orthotopic cancer mice models are needed to simultaneously assess efficacy and toxicity and establish dose-response relationships tor L-PTX. High paclitaxel exposure in the lungs following administration of L-PTX further supports potential use of this formulation for lung cancer.

Assessment of drug concentration in target tissues is important for establishing dose-response relationships for efficacy and toxicity. Previously, we developed a physiologically-based pharmacokinetic (PBPK) model to describe paclitaxel biodistribution after Taxol® administration based on published data (218). Large variability in reported tissue concentrations was found across multiple publications. Some of the differences were attributed to bioanalytical procedures and other experimental techniques. Observed tissue concentration data of paclitaxel after Taxol® dosing obtained in this study were in good agreement with model-based predictions generated based on our previously developed PBPK model (**Figure 3.6)** (218).

In majority of previous studies paclitaxel disposition to the brain and other parts of the nervous system was not reported. Furthermore, assessment of drug disposition into skin and muscle is rarely evaluated, and these tissues are lumped in a “remainder” compartment in PBPK models. In this study, we evaluated concentrations of paclitaxel in tissues that may help establish dose-CIPN relationships, including peripheral tissues (skin and muscle) where sensory axons are located (202) and the central nervous system (spinal cord and brain). Changes in the CNS due to administration of paclitaxel have been previously reported, e.g. increased reactive nitrogen species production in the spinal cord of rats (68) and increased expression of voltage gated sodium channel in forebrain of mice (219). Persistent muscle and cutaneous hyperalgesia were observed in Taxol® induced

peripheral neuropathy in rats (220). Administration of L-PTX led to a significantly lower drug exposure in the brain, spinal cord, muscle and skin compare to Taxol®-treated group, which corresponds to the results of mechanical and thermal sensitivity testing.

Surprisingly low concentrations of paclitaxel in the plasma and short circulation half-life were obtained after L-PTX dosing, which may be related to efficient uptake by the reticuloendothelial system. The size of the particles was relatively small for liposomes with mPEG 2000, which might be caused by probe sonication during formulation preparation. Future studies are needed to determine the optimal size of particulates for preserving (or enhancing) efficacy and minimizing neurotoxicity. In a previous animal study, no correlation was found between Taxol® dose (0.5-2 mg/kg) and the extent of neuropathy (183). However, the exposure of the nervous system to paclitaxel was not tested. Dose-response relationships for L-PTX will be addressed in future studies that will require more sensitive bioanalytical methods.

3.5 CONCLUSION

Proof of concept study was performed and showed that formulation in nanoparticles is a promising approach for reducing (or preventing) neurotoxicity caused by cancer drugs. L-PTX significantly reduced cytotoxicity *in-vitro* in neuronal cells and prevented development of peripheral neuropathy *in-vivo.* Future studies are needed for development of an optimized formulation for paclitaxel; and this approach can be potentially extended to other neurotoxic compounds.

Table 3.1 Plasma pharmacokinetic parameters of paclitaxel after single IV administration of Taxol® and L-PTX formulations to rats

PK Parameters	$t_{1/2}$	C_0	AUC_{last}	V_{ss}	CL_T	MRT
	h	ng/mL	ng*h/mL	mL/kg	mL/h/kg	h
Taxol®	1.06	9126	7872	857	721	0.94
L-PTX	0.33	2599	1275	2283	4630	0.46

AUC_{last}, area under the curve to the last measurable concentration; C_0, concentration at time 0 h; CL_T, total body clearance; MRT, mean residence time; $t_{1/2}$, half-life; V_{ss}, volume of distribution at steady state.

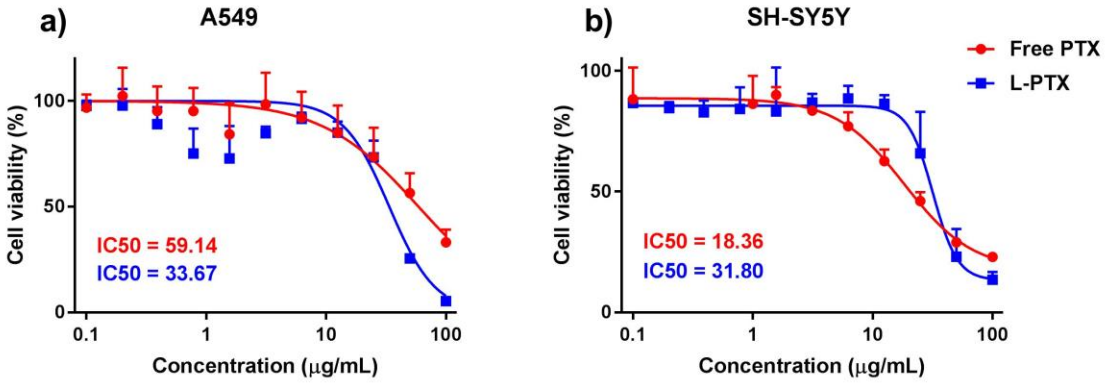

Figure 3.1 Cell viability after incubation with various concentrations of L-PTX formulation and paclitaxel solution for 24 hours **a)** cancer cell line A549 and **b)** neuroblastoma cell line SH-SY5Y from 0.1 – 100 µg/mL. Data are shown as mean ± SD. Lines are fitted curves.

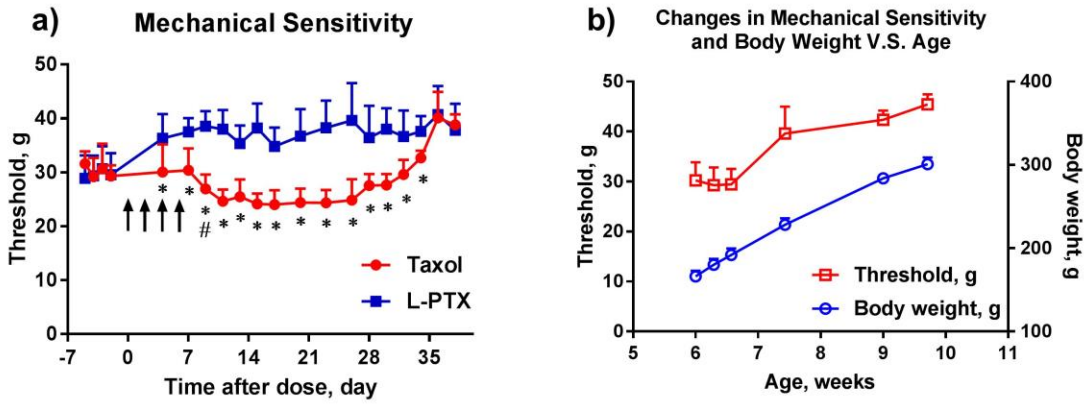

Figure 3.2 a) Threshold for withdrawal in response to mechanical stimulation to the plantar surface of hind paw before and after injection of L-PTX or Taxol® at 2 mg/kg for 4 times (n = 10 each group). Statistically significant difference between treatment groups (* $p < 0.05$), and before and after Taxol® treatment (# – the first day that the significance ($p < 0.05$) vs. baseline was reached). Arrows indicate days of drug administration. **b)** Changes to the mechanical sensitivity threshold and animal body weight in a group without drug administration. Data are shown as mean ± SD.

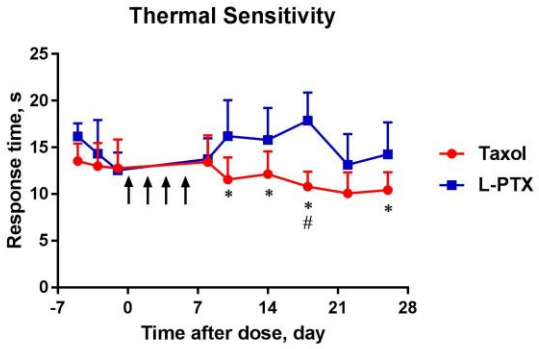

Figure 3.3 Response time to thermal stimulation to the plantar surface of hind paw before and after injection of L-PTX or Taxol® at 2 mg/kg for 4 times (n = 10 each group). Statistically significant difference between treatment groups (* $p < 0.05$) or before and after Taxol® treatment ($^{\#}$ $p < 0.05$). Arrows indicate days of drug administration. Data are shown in mean ± SD.

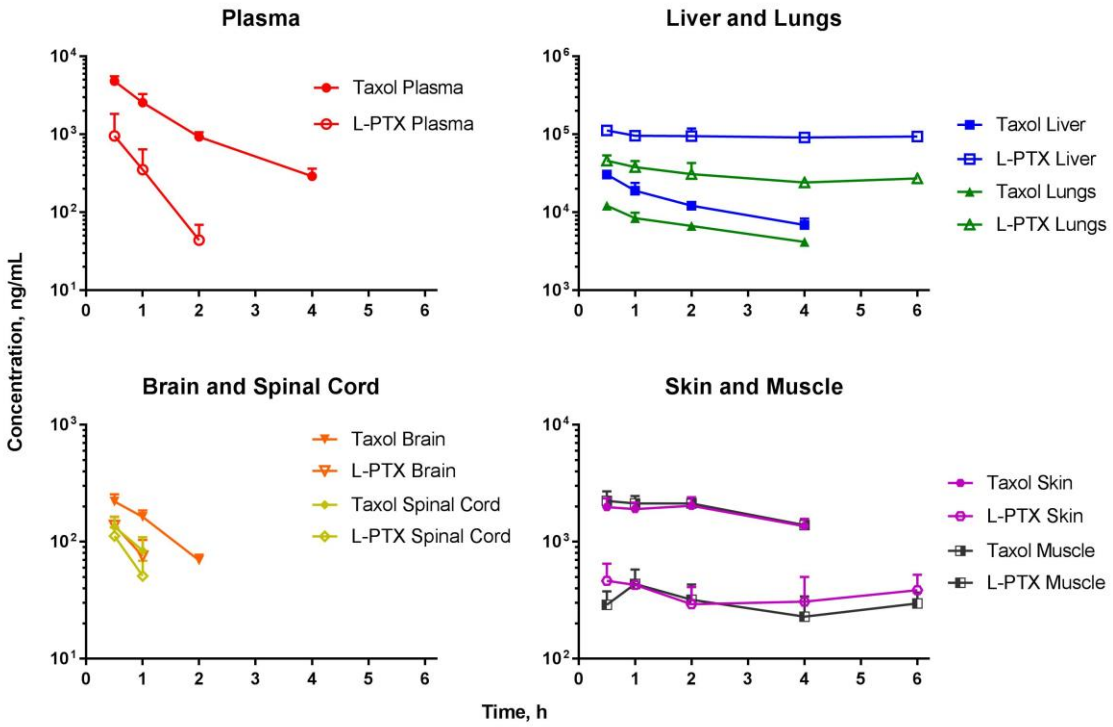

Figure 3.4 Exposure to paclitaxel in the plasma, liver, lungs, brain, spinal cord, skin, and muscle, for Taxol® (filled symbols) and L-PTX (open symbols) groups after IV administration at a dose level of 6 mg/kg to rats. Data are presented as the mean ± SD (n=3-4).

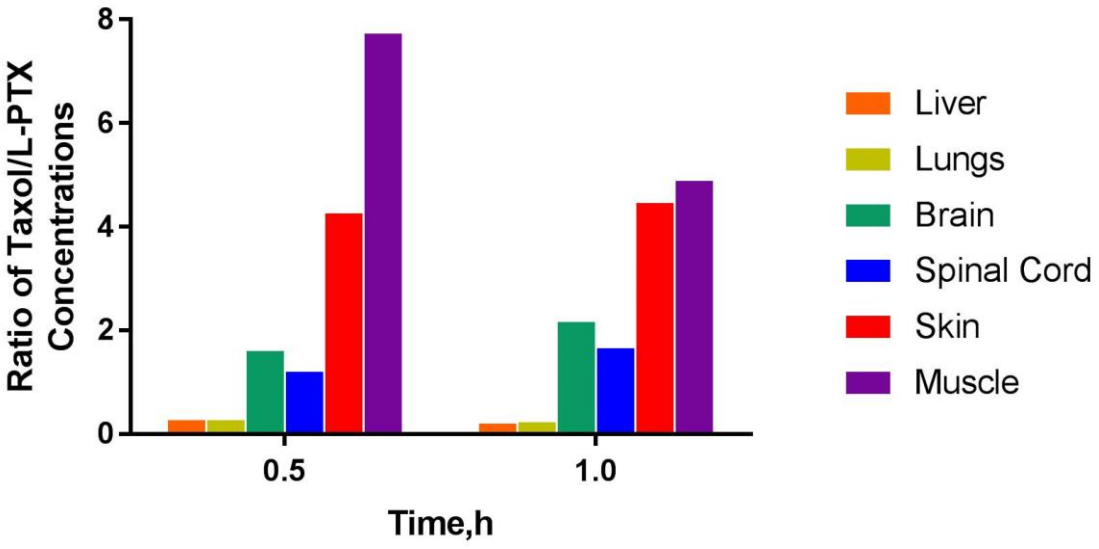

Figure 3.5 Ratio of paclitaxel concentrations in the liver, lungs, brain, spinal cord, skin, and muscle at 0.5 and 1 h in rats following IV bolus administration of Taxol® or L-PTX at 6 mg/kg.

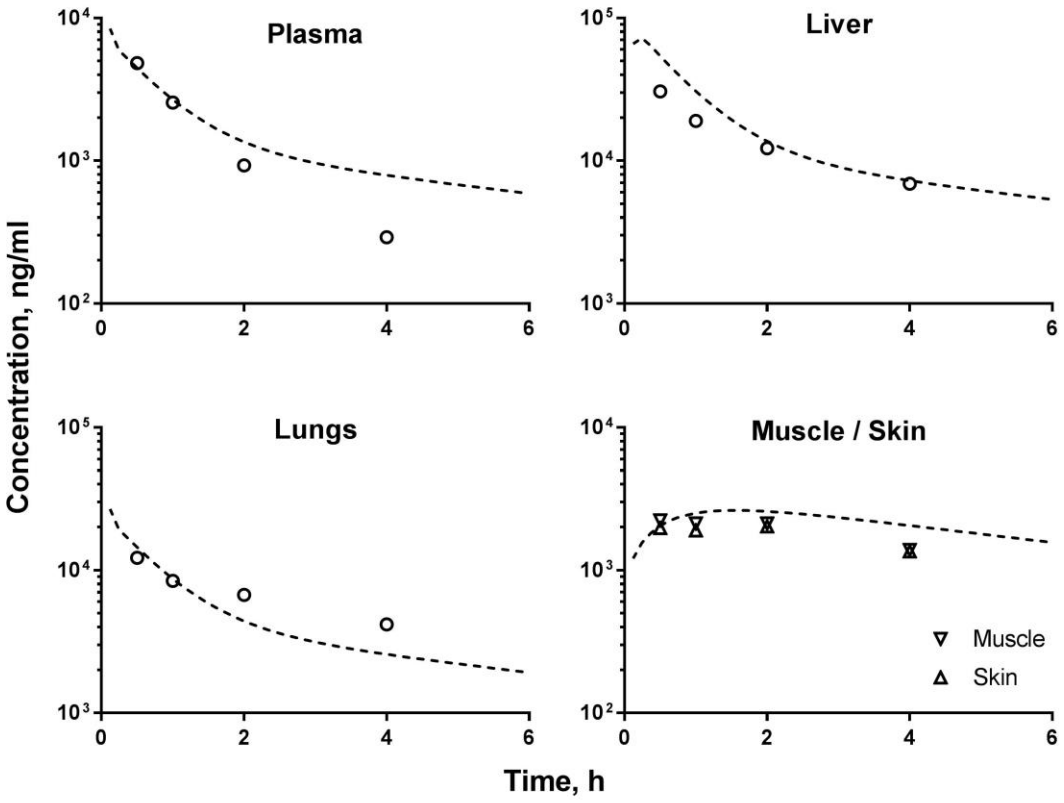

Figure 3.6 Observed paclitaxel tissue distribution (open symbols) after IV administration of Taxol® 6 mg/kg overlaid with predictions generated using previously developed physiologically-based pharmacokinetic model (218) (dotted lines) for plasma, liver, lungs, skin, and muscle tissues. In the model, skin and muscle were lumped into a 'remainder' compartment; the simulated line on skin/muscle panel represents a profile for the 'remainder' compartment.

Chapter 4. Pharmacokinetic-Pharmacodynamic Model of Paclitaxel-induced Peripheral Mechanical Sensitivity After Administration of Taxol® to Rats

4.1 INTRODUCTION

Chemotherapy-induced peripheral neuropathy (CIPN) is a major, often dose-limiting adverse effect of various drugs, including taxanes (paclitaxel, docetaxel), platinum-based drugs (cisplatin, carboplatin, oxaliplatin), proteasome inhibitor (bortezomib), immunomodulator (thalidomide), epothilones (ixabepilone), and vinca alkaloids (vincristine and vinblastine) (198). Up to 40-90% of patients treated with chemotherapy develop CIPN. The symptoms of CIPN may be severe and long-lasting (up to 11 years after discontinuation of chemotherapy) (200). The quality of life of cancer patients are significantly affected by CIPN since current treatments are often not effective and no effective prevention is available, which leaves the discontinuation of chemotherapy or dose reduction the only clinical solution (202).

Paclitaxel is one of the chemotherapeutic drugs for treatment of various cancers, including ovarian, breast, small and non-small-cell lung, colon, bladder, esophagus, head and neck, multiple myeloma, and advanced forms of Kaposi's sarcoma (32, 33). It was the first in a new class of microtubule stabilizing drugs that defect in mitotic spindle assembly and normal cell division by stabilizing microtubule polymers and protect them from disassemble (102, 133-135). Paclitaxel is highly lipophilic (logP~4) and poor aqueous soluble (0.77 - 35 μM) (35-38). Taxol® (Bristol-Myers Squibb, Princeton, NJ) is the first approved formulation of paclitaxel, which is formulated with polyoxyethylated castor oil (Cremophor EL) and ethanol (1:1, v/v) due to the poor solubility of the drug. Although several adverse events were reported with Taxol® treatment, such as peripheral neurotoxicity (42-70%), nephrotoxicity (18-34%) and hypersensitivity (31-45%) (reported

as percentages of patients after single-agent therapy) (40), Taxol® is the standard of care for many cancers and is used on a daily basis in the clinic.

Several risk factors for CIPN have been described, including dose, schedule, exposure, and genetic polymorphism. In patients with metastatic breast cancer, Taxol® given at 250 mg/m^2 dose level every 3 weeks was found to cause more grade 3 CIPN compared to 210 and 175 mg/m^2 every 3 weeks dosing (221). In another study, weekly Taxol® at 80 mg/m^2 for 6 cycles (combined with carboplatin for treatment of ovarian cancer patients) resulted in higher rate of neuropathy (grade≥2) compared to Taxol® at 175 mg/m^2 administered every 3 weeks for 6 cycles (222). Other studies reported that patients with polymorphism in a congenital peripheral neuropathy gene (223) and women who were CYP3A4*22 carriers (224) had a higher risk of CIPN development. Higher area under the time-course curve of paclitaxel concentrations above 0.05 µM was also correlated with the severity of CIPN (224, 225). However, no dose-response relationship was discovered in rats that received Taxol® at 0.5, 1, or 2 mg/kg dose levels on alternate days for four times (183). Despite all these studies, it remains challenging to predict the time course and extent of CIPN development in patient receiving Taxol®.

Because dose level and administration schedule are widely recognized as risk factors for CIPN development, CIPN is commonly managed by dose reduction and treatment discontinuation. However, the quantitative relationship between the dose, plasma pharmacokinetics, and paclitaxel induced peripheral neurotoxicity has not been established. To optimize the efficacy and toxicity of paclitaxel, there is an urgent need to establish a model-based approach for connecting between the pharmacokinetics and toxicokinetic profile (for peripheral neurotoxicity). Since there are no widely accepted and standardized assessment tools to reliably classify patients with CIPN (23), animal models have been utilized to study neurotoxicity (response to mechanical or thermal stimuli) after

Taxol® administration. The first aim of this work was to utilize the data from previous publications as well as our experimental data to describe the quantitative relationship between the dosing regimen and paw withdrawal threshold due to mechanical stimuli after IV administration of Taxol® to rats. The second aim was to perform simulations to compare paw withdrawal threshold to mechanical stimuli in order to propose an optimized dosing regimen of paclitaxel.

4.2 MATERIALS AND METHODS

4.2.1 Data Sources

To investigate the pharmacokinetic-pharmacodynamic (PK-PD) relationship between Taxol® dose and degree of sensitivity to mechanical stimulus in rats, paclitaxel PK profile in plasma and paw withdrawal threshold to mechanical stimuli after IV administration of Taxol® were collected from the literature or acquired experimentally.

PK data

Paclitaxel pharmacokinetic profile in plasma after a single intravenous (IV) bolus administration at 6 mg/kg to Sprague Dawley rats were obtained. The detailed experimental design, material and methods were reported previously in Chapter 2. Briefly, rats were randomly divided to receive a single dose of 6 mg/kg of Taxol® (1 mg/mL diluted with saline) via the tail vein. Animals were sacrificed (n=3-4 for each time point) and blood samples were collected at 0.5, 1, 2, and 4 h after drug administration. Blood samples were collected into heparinized tubes and immediately processed for plasma by centrifugation. Samples were stored at -80 °C until analysis using an HPLC-UV system (Agilent 1260 Infinity, Santa Clara, USA). The lower limit of quantification for paclitaxel was 50 ng/mL, and the method was linear between up to 20,000 ng/mL. Plasma was mixed with N-benzylbenzamide (100 µg/mL in acetonitrile, internal standard) and extracted using liquid-liquid extraction method with 300 µL of acetonitrile, and 3 mL of methyl tert-butyl ether. After extraction, the injection volume was 40 µL.

PD data

Several sets of paw withdrawal threshold to mechanical stimuli data after IV Taxol® administration were collected from the literature. Previous publications have reported in-vivo model of Taxol® induced peripheral neurotoxicity (increased sensitivity of hind paws to mechanical stimuli) following administration of Taxol® (209, 214, 226). Only studies that evaluated Taxol® formulation administered by the IV route were included in the analysis.

Mean data (paw withdrawal threshold to mechanical stimuli before and after Taxol® administration) and standard error of the mean (SEM) in each publication were captured by Plot Digitizer (Version 2.6.8). Three publications reporting Taxol® induced peripheral sensitivity to mechanical stimuli after multiple IV bolus dosing to rats were identified after screening (**Table 4.1**) (209, 214, 226).

In addition, experimental data collected in our laboratory after multiple IV bolus doses of Taxol® to rats were included (**Table 4.1**). The assessment of sensitivity of rats to mechanical stimuli was performed using dynamic plantar aesthesiometer (Ugo Basile, Italy), as previously described in Chapter 2. Briefly, a baseline of paw withdrawal threshold was measured on at least 3 consecutive days before Taxol® administration. Peripheral sensitivity was induced by repeated IV dosing of paclitaxel at a cumulative dose of 8 mg/kg (2 mg/kg, every other day for a total of 4 doses). A linearly increasing force was applied on the plantar surface of hind paws of rats using a metal filament which was programmed with the microprocessor (2.5 g/s, with a cut-off of 50 g). paw withdrawal threshold in response to the mechanical stimuli was automatically recorded in grams when the animal withdrew the paw.

4.2.2 PK-PD Model Structure

A one-compartment model with first order elimination was used as the structural model to describe the concentration time course of paclitaxel **(Figure 4.1)**. An indirect response model (IDR) linked to plasma concentrations through a biophase compartment was utilized to describe the time course of paw withdrawal threshold to mechanical stimuli. The onset of peripheral neurotoxicity occurs gradually over several days, and hence, a direct effect model could not be used because the plasma half-life of paclitaxel is relatively short. After initial assessment of the data using biophase model alone, IDR model alone, or a combination of biophase model and IDR, the later one was selected (**Figure 4.1.**).

Since the mechanisms of paclitaxel-induced peripheral neuropathy are not fully understood, IDR model I and IDR model IV were both evaluated to describe the PK-PD relationship.

Model I

The mechanisms that contribute to paclitaxel-induced neuropathy includes loss of neuronal fibers, demyelination, axon degeneration and subsequently changes axon morphology; changes of cell shape and cell stability in microtubules; and alters calcium homeostasis and mitochondrial function in neurons (4). It was assumed that baseline sensitivity of animals to mechanical stimuli (paw withdrawal threshold before administration of chemotherapy) can be described using a homeostasis equation ${dR}/{dt} = k_{in} - k_{out} \cdot R$, with a hypothetical production rate and elimination rate constants. IDR models have been utilized to describe such data before (227). IDR model I (inhibition of production) was evaluated and ascribed the action of paclitaxel to inhibition of the factors regulating the production of the response variable. The following equation was used to describe the model I:

$$ {dR}/{dt} = k_{in} \cdot (1 - \frac{I_{max} \cdot C_{bio}}{IC_{50} + C_{bio}}) - k_{out} \cdot R \qquad \text{where} \qquad R(0) = R_0 $$

(1)

where R is the response variable, R_0 is the baseline value for paw withdrawal threshold to mechanical stimuli, k_{in} and k_{out} are zero- and first-order rate constants for the appearance and disappearance of the peripheral sensitivity, respectively, C_{bio} is the concentration in biophase, I_{max} is the maximum inhibition, and IC_{50} is the drug concentration that produces 50% of the maximum inhibition.

Model IV

On the other hand, the paclitaxel induced peripheral neurotoxicity results in maladaptive responses in nociceptive pathways that drives sensory amplification. In

somatosensory pathway, an enhanced response to noxious stimuli and low-threshold sensory in amplitude, duration and spatial extent, and subsequently active the pain circuit (228). Therefore, IDR model IV was also evaluated due to the amplification the neural signaling within central nervous system that elicits pain hypersensitivity. The following equation was used to describe the model IV:

$$dR/dt = k_{in} - k_{out} \cdot (1 + \frac{S_{max} \cdot C_{bio}}{SC_{50} + C_{bio}}) \cdot R \qquad \text{where} \qquad R(0) = R_0$$

(2)

where S_{max} is the maximum stimulation, and SC_{50} is the drug concentration that produces 50% of the maximum stimulation. However, the parameters could not be identified and a simplified model was used. When $C_{bio} \ll SC_{50}$, k represents the ratio of S_{max}/SC_{50}, and the model was described as below:

$$dR/dt = k_{in} - k_{out} \cdot (1 + k \cdot C_{bio}) \cdot R \qquad \text{where} \qquad R(0) = R_0$$

(3)

where k represents the ratio of S_{max}/SC_{50} when $C_{bio} \ll SC_{50}$.

When there is no drug present, the baseline (paw withdrawal threshold to mechanical stimuli) was determined by $R_0 = k_{in}/k_{out}$. The baseline (without intervention) animal sensitivity measured in an experiment can be dependent on multiple factors, including animal-dependent, method of measurement-dependent and investigator-dependent; and conversion (or scaling factors) have not been determined. The baseline value in all utilized data sets varied significantly. Therefore, for each of the four data sets, baselines were calculated based on starting value (29.6 g for Yilmaz et al. and 14.9 g for Ochi-ishi et al.) or an average of starting and returning response values (12.2 g for Yamashita et al. and 34.0 g for Zang et al.). Since R_0 is fixed to paw withdrawal threshold values before drug administration and determined by k_{in} and k_{out}, two cases can be

explored, namely that the parameterization is in either k_{in} or k_{out}. Therefore, the following four models were evaluated and compared:

a) Indirect response model I, parameterization in k_{in}
b) Indirect response model I, parameterization in k_{out}
c) Indirect response model IV, parameterization in k_{in}
d) Indirect response model IV, parameterization in k_{out}

4.2.3 Simulations

To assess the effect of dose and dosing frequency on the development of peripheral neurotoxicity after IV administration of Taxol® to rats, simulations were performed under three scenarios. First, the same total dose (8 mg/kg) was given within one week at different dose for each administration (1, 2, 4, or 8 mg/kg); second, the same total dose (8 mg/kg) given at daily, 2, 3, or 4 days apart, or weekly at 2 mg/kg for each administration; and third, 2 mg/kg every other day for 4 times or 4 mg/kg every 6 days for 4 times.

4.2.4 Data Analysis

PK data are presented as individual observed value. PD data from different experiments are presented as mean ± SEM. Modeling and simulation were conducted using MATLAB R2015b software (The MathWorkds, Natick, MA). All pharmacokinetic parameters were estimated using the maximum likelihood method. The variance model was defined as $VAR_i = (\sigma \cdot Y(\theta, t_i))^2$, where VAR_i is the variance of the ith data point, σ is the variance model parameter, and $Y(\theta, t_i)$ is the ith predicted value from the PK-PD model. The goodness-of-fit was assessed by system convergence, Akaike Information Criterion, estimator criterion value for the maximum likelihood method, and visual inspection of residuals and fitted curves.

RESULTS

To evaluate the quantitative relationship between dose and paw withdrawal threshold to mechanical stimuli after IV administration of Taxol® to rats, PK-PD modeling was performed using experimental PK and PD data from our laboratory, and additional three published PD data sets. Since baseline values for each study were all different, R_0 was fixed according to individual data sets, and either k_{in} or k_{out} was calculated based on R_0. The model fitting among four models were very similar to each other (final fits of d, IDR IV, difference in k_{out} for are shown in **Figure 4.2**). The PK-PD model provided a good description of the experimental plasma PK data and paw withdrawal threshold to mechanical stimuli PD data. All the parameters from four different models were estimated with sufficient precision **(Table 4.2)**.

The changes of paw withdrawal threshold to mechanical stimuli were not very significant when the total dose was the same but given as one of the four dosing regimens: 1 mg/kg daily for 8 days; 2 mg/kg on day 0, 2, 4, and 6; 4 mg/kg on day 0 and 4; 4 mg/kg on day 0 and 7; 8 mg/kg on day 0 (**Figure 4.3a**). The maximum changes in paw withdrawal threshold for all the dosing regimens were approximately 71-73% compared to the baseline level. The onset of the peripheral neurotoxicity was slight different, depending on the frequency of the dose. On the other hand, the changes of paw withdrawal threshold to mechanical stimuli varies among different frequencies of administration at 2 mg/kg of Taxol® for 4 times (**Figure 4.3b**). Taxol® given as daily, every 2, 3, or 4 days, or weekly doses of 2 mg/kg yielded distinct response on mechanical sensitivity, range from 71% - 78% compared to the baseline level. The onset of peripheral neurotoxicity delayed with the increased dosing interval (from daily to weekly). A third simulation was conducted to compare with previously reported clinical study in comparison of lower dose at higher frequency or higher dose at lower frequency (**Figure 4.3c**). The lower dose at higher

frequency (2 m/kg on day 0, 2, 4, and 6) yielded a less sensitivity to mechanical sensitivity compared to higher dose at lower frequency (4 mg/kg on day 0, 6, 12, and 18).

4.3 DISCUSSION

CIPN is a very common, serious, and debilitating adverse effect of paclitaxel and many other anticancer drugs. A recent systematic review (31 studies, 4179 patients) reported CIPN prevalence of 68% when measured in the first month after chemotherapy, 60% at 3 months and 30% at 6 months or more (6). Different drugs may result in a different clinical presentation of neuropathy symptoms; the underlying mechanism of development of CIPN are complex (212, 213) and not fully understood. Treatment of CIPN is mostly symptomatic (using anticonvulsants, gabapentin, opioids (202)) and remains largely ineffective (201). Some prevention treatments using vitamin E, amifostine, and glutathione were reported (202); however, discontinuation of chemotherapy or dose reduction remains the only clinical solution (202). Therefore, there is an urgent need to evaluate possible risk factors of CIPN and prevent CIPN development.

Previous studies have raised several risk factors for CIPN, including dose (221) or schedule (222), genetic polymorphism (223), and drug exposure in plasma (224, 225). However, the quantitative analysis of the PK-PD relationship has not been conducted. A kinetic-pharmacodynamic model of CIPN induced by Taxol® was developed in patients with metastatic breast cancer (227). Indirect response model with linear drug effects was able to describe the CIPN development using patient reported CIPN score. However, no plasma PK data were available, and hence, no PK-PD relationship was established. The current model may have less translational significance to clinical use because the approach for neurotoxicity assessment are different from preclinical model to human. However, surrogate models can be generated to simulate the dosing regimen that is being clinically used. For example, our simulations show that there is no significant difference in paw withdrawal threshold after administering the same total dose of Taxol® using different dosing schedules (**Figure 4.3a**). Administration of the same dose on weekly basis yield less neurotoxicity compared to daily doses (**Figure 4.3b**). **Figure 4.3** demonstrated a

simulation of similar dose and frequency compared to a clinical study. In the clinical study, lower dose with higher frequency (80 mg/m^2 with weekly administration for a total of 6 cycles) resulted in higher rate of neuropathy compared to higher dose with lower frequency (175 mg/m^2 with every 3 weeks for a total of 6 cycles) (222). Interestingly, the model simulation with lower dose but higher frequency (2 mg/kg on day 0, 2, 4, and 6) results in a lower peripheral sensitivity compared to the other group (4 mg/kg on day 0, 6, 12, and 18). Another preclinical study claimed no-dose response relationship was found for rats administered with different doses of Taxol® (0.5 - 2 mg/kg on alternate days for four times) (183). Additional information of dosing schedule with a wide range of doses would help to determine the relationship between dose and the severity of paclitaxel-induced peripheral neurotoxicity in the future.

In current PK-PD model development, model I and model IV of IDR were both evaluated and compared to describe the relationship between paclitaxel plasma PK and paclitaxel-induced neurotoxicity. Since the mechanisms that contribute to CIPN are not fully understood, the PK-PD relationship can be explained as inhibition of factors regulating the production of response to mechanical stimuli, such as changes in axon morphology functions, cell shape and stability in microtubules, calcium homeostasis in mitochondria, etc. (4); or as stimulation of factors controlling the dissipation of the response to mechanical stimuli, such as amplification the neural signaling within central nervous system that elicits pain hypersensitivity (228). In fact, both models adequately described the observed data with comparable estimated parameters and sufficient precision. In model I development, I_{max} was fixed to the maximum possible value (1.0) to accommodate the algorithm of the modelling, which may indicate that the maximum fractional ability of the drug to affect the process can reach 100%. Future studies on the mechanism of CIPN are necessary to determine the appropriate model for paclitaxel plasma PK and its neurotoxicity development.

The baseline response values among all data sets were different, which may be due to the age differences of rats, the differences in measurement equipment, and individual researchers. Von Frey filaments yielded a lower baseline while electronic Von Frey and dynamic plantar yielded a higher baseline. The underlying protocols and principles are different, it remains unclear if electronic Von Frey activates a different subset of sensory neurons (high-threshold mechanoreceptors) compared to traditional Von Frey filaments (low-threshold mechanoreceptors) (26). However, both methods can be used to measure mechanical sensitivity. To accommodate the different baselines, original data sets may be computed as ratio relative to the baseline, change from the baseline (subtraction), and percent change relative to the baseline. However, it is highly recommended to use original experimental data rather than normalized data to model because any normalization would cause absence of individual differences in basal conditions between subjects or study groups (229). In addition, model parameters of the IDR models are interrelated with baseline values (k_{in} and k_{out}), baseline normalization is not a frequent practice to handling IDR models. In the current model, original data sets were used for modeling and baselines were not estimated, which reduced the number of model parameters to be estimated. Importantly, all data sets could be captured with a single set of parameters (except for the baseline values).

Modelers have been debating as to whether the baseline should be estimated or fixed. Woo et al. have discussed the handling of baseline values by estimation, fixing at the starting value, and fixing at an average of starting and returning values of response profiles (229). Estimation led to the least bias and imprecision when the data is sufficient to capture a full response profile compared to other two approaches. However, if the profile does not completely return to baseline, estimation and fixing approaches are comparable. The overall relative performance between estimation and fixing are very similar when there are more sampling points in the return phase (229). In the current model, 2 out of 4 data

sets have a complete response profile. Therefore, the baselines were fixed to the average of initial and late measurements for these two data sets, and to the initial observations for the rest of the data sets.

Since baselines were fixed to either starting value or the average of starting and returning response value, k_{in} and k_{out} can be calculated based on the $R_0 = {k_{in}}/{k_{out}}$. Therefore, two cases were compared, namely that there was a difference in either k_{in} or k_{out}. The fitted profiles, estimated parameters, variances, and Akaike Information Criterion were very similar between estimating k_{in} and k_{out}. The ratio of estimated k_{in} and k_{out} were 18.33 g and 65 g for model I and model IV, which are not directly correlated with the fixed baseline levels (R_0). If a more informative data sets with wider range of dosing regimen were available for model development in the future, estimating R_0 would be another way to evaluate the quantitative relationship.

Dansirikul et al. have discussed different ways of modeling baseline responses while taking into consideration between- and within-individual variability (230). The baseline normalization yields the largest bias and imprecision of parameter estimates. However, the population modeling approach is not suitable for the data sets in the current study since only mean ± SEM were available from publications.

4.4 CONCLUSION

In this study, we established a quantitative approach to link between the plasma concentration of paclitaxel and paclitaxel-induced peripheral neurotoxicity after IV administration of Taxol® to rats. Simulations of different dose and schedule may enhance the understanding of CIPN development and direct the future Taxol® usage in the clinic. Our previous study (Chapter 2) showed slow elimination of paclitaxel from peripheral tissues (skin and muscle) after IV administration Taxol® to rats at 6 mg/kg. In the future studies, the estimates half-life of the drug in the hypothetical biophase should be compared to actual half-lives of paclitaxel in various tissues.

Table 4.1 Data sources for Taxol® induced peripheral sensitivity to mechanical stimuli in rats used for PK-PD model development

References	Species	Age/Weight	Sex	Number	Dose regimen	Total dose (mg/kg)	Method
Yamashita et al., 2011 (214)	Sprague Dawley rats	- [a]	Male	10-11	6 mg/kg/week x 4 times	24	Von Frey Filaments
Ochi-ishi et al., 2014 (226)	Sprague Dawley rats	8-11 weeks	Male	6	18 mg/kg, day 0 and 4	36	Von Frey Filaments
Yilmaz et al., 2015 (209)	Sprague Dawley rats	250-320 g	Male	7	2 mg/kg/2 days x 4 times	8	Plantar test analgesia meter (IITC Life Sciences Inc. CA)
Zang, 2017 [b]	Sprague Dawley rats	250-350 g	Male	10	2 mg/kg/2 days x 4 times	8	Dynamic Plantar aesthesiometer (Ugo Basile, Italy)

[a] Not available
[b] data was acquired by the investigator rather than a published resource

Table 4.2 Estimated PK-PD parameters of Taxol® induced peripheral mechanical sensitivity in rats

Estimated parameters, units	Model I				Model IV			
	Parameterization in k_{in}		Parameterization in k_{out}		Parameterization in k_{in}		Parameterization in k_{out}	
	Estimate	%CV	Estimate	%CV	Estimate	%CV	Estimate	%CV
k_{el}, day^{-1}	18.67	4	18.67	4	18.67	4	18.67	4
V_p, L	0.35	8	0.35	8	0.35	8	0.35	8
k_{eo}, day^{-1}	0.07	20	0.07	19	0.06	22	0.14	56
k_{in}, g/day	8.98	23	- [a]	-	5.20	31	-	-
k_{out}, day^{-1}	-	-	0.49	22	-	-	0.08	56
I_{max}	1.0 [b]	-	1.0 [a]	-	-	-	-	-
IC_{50}, ng/mL	32.42	10	32.17	10	-	-	-	-
k, mL/ng	-	-	-	-	0.03	13	0.03	8
Variance_PK	0.033	38	0.033	38	0.033	38	0.033	38
Variance_PD	0.015	19	0.015	19	0.016	19	0.012	19
OBJ	377		377		385		368	
AIC	768		768		783		750	

[a] not applicable
[b] Imax was fixed to 1.0
%CV, estimator criterion value for the maximum likelihood method; OBJ, objective function value; AIC, Akaike information criterion

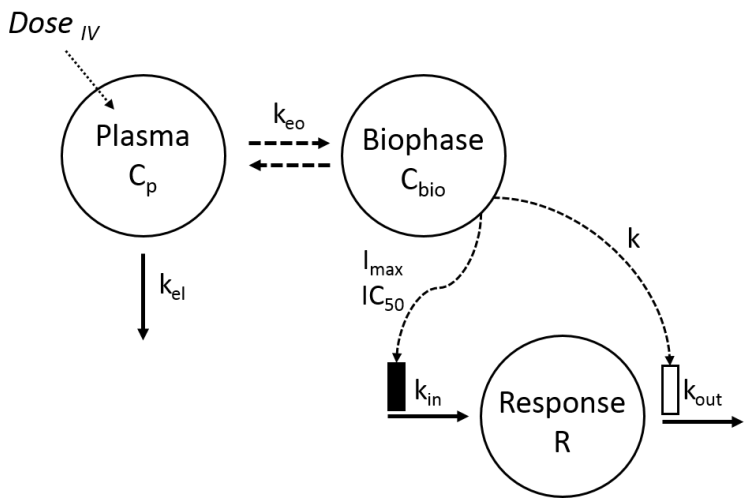

Figure 4.1 Integrated model used to characterize PK and PD of Taxol® induced peripheral sensitivity to mechanical stimuli.

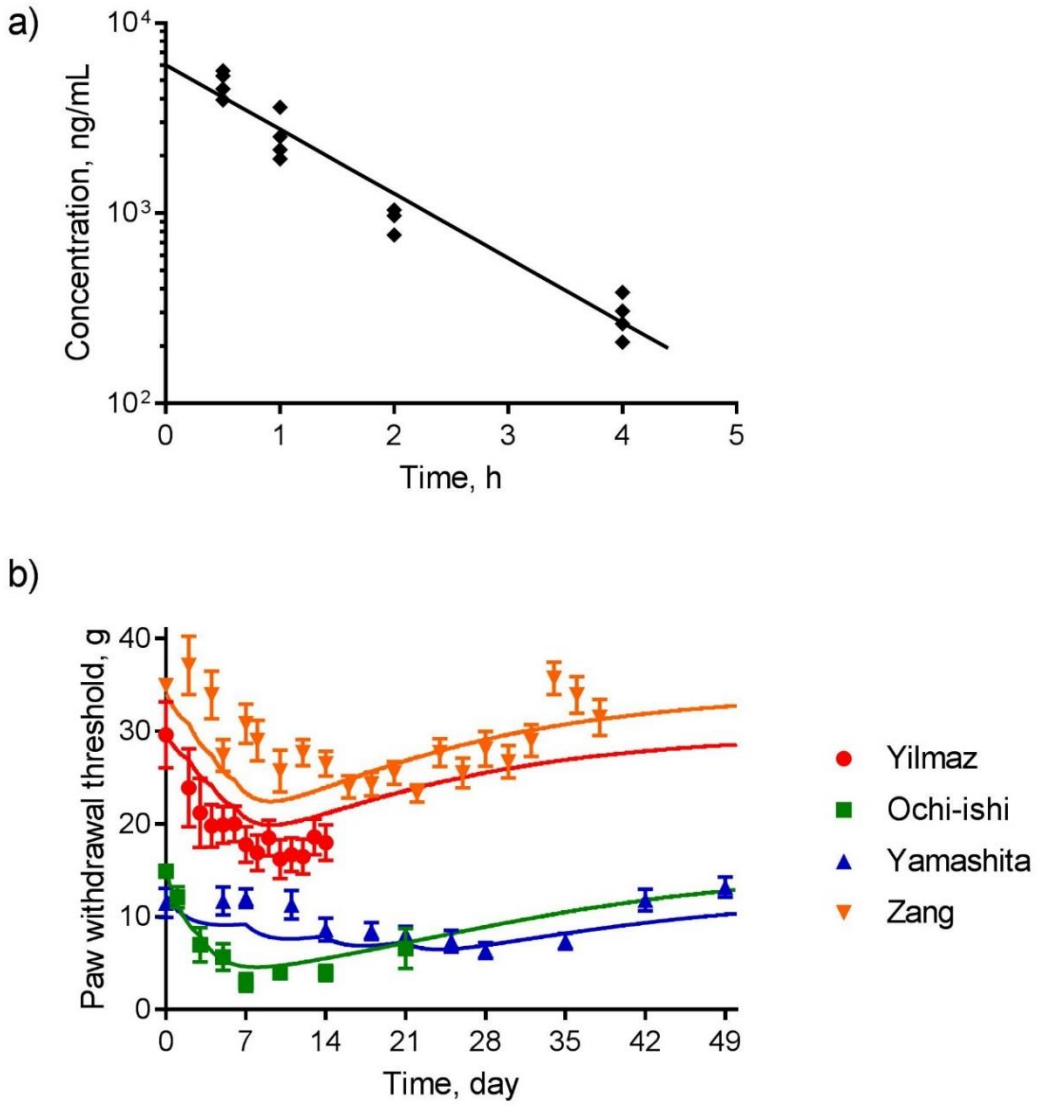

Figure 4.2 a) Time-course of plasma paclitaxel following Taxol® IV bolus administration at 6 mg/kg to rats (n = 3-4). Data are shown as individual measurement. b) Time-course of paw withdrawal threshold in response to mechanical stimulation to plantar surface of hind paw before and after injection of Taxol® at 2 mg/kg for 4 times (n = 6-10). Data are shown in mean ± SEM. The symbols represent experimental data or data extracted from references (209, 214, 226), and lines are model-predicted profiles after simultaneous fitting PK-PD data.

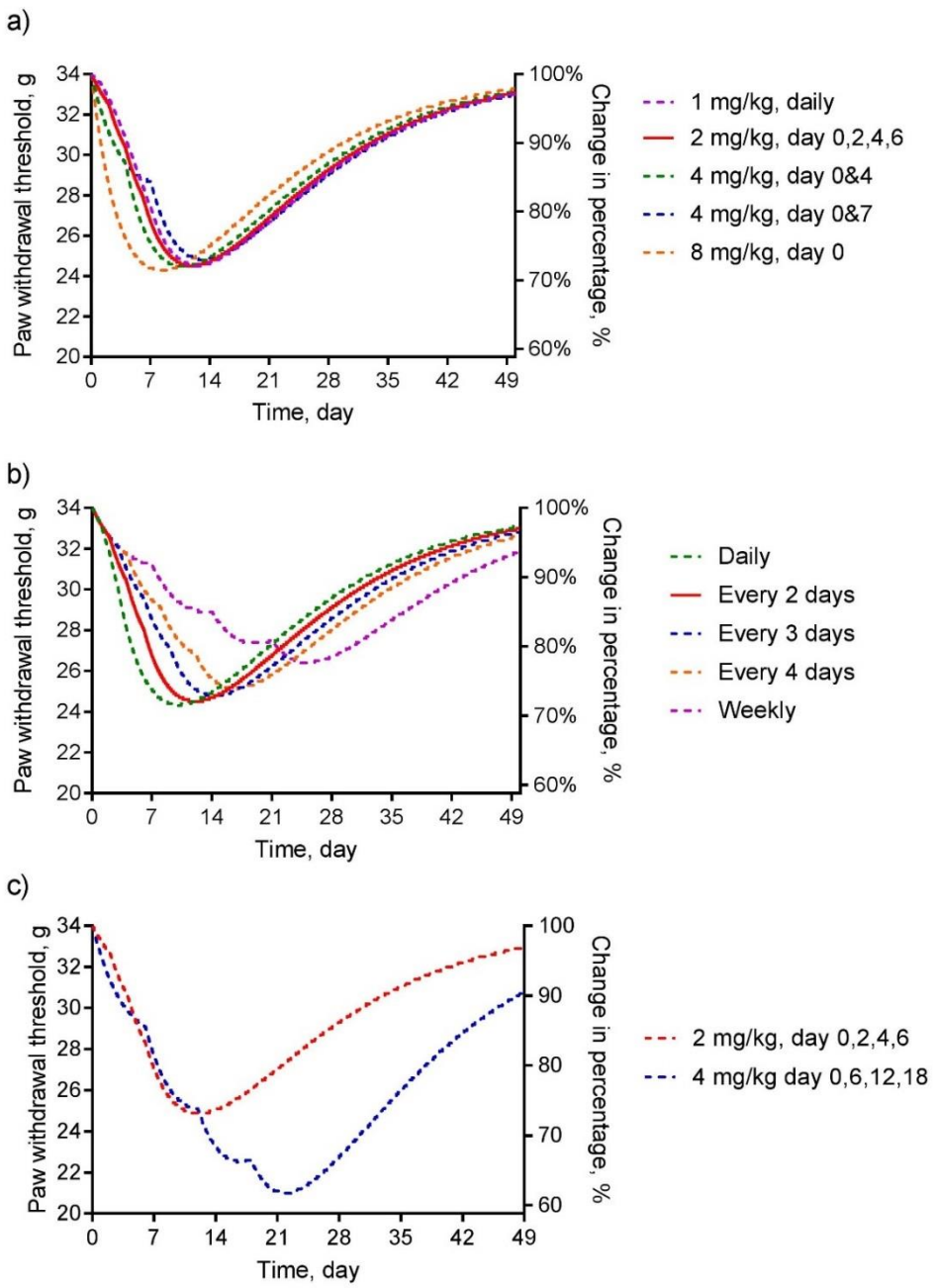

Figure 4.3 Time-course of paw withdrawal threshold to mechanical stimuli after IV administration of Taxol® to rats. Lines represent PK-PD model predicted profiles using a) same total dose (8 mg/kg) given within one week at different dose for each administration (1, 2, 4, or 8 mg/kg) and b) same total dose (8 mg/kg) given at daily, 2, 3, or 4 days apart,

or weekly at 2 mg/kg for each administration c) 2 mg/kg every other day for 4 times or 4 mg/kg every 6 days for 4 times.

Chapter 5. Physiologically-Based Modeling and Interspecies Prediction of Cisplatin Pharmacokinetics

5.1 INTRODUCTION

Cisplatin (*cis*-diamminedichloroplatinum(II) or CDDP) is an effective anti-neoplastic therapy for various types of cancer, including metastatic testicular tumors, metastatic ovarian tumors, advanced bladder cancer, non-small cell lung cancer (44). Off-label use has been extended to head and neck, esophageal, gastric, colorectal, hepatocellular, metastatic melanoma, and second-line to metastatic breast and prostate cancers (43). Cisplatin is a platinum-based alkylating compound which causes formation of inter- and intra-strand DNA cross-links resulting in inhibition of replication and apoptosis of the cell (231).

Cisplatin is usually administered to patients as slow intravenous infusion (6-8 h) in cycles. For example, treatment for testicular cancer is 20 mg/m^2 daily for 5 days per cycle in combination with other chemotherapeutic agents, or 75-100 mg/m^2 every 4 weeks for ovarian cancer in combination with cyclophosphamide (44). Cisplatin and its metabolites are mainly renally excreted and can accumulate in the renal proximal tubules. Cisplatin-induced nephrotoxicity is the most common (about one third of the patients) and dose-limiting side effect, and cisplatin use is normally limited to patients with a creatinine clearance greater than 60 mL/min (45). Neurotoxicity has developed in nearly 50% of patients who received cisplatin-containing regimen compared to 25% of patients treated with non-cisplatin-containing regimen. Additionally, the severity of neurotoxicity in cisplatin treated patients were much higher (46). Other side effects of cisplatin treatment include ototoxicity (31%), myelosuppression (25% - 30%), and nausea and vomiting (~100%) (reported as percentages of patients after single-agent therapy) (44). Alternative formulation of cisplatin has been investigated to reduce cisplatin-induced side effects. The

liposomal cisplatin formulation (Lipoplatin™) has shown in phase I, II, and III clinical trials to substantially reduce renal toxicity, peripheral neuropathy, and other side effects with enhanced or similar efficacy (43).

Cisplatin is not subjected to enzymatic metabolism, it exhibits an uncommon metabolism and binding pattern. Cisplatin (parent drug) irreversibly binds to low molecular weight nucleophiles and nucleophilic sites on macromolecules to form mobile and fixed metabolites **(Figure 1)** (105, 106). Plasma profiles of parent drug show monoexponential decay with a half-life of approximately 0.5 h following intravenous (IV) bolus administration to humans at a dose level of 50 or 100 mg/m^2, or 2 h infusions at 100 mg/m^2 (44). Majority of studies measured the total platinum concentration without differentiating between parent drug and metabolites. Tight and irreversibly binding between platinum and macromolecules results in a long half-life of total platinum due to slow elimination of fixed metabolites (44). Cisplatin clearance and volume of distribution at steady state in humans were reported as 15-16 L/h/m^2 and 11-12 L/m^2 respectively. Fecal excretion of platinum is insignificant because very minimal amount of platinum is present in the bile and large intestine (44).

The goals of this work were to develop a PBPK model based on multiple published data sets from preclinical species and to evaluate the utility of the PBPK model for predicting cisplatin pharmacokinetics in humans.

5.2 MATERIALS AND METHODS

5.2.1 Data sources

To investigate whole-body biodisposition of cisplatin, pharmacokinetic data were collected from the literature. Mean data (total platinum, parent, or filterable platinum concentration in plasma and tissues) in each publication were captured by Plot Digitizer (version 2.6.8). Eleven publications reporting cisplatin pharmacokinetic profiles in plasma and tissues after a single intravenous (IV) bolus administration to mice (232-242) and four publications to rats (106, 243-245) were identified after screening. Four publications were excluded because too few tissue concentration profiles (≤ 3 tissues) were reported. Seven publications with mice data (232, 234, 236, 238, 240-242) **(Table 5.1)** and four publications with rats data **(Table 5.2)** were included for model development. Instead of plasma, two studies reported blood or serum concentration were excluded from plasma concentrations from the rest of the studies (234, 241). Due to technical difficulties were associated with extracting data from the spleen concentration profiles of Staffhorst et al. (238) and Oberoi et al. (240), both were excluded from model development. Selected studies have a dose level of 3 to 10 mg/kg for mice and 2 to 5 mg/kg for rats, which were used to construct the PBPK model of cisplatin disposition. Reported tissue distribution profiles includes plasma, spleen, liver, kidneys, lungs, gastrointestinal (GI) tract, muscle, skin, heart, brain, and platinum concentrations in urine.

Human data were used for evaluating interspecies prediction using the PBPK approach. Three studies were identified that reported plasma pharmacokinetic data and urine profile of cisplatin following single IV infusion in cancer patients at dose level of 70, 75, and 100 mg/m^2 over 1 h (246-248); and three studies were identified that reported tissue concentrations (autopsy data), including kidneys, liver, heart, spleen, lung, GI, brain, and muscle (249-251). Only total dose information was reported in two studies, ranging 80-174 mg/m^2 (251) and 90-265 mg/m^2 (250). In the third publication, data were reported

as normalization to 100 mg platinum/m^2 for all patients (249). All dose information and concentrations were converted to molar unit (µmol/kg for cisplatin, and nmol for platinum concentration).

5.2.2 Physiological parameters

Physiological parameters, such as tissue weights, fractions of vascular space in tissues, and plasma flow rates to tissues, were fixed to previously reported literature values (120-122). Plasma cardiac output (CO) for rats and mice were calculated using allometric relationships: $CO_{rat}(L/h) = 14.1 \cdot (1 - Hematocrit) \cdot (body\ weight\ in\ kilograms)^{0.75}$ and $CO_{mouse}(L/h) = 16.5 \cdot (1 - Hematocrit) \cdot (body\ weight\ in\ kilograms)^{0.75}$ (120). Plasma cardiac output for humans was fixed to $312 \cdot (1 - Hematocrit)$ L/h (120). All tissues that were not reported in the publications were lumped into a hypothetical remainder compartment (107). The densities of all tissues were assumed to be 1 g/mL. Body weights (BW) of 0.02, 0.25, and 69 kg were used for mice, rats, and humans by taking the mean of the reported values from used publications.

5.2.3 Elimination Mechanisms

The renal clearance and biliary clearance of cisplatin in rats were reported as 12.3 and 0.27 mL/min/kg (232). Similarly, biliary excretion of platinum has only accounted for 1-4% in rabbits (252), dogs (253), and humans (254), which was assumed to be negligible compare to renal clearance. Therefore, biliary clearance was fixed to zero and only renal clearance was included in the PBPK model. Previous clinical studies suggested that ultrafilterable platinum is predominantly excreted by glomerular filtration (246). Therefore, the clearance of parent cisplatin and mobile metabolites were fixed to glomerular filtration rate (GFR) for all species. Mice GFR values was fixed at 283.5 µL/min (0.01701 L/h), which were calculated based on conscious C57BL/6 male mice (255). Rats GFR values

was fixed at 1.1 mL/min (0.066 L/h) (106). Human GFR values is assumed at 99 mL/min per 1.73 m^2 (6.21 L/h), which is based on the average GFR of people age 40-49 according to National Kidney Foundation (256).

5.2.4 Modeling Strategy

A whole-body PBPK model was develop in this work based on tissue disposition data in mice and rats, and human plasma and autopsy tissue data were used for qualification of interspecies scaling approaches. Due to a unique nature of cisplatin metabolism and binding, common approaches for data-driven PBPK model building (such as using equilibrium partition coefficients or permeability-surface terms to describe individual organs) were inadequate. A more mechanistic tissue model with separate parent drug and mobile and fixed metabolites compartments suggested by Farris and colleagues in the 1980s was implemented (106), as described below. Important distinction of our work is that 1) model parameters were estimated by fitting the model to the data, 2) multiple data sources were used, 3) additional tissues were included, and 4) approaches for interspecies scaling of the model parameters were developed.

5.2.5 PBPK model structure

PBPK models for cisplatin had been reported over 30 years ago by the same group in rats, rabbits, dogs, and humans (106, 257). While the overall structural model was shared across all species, species-specific parameters were utilized. More importantly, no model fitting was performed. Initial model parameters were calculated based on certain *in-vitro* and *in-vivo* experiments, and some of them were manually adjusted to provide description of the experimental data. In this work, we adopted the tissue-level model and underlying set of assumptions as proposed by Farris and colleagues (106). In each tissue, the parent drug is assumed to undergo biotransformation to mobile and fixed metabolites,

with a first-order rate constants k_{1i} and k_{2i}, and the fixed metabolites are converted to mobile metabolites with a first-order rate constants k_{3i} **(Figure 5.1)**. Cisplatin and mobile metabolites (any platinum containing low molecular weight nucleophile species) are assumed to freely traverse cell membranes, moves readily between compartments, and follow flow-limited kinetics. On the other hand, fixed metabolites - platinum bound to various macromolecules (mostly protein) - are assumed to be confined to the compartment where they are formed and can only be eliminated from a compartment by catabolism of platinum-macromolecule complexes to form mobile metabolites. Elimination of platinum from the body occurs in the kidneys, and the excretion rate of cisplatin and mobile metabolites is assumed to be the same. The representative model equations for kidney compartment is illustrated below:

Parent cisplatin

$$dC_{kdp}/_{dt} = \frac{Q_{kd} \cdot (C_{plp} - C_{kdp}) - Cl_{kd} \cdot C_{kdp}}{V_{kd}} - k_{2kd} \cdot C_{kdp} - k_{1kd} \cdot C_{kdp}$$

Mobile metabolite

$$dC_{kdm}/_{dt} = \frac{Q_{kd} \cdot (C_{plm} - C_{kdm}) - Cl_{kd} \cdot C_{kdm}}{V_{kd}} + k_{1kd} \cdot C_{kdp} + k_{3kd} \cdot C_{kdf}$$

Fixed metabolite

$$dC_{kdf}/_{dt} = k_{2kd} \cdot C_{kdp} - k_{3kd} \cdot C_{kdf}$$

where Q_{kd} is kidney plasma flow, V_{kd} is kidney volume, CL is the renal clearance, $k_{1kd}$is the rate constant for the biotransformation of cisplatin to mobile metabolite in kidney, $k_{2kd}$is the rate constant for the biotransformation of cisplatin to fixed metabolite in kidney, $k_{3kd}$is the rate constant for the biotransformation of fixed to mobile metabolite in kidney. The initial conditions for all equations were set to zero.

5.2.6 PBPK Modeling Process

Multiple publications reported plasma and tissue concentration-time profiles of total platinum in mice and rats following intravenous administration of a range of doses of cisplatin. Initial visual data evaluation did not reveal any nonlinearities, and urinary excretion was reported to be dose independent (258). Pharmacokinetic data for some tissues was not available in mouse studies and for some other tissues in rat studies (heart and brain profiles were only reported in mice, and GI profile was only reported in rats); therefore, PBPK model was developed using data from both species simultaneously. The PBPK model included the following tissues and organs: plasma (pl), GI tract (gi), spleen (sp), liver (li), kidneys (kd), lungs (lu), heart (hr), muscle (mu), skin (sk), brain (br), and remainder (rm) (lumped all non-sampled tissues) compartments **(Figure 5.2)**. During initial model runs, all cisplatin biotransformation rate constants (k_{1i}, k_{2i}, k_{3i}) were estimated separately; however, many parameters could not be estimated with sufficient precision due to lack of data. Therefore, the number of parameters was reduced based on the approach proposed by Farris and colleagues (106). In each tissue, the biotransformation rates from parent to mobile (k_{1i}) and fixed (k_{2i}) metabolites were assumed to be correlated (i.e., $k_{1i} = k_{2i} \times SF$, where *SF* is a scaling factor). SF was assumed to be tissue independent. To further reduce the number of parameters, the biotransformation rate from fixed to mobile metabolite (k_{3i}) that represents protein turnover in each tissue, was assumed to be the same in all tissues except for plasma and kidney.

Parameter estimation was initially performed using two the most informative data sets, one for mice (232) and one for rats (106) because they contained the largest number of observed tissue profiles. After the model structure was finalized, other data were included (7 mice and 4 rats data sets); in addition, the value for the skin compartment ($k2_{sk}$) was fixed for subsequent model runs because none of the other data sets contained information on this tissue.

5.2.7 Interspecies scaling and PBPK simulations for predicting pharmacokinetics in humans

When PBPK models are used for interspecies modeling, certain parameters can be fixed to known values (physiological parameters, fraction unbound in plasma, clearance terms), shared (partition coefficients) or scaled (permeability-surface area terms, clearance terms) across the species. It was hypothesized that binding of cisplatin to low and high molecular weight nucleophiles is a cellular level process independent of species size; and therefore, the corresponding rate constants, k_1 and k_2 can be shared across the species. On the other hand, degradation rate of fixed metabolites to mobile metabolites was assumed to be dependent on the protein turnover rate. Whole body protein turnover was previously shown to scale allometrically (259). Data from six species (mouse, rat, rabbit, sheep, human, and cow) were included and plotted against species body weights on a log-log scale, and a power-based regression was performed. The rate constant k_{3i} was assumed to scale allometrically across the species with the same exponent as the whole body protein turnover: $P = P_{mouse} \cdot (\frac{BW}{BW_{mouse}})^B$, where P is the parameter of interest, BW is species body weight, and B is an allometric exponent (**Figure 5.3**).

To evaluate predictive performance of the PBPK model, plasma and tissue pharmacokinetic profiles of platinum in humans were simulated (using the final PBPK model structure, estimated parameters, and interspecies scaling approaches) and compared visually with the observed data from literatures.

5.2.8 Data analysis

Modeling and simulation were conducted using MATLAB R2015b software (The MathWorks, Natick, MA). All pharmacokinetic parameters were estimated using the

maximum likelihood method. The variance model was defined as $VAR_i = (\sigma_1 + \sigma_2 \cdot Y(\theta, t_i))^2$, where VAR_i is the variance of the ith data point, σ_1 and σ_2 are the variance model parameters, and $Y(\theta, t_i)$ is the ith predicted value from the pharmacokinetic model. The goodness of fit was assessed by system convergence, Akaike Information Criterion, estimator criterion value for the maximum likelihood estimation method, and visual inspection of residuals and fitted curves.

5.3 RESULTS

A whole-body PBPK model was constructed according to the schematic presented in **Figures 5.1 and 5.2**, and included biotransformation of cisplatin to mobile and fixed metabolite and from fixed to mobile metabolites in each tissue compartment. The allometric relationship between species body weight and whole-body protein turnover is shown in **Figure 5.3**. Data were fitted well by power-based regression and the resulting allometric equation was $Protein\ turnover\ rate = 16.18 \cdot BW^{-0.28}$ ($R^2 = 0.99$). Therefore, the allometric exponent of -0.28 was used for interspecies scaling of the rate constant k_3 that describes biotransformation of fixed metabolites to mobile metabolites.

The PBPK model provided a good description of the experimental plasma and tissue total platinum data for mice **(Figure 5.4)** and rats **(Figure 5.5)**, and all parameters were estimated with sufficient precision **(Table 5.3)**. The reported values of k_3 in **Table 5.3** are for rat species. Values of k_3 for mice and humans can be calculated using the allometric equation reported above. In Figures 4 and 5, different colors represent different dose levels. The urine data were not used for fitting due to cumulative nature of this measurement. PBPK model predicted cumulative excretion was overlaid with the observed data for visual comparison. The model provided good prediction of the time course of platinum excretion into urine in mice and rats.

To evaluate the performance of the PBPK model in predicting cisplatin biodisposition in humans, pharmacokinetics profiles of total platinum in humans were simulated and visually compared with published results. The allometric relationship between species body weights and whole-body protein turnover (k_3) was incorporated as described before. **Figure 5.6** shows simulated total platinum plasma and tissue concentration-time profiles following administration of 100 mg/kg of cisplatin as an IV infusion over 1 h to humans. To facilitate the comparison, the observed data were

normalized to 100 mg/kg dose level. For tissues other than plasma and urine, only information on cumulative dose of cisplatin were available (and exact dosing schedule was not reported in the original publications). Since precise dosing regimen was not available, the total dose was assumed to be given to patients as a single IV infusion over 1 h. In general, reasonable prediction of cisplatin pharmacokinetics in humans was obtained for plasma, kidneys, lungs, liver, spleen, muscle, heart, brain, GI tract and urine.

5.4 DISCUSSION

A better understanding of the time-course of cisplatin biodistribution into tissues is required for establishing the connection between pharmacokinetics and pharmacodynamics and for optimization of cisplatin therapy (providing efficacy with minimal adverse sequalae). Since a comprehensive evaluation of drug disposition to various human tissues is rarely feasible, a combination of preclinical whole-body disposition studies, PBPK modeling and interspecies scaling is a valuable translation approach for achieving this goal.

In this work, the PBPK model was successfully developed based on preclinical data, and all model parameters were estimated with sufficient precision. Incorporation of interspecies scaling allowed for reasonable prediction of plasma and tissue time course of platinum in humans. While current PBPK model utilized previously suggested assumptions and model structure (106), several important advancements have been made. The model utilized more than ten different data sources which allowed for expanding the model to include additional tissue compartments (lungs, brain, heart, and spleen). Advancement in computational power over recent decades allowed for successful estimation of model parameters, in comparison to approach taken by Farris and colleagues (106), where some parameters were manually adjusted to provide reasonable data description. Furthermore, we shown that the number of model parameters can be significantly reduced (from 33 to 15), and model parameters can be effectively shared or scaled across species.

The relationship between the whole-body protein turnover and species body weight was reported before (259); however, to the best of our knowledge, this relationship has not been utilized for pharmacokinetics before. Initially, all three rate constants (k_1, k_2, k_3) were shared between mice and rats; and the model could be fitted reasonably well. However, an attempt of using the same approach for predicting kinetics in humans

resulted in a significant underestimation of plasma concentrations. Drug biodisposition data in human tissues is rarely available. In this work, the PBPK model was partly qualified using historic autopsy data. Overall, a reasonable prediction was obtained. Some discrepancies between the predicted profiles and observed data can be attributed to the following reasons: 1) lack of precise dosing regimen information in human subjects, 2) significant differences between the time scales for animal studies (hours and days) used for model development and human data (weeks), 3) use of autopsy data (unknown physiological status of these patients, which might have been different from “normal” physiological parameters used in modeling), and 4) potential drug interactions. In some of the utilized clinical studies, patients were given mannitol (246, 251) or 5-fluorouracil (247, 251) with cisplatin treatment. Previously, it was shown that these co-medications did not affect the plasma Cmax and terminal half-life, and urinary excretion (260). Effect of co-medications on tissue disposition should be evaluated in future studies.

5.5 CONCLUSION

In conclusion, a PBPK model for cisplatin and metabolites was developed using mice and rats data. The model successfully captured complex pharmacokinetics of platinum from multiple publications using a single set of parameters. Scaled PBPK model that included an allometric expression for conversion of fixed to mobile metabolites (that was based on total protein turnover) provided reasonable prediction of cisplatin pharmacokinetics in humans. Future studies, that separately measure parent drug and metabolites in various tissues are needed to further understand the pharmacokinetics of cisplatin and its metabolites.

Table 5.1 Sources of cisplatin pharmacokinetic data in mice used for model development.

Author	Route of Administration	Dose (mg/kg)	Strain	Tumor	Sex	Weight (g) / Age (weeks)	Analysis Method
Zamboni et al., 2002	IV Bolus	3 and 10	C57BL/6	B16 melanoma	F	4-6 weeks	FAAS
Xiao et al., 2012	IV Bolus	7.69 [a]	-	Cervical cancer	-	-	ICP-MS
Oberoi et al., 2012	IV Bolus	7.5	Athymic	Ovarian carcinoma	F	6 weeks	ICP-MS
Yu et al., 2015	IV Bolus	5	C57Bl/6J	Lewis lung carcinoma	F	17g	ICP-MS
Siddik et al., 1988	IV Bolus	4	BABL/c	No	M	20-25 g	FAAS
Staffhorst et al., 2008	IV Bolus	4	-	Ovarian carcinoma	F	28-35 g	FAAS
Ichinose et al., 2000	IV Bolus	3	BALB/c	Colon cancer	M	9 weeks	FAAS

FAAS, flameless atomic absorption spectrophotometer; ICP-AES, inductively coupled plasma-atomic emission spectroscopy; ICP-MS, inductively coupled plasma mass spectrometry; IV, intravenous

[a] Dose was reported as 5 mg of platinum per kg. 7.69 mg/kg was calculated based on the molecular weights of platinum and cisplatin.

Table 5.2 Sources of cisplatin pharmacokinetic data in rats used for model development.

Author	Route of Administration	Dose (mg/kg)	Strain	Tumor	Sex	Weight (g) / Age (weeks)	Analysis Method
Uchino et al., 2005	IV Bolus	5	Sprague Dawley	No	F	-	FAAS
Zhang et al., 2000	IV Bolus	5	Wistar	No	M	7 weeks	FAAS
Farris et al., 1985	IV Bolus	4	Sprague Dawley	Warlker 256 Carcinoma	F	200-250 g	Gamma-ray spectrometer
Zhang et al., 2002	IV Bolus	2	Wistar	No	M	7 weeks	FAAS

FAAS, flameless atomic absorption spectrophotometer; IV, intravenous

Table 5.3 Estimated pharmacokinetic parameters of cisplatin in mice and rats

Parameter	Units	Estimate	%CV	Parameter	Units	Estimate	%CV
$k2_{pl}$	h^{-1}	1.65	14	$k2_{lu}$	h^{-1}	2.53	18
$k2_{kd}$	h^{-1}	30.84	15	$k2_{sk}$	h^{-1}	21.92[a]	-
$k2_{gi}$	h^{-1}	1.54	24	$k2_{rm}$	h^{-1}	15.90	30
$k2_{sp}$	h^{-1}	1.45	15	$k3_{pl}$[b]	h^{-1}	0.012	12
$k2_{li}$	h^{-1}	5.90	14	$k3_{kd}$[b]	h^{-1}	5.50×10^{-3}	13
$k2_{hr}$	h^{-1}	0.90	18	$k3_{ti}$[b]	h^{-1}	8.50×10^{-4}	41
$k2_{br}$	h^{-1}	0.11	25	**SF**		0.74	16
$k2_{mu}$	h^{-1}	0.52	21				

%CV estimator criterion value for the maximum likelihood method,
[a] fixed to estimates using one mouse profile (232) and one rat profile (106)
[b] Values of k_3 are reported for rat species. Values of k_3 for other species can be calculated using the allometric equation reported in the result.

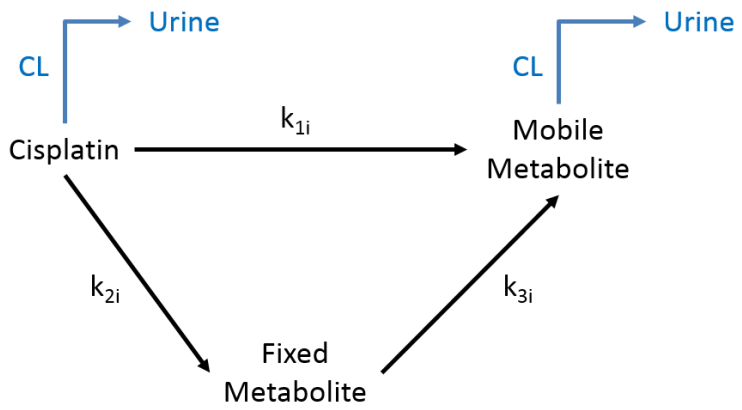

Figure 5.1 Schematic of the biotransformation and elimination pathways of cisplatin. It represents tissue-level model in the proposed PBPK. *k1i*, rate constant for the biotransformation of cisplatin to mobile metabolites; *k2i*, rate constant for the biotransformation of cisplatin to fixed metabolites; *k3i*, rate constant for the biotransformation of fixed to mobile metabolites. *CL*, clearance was only included in the kidneys.

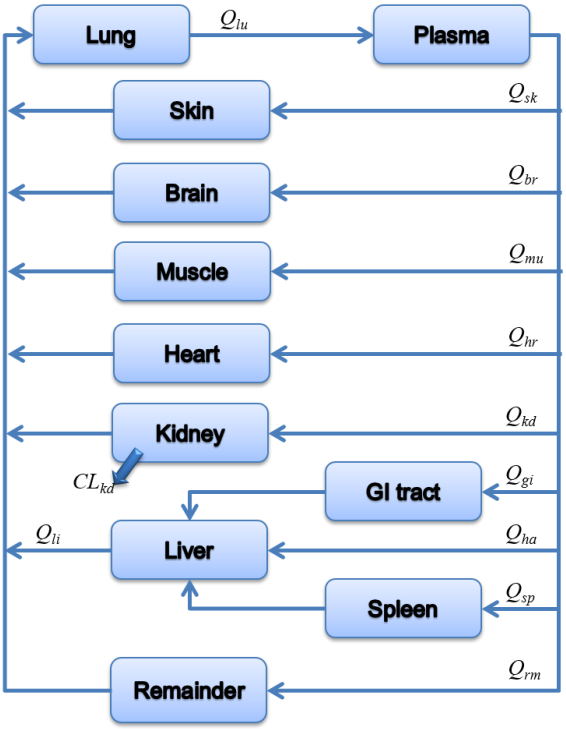

Figure 5.2 Schematic of the whole-body PBPK model used to describe the disposition of platinum in mice, rats, and humans following intravenous injection of cisplatin. Q_{ti} plasma flow rate to different organs, CL_{kd} renal clearance, *gi* gastrointestinal, *br* brain, *hr* heart, *kd* kidneys, *li* liver, *lu* lungs, *mu* muscle, *pl* plasma, *rm* remainder, *sk* skin, *sp* spleen

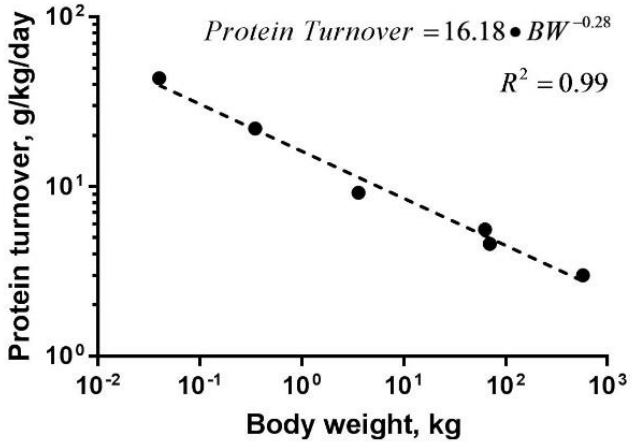

Figure 5.3 Allometric scaling plot of whole body protein turnover versus species body weights. Data included mouse, rat, rabbit, sheep, human, and cow (259).

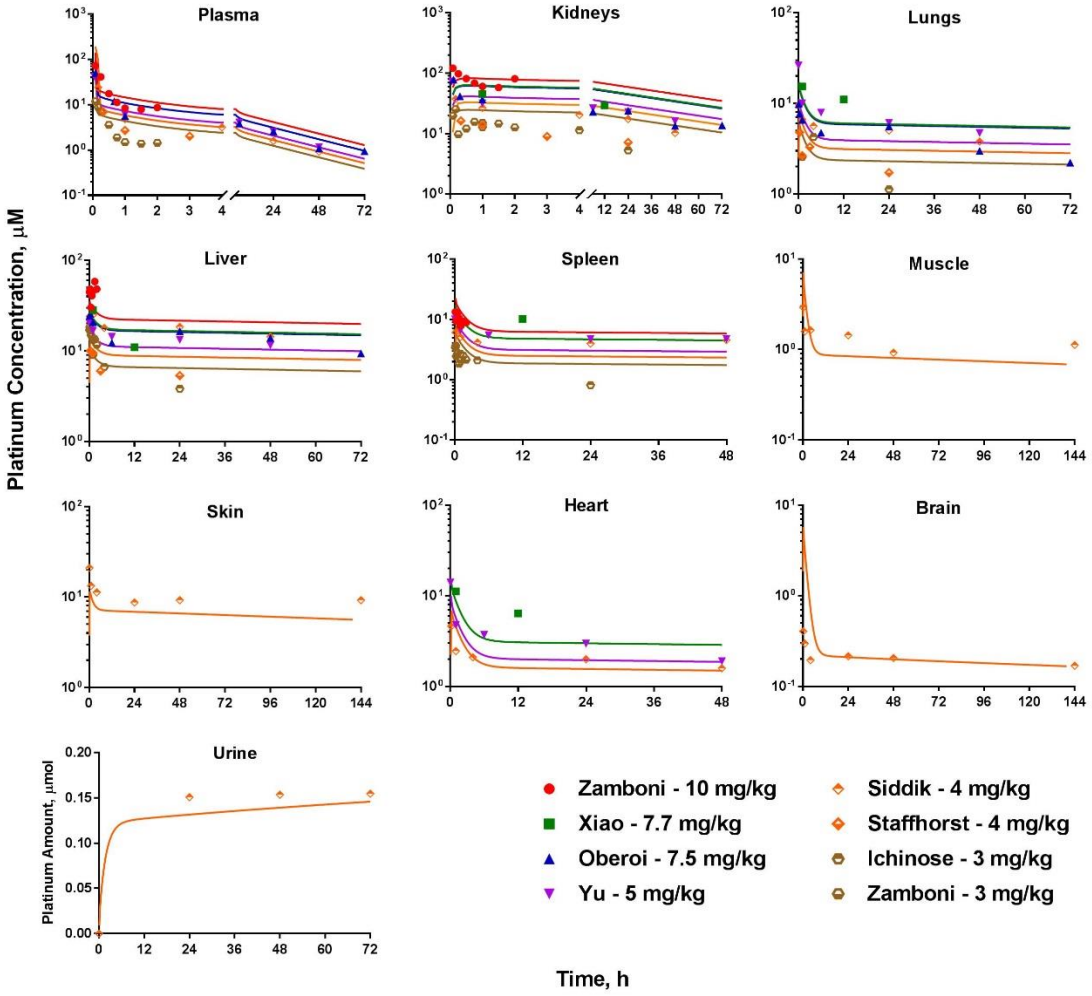

Figure 5.4 Observed (symbols) and the PBPK model fitted (lines) pharmacokinetic profiles of total platinum in plasma and tissues of mice following single IV bolus administration of 3-10 mg/kg of cisplatin (232, 234, 236, 238, 240-242). The urine data were not used for fitting, model predicted line was overlaid with observed data.

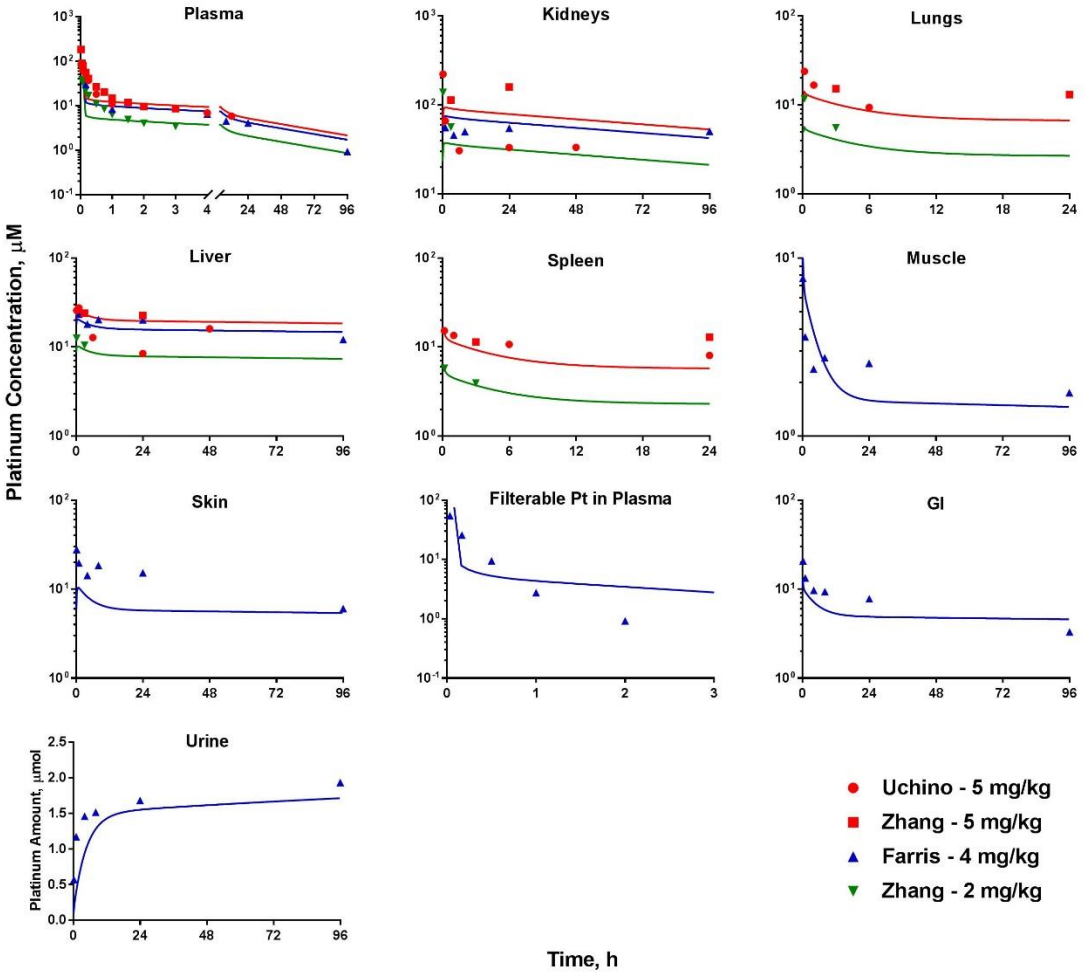

Figure 5.5 Observed (symbols) and the PBPK model fitted (lines) pharmacokinetic profiles of total platinum in plasma and tissues of rats following single IV bolus administration of 2-5 mg/kg of cisplatin (106, 243-245). The urine data were not used for fitting, model predicted line was overlaid with observed data.

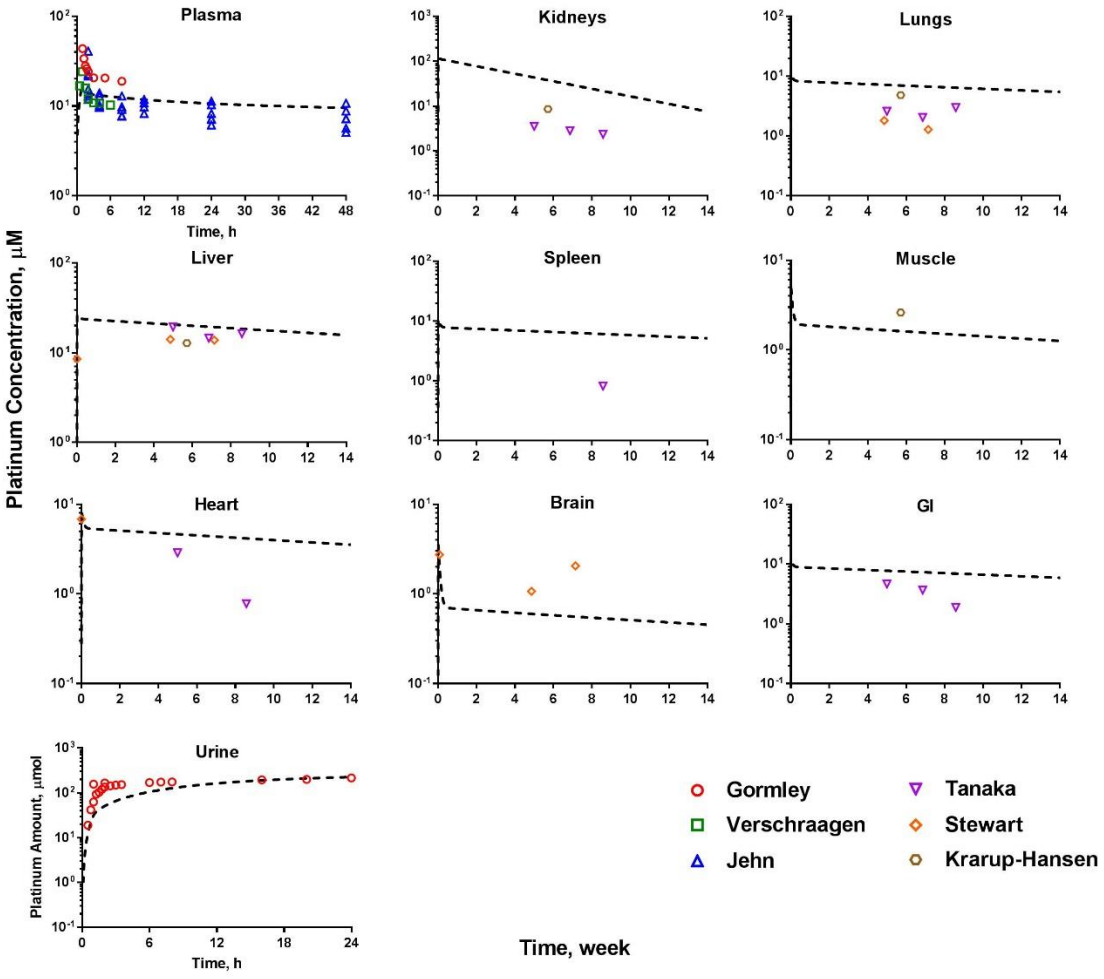

Figure 5.6 Time-course of total platinum in plasma and tissues of humans following single IV infusion administration for plasma and urine profiles, and multiple IV infusion administrations for tissue profiles. Symbols represent data extracted from 6 references, 3 for plasma and urine (246-248), and 3 for tissues (249-251). Lines represent PBPK model predicted profiles using parameters estimated from the preclinical model. The data were dose-normalized and simulation performed for 100 mg/m2 cisplatin dose level. Plasma and urine data were plotted using hour units for time axis, and tissue data were plotted using weeks units for time axis.

Chapter 6. General Discussion and Future Work

6.1 General Discussion

In this PhD project, quantitative modeling approaches were developed to understand the dose-response relationships between drug concentration in target tissues and chemotherapy-induced peripheral neuropathy focusing on paclitaxel and cisplatin, two commonly used chemotherapeutic drugs.

A better understanding of PK-PD relationship for paclitaxel is required for improving efficacy and minimizing toxicity of chemotherapy. Multiple preclinical and clinical pharmacokinetic studies with paclitaxel have been conducted mostly focusing on the time-course of plasma concentration of the drug. However, definitive quantitative relationships between the exposure profile to paclitaxel *in-vivo* and the efficacy and toxicity have not been established. For example, no relationship between the steady-state concentration of paclitaxel in plasma and the response rate to treatment, time to treatment failure, survival, or development of neurotoxicity was found in non-small cell lung cancer patients (179). A PBPK model of paclitaxel disposition after administration of Taxol was developed in mice and adequately predicted the tissue concentration-time profiles of paclitaxel in rats and humans utilizing interspecies modeling approach.

An important advantage of PBPK modeling is the ability to predict distribution to human tissues, which can be rarely tested experimentally. However, approaches for combining PBPK with interspecies scaling are not fully developed. Recently, the plasma PK of moxifloxacin in 5 species was simultaneously fitted using a minimal PBPK model (192), and the allometric exponent for the clearance term was estimated to be 0.59. In addition, renal and biliary clearance of amphotericin B were scaled among species using an allometric exponent of 0.75 (173, 174). Determining species differences in clearance for compounds eliminated through metabolism can be challenging (195). In their analysis

of published data for multiple compounds, an allometric exponent of 0.67 for clearance of compounds eliminated mainly by renal excretion, and 0.75 when substances are mostly eliminated by metabolism or by metabolism and excretion combined were suggested (196). They further noticed that often the exponent values of 0.67 and 0.75 cannot be differentiated statistically. In this work, the allometric exponent for clearance term was determined using non-compartmental analysis of plasma paclitaxel concentration-time profiles incorporated into PBPK model for interspecies simulations. Allometric exponent of 0.86 was incorporated and a reasonable prediction of paclitaxel disposition in humans was achieved.

The extent of neurotoxicity of chemotherapeutics in humans has not been directly connected with exposure profile but shown to increase with cumulative dose (182). On the other hand, in an animal model of paclitaxel-induced neurotoxicity, no correlation was found between paclitaxel dose (0.5-2 mg/kg) and the mechanical and thermal sensitivity (183), which may be related to a similar exposure of the central or peripheral nervous system or peripheral tissues to the drug at tested dose levels. In this work, dose-response relationship was established between PK of paclitaxel and PD (neurotoxicity). An indirect response model was developed to describe the time course of paclitaxel-induced peripheral neurotoxicity in rats. This model may not be directly translatable to clinical use (because the approach for neurotoxicity assessment are different from preclinical model to human). However, similar models can be constructed in combination with PBPK to simulate the dosing regimen in clinical use.

Many researchers focused on development of alternative formulations for Taxol® to modulate pharmacokinetics, toxicity, and efficacy (137, 177, 179). However, Taxol® remains the standard paclitaxel formulation in clinical practice. In this work, PBPK was constructed for Taxol® and PK-PD relationship was established between exposure and paclitaxel-induced peripheral neurotoxicity. Development of alternative formulations is a

promising approach to achieve better efficacy and reduce toxicities. Preclinical formulation development for paclitaxel and other cancer agents is often focused only on tumor targeting and overall efficacy, without specifically considering adverse effects and especially neurotoxicity.

CIPN is one of the most common, and often dose-limiting side effect of paclitaxel treatment. In this work, PEGylated liposomal paclitaxel formulation was developed and investigated for one of the toxicities. The liposomal formulation of paclitaxel was less toxic to neuronal cells than paclitaxel solution and prevented development of neurotoxicity *in-vivo* as compared to Taxol® administration (that resulted in a significant increase in sensitivity of rats to mechanical and thermal stimuli). The difference observed in development of neurotoxicity may be explained by alteration of drug exposure in peripheral tissues (skin and muscle). Persistent muscle and cutaneous hyperalgesia were observed in Taxol® induced peripheral neuropathy in rats (220). However, in majority of previous studies paclitaxel disposition to brain, spinal cord, skin, or muscle were not reported. In our study, assessment of drug concentration in target tissues were shown to be important for establishing dose-response relationship for efficacy and toxicity. Administration of L-PTX led to a significantly lower drug exposure in the brain, spinal cord, muscle and skin compare to Taxol® treated group, which corresponds to the results of mechanical and thermal sensitivity testing.

Cisplatin is another commonly used chemotherapeutic agent leading to peripheral neurotoxicity. In this work, the time-course of cisplatin biodistribution into tissues was investigated. The cisplatin PBPK model demonstrated reasonable prediction of human tissue distribution after cisplatin IV administration in both plasma and tissues. Cisplatin exhibits an uncommon metabolism and binding pattern in plasma and tissues which was well fitted using the current model structure. The rate constant of fixed to mobile metabolite was assumed to scale allometrically across the species with the same exponent as the

whole body protein turnover. This model was built based on multiple publications with plasma and 9 other tissues, including brain, muscle and skin. Future investigations on the relationship between drug exposure in central nervous system and peripheral tissues and cisplatin induced peripheral neurotoxicity could help us better understand the CIPN development.

6.2 Future Work

The understanding of paclitaxel biodistribution into central nervous system and peripheral tissues is limited with the developed PBPK model because published concentration-time profiles in these tissues are scarce. A more comprehensive and informative PBPK model of Taxol® and L-PTX is needed by expanding the current tissue disposition profile of Taxol® and L-PTX with more sampling time points. The biophase compartment was required for the PK-PD model reflecting a slow half-life, which may be correlated with the slow elimination of paclitaxel observed in peripheral tissues (skin and muscle). In future studies, estimated half-life of paclitaxel in the biophase should be compared to actual half-lives of paclitaxel in various tissues.

It has been shown that non-targeted and targeted liposomal formulations of paclitaxel are effective in suppression of tumor growth in nude mice bearing human A540 lung carcinoma xenografts (208). Future studies in orthotopic cancer mice models are needed to simultaneously assess efficacy and toxicity and establish dose-response relationship for L-PTX. In addition, surprisingly low concentrations of paclitaxel in plasma and short circulation half-life were obtained after L-PTX dosing, which may be related to efficient uptake by the reticuloendothelial system. The size of the particles was relatively small for liposomes with mPEG2000, which might be caused by probe sonication during formulation preparation. Future studies are needed to determine the optimal size of particulates for preserving (or enhancing) efficacy and minimizing neurotoxicity. The dose-

response relationship for L-PTX will be addressed in future studies, which will require more sensitive bioanalytical methods.

The PBPK model of cisplatin successfully described a complex data sets from multiple publications with plasma and 9 other tissues using a modified and simplified PBPK model compared to a previously reported PBPK model. However, the information on concentration-time profiles of mobile metabolite, fixed metabolites, parent drug, or filterable platinum are very limited. Future studies in metabolites tissue distribution are needed to fully understand the pharmacokinetics of cisplatin metabolites. Furthermore, a link between cisplatin exposure and cisplatin-induced neuropathy should be explored.

Appendix 1 Postprandial administration but not controlled release in the colon increases oral bioavailability of DF030263, a promising drug candidate for chronic lymphocytic leukemia[2]

A1.1 INTRODUCTION

Treatment of cancer is often limited by lack of efficacy and serious adverse effects. Unsatisfactory efficacy in many cases is related to unfavorable pharmacokinetics and biodistribution profiles including poor bioavailability, rapid clearance and limited distribution to the tumor tissues (261). The key aspect of this is that sufficient drug concentration has to be achieved and maintained at the site of action for the optimal anticancer efficacy. (262). Therefore, along with the development of targeted anticancer therapies by means of well-defined molecular targets or biologic signaling streams, pharmacokinetic development and optimization of chemotherapeutic agents are important to improve the treatment outcomes of cancer (263, 264).

While the majority of chemotherapy regimens in cancer depends on parenteral delivery, oral administration of anticancer agents is desired for several reasons. Oral dosing allows self-administration by the patients and avoids the inconvenience of intravenous injections which needs hospitalization (265, 266). Therefore, it improves patient compliance and reduces costs of therapy. It also prevents risk of infection that might be caused as a complication of injectable routes of administration. Most importantly, it makes treatment of chronic diseases more practical (266, 267). However, many anticancer agents possess unfavorable properties that make sufficient systemic exposure following oral administration challenging. These properties are mainly physicochemical

[2] Part of this chapter has been published by University of Nottingham, Ph.D. thesis (J.B. Lee), 2017

characteristics that result in low solubility, poor permeability, high efflux and rapid pre-systemic metabolism (262).

Cyclin-dependent kinases (CDKs) are essential in cell growth as they control progression of cell cycles and regulate transcription (268). CDK inhibitors have been discovered and developed on this premise to seek inhibition of unsuppressed cancer cell proliferation (268, 269). Among the CDK family, CDK9 is particularly related to regulation of RNA transcription. High expression of CDK9 and cyclin T1, corresponding cyclin partner of CDK9, is observed in chronic lymphocytic leukemia (CLL), indicating their key roles in pathologic mechanism of the disease (269-271). We have recently reported a series of highly active and selective inhibitors of CDK9 as candidates for treatment of CLL. Among the candidates, DF030263 was one of the most efficacious and selective compounds *in-vitro* [Ref].

Therefore, the aim of this work was to assess and to optimize the biopharmaceutical properties of DF030263 in order to achieve efficient treatment of CLL following oral administration of this compound. An *in vitro-in vivo-in silico* approach was applied to provide adequate solution towards improvement of the oral bioavailability. Biopharmaceutical optimization approaches including controlled release in the colon and postprandial conditions have also been assessed in this work.

A1.2 MATERIALS AND METHODS

A1.2.1 Materials

DF030263 (5-(2-((3-(1,4-diazabicyclo[3.2.2]nonan-4-yl)phenyl)amino)-5-methylpyrimidin-4-yl)-N,4-dimethylthiazol-2-amine, **Figure A1.1**) was synthesized in School of Pharmacy, University of Nottingham (Nottingham, UK) as previously reported [Ref]. Sodium taurocholate (NaTc), NaCl, NaOH (pellets), NaH_2PO_4, glacial acetic acid, lecithin, chlorpromazine and dexamethasone were obtained from Sigma (Gillingham, UK). Rat plasma was purchased from Sera Laboratories International (West Sussex, UK). Polyethylene glycol (PEG) 400 and all solvents (HPLC grade or higher) were obtained from Fisher Scientific (Leicestershire, UK). All other chemicals were analytical reagent grade or higher.

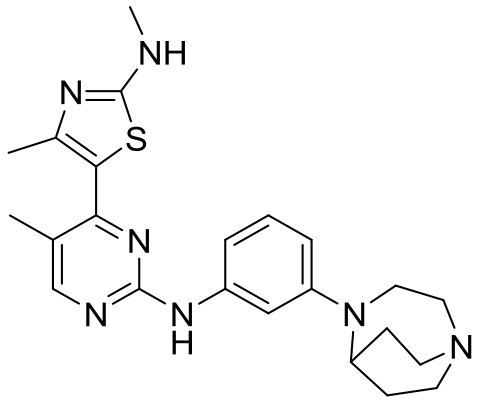

Figure A1.1 Chemical structure of DF030263 [ref].

A1.2.2 *In-vitro* solubility assay

<u>Preparation of simulated fluids</u>

Three different types of fluids simulating the gastrointestinal environment were prepared according to previously reported preparation methods (272-274): fasted state simulated gastric fluid (FaSSGF), fasted state simulated intestinal fluid (FaSSIF) and fed state simulated intestinal fluid (FeSSIF). The composition of these three simulated fluids were as described in **Table 1.1**. Prior to the assay, the pH of FaSSGF was adjusted to 1.6 and

3.0 using HCl and the pH of FaSSIF and FeSSIF was adjusted to be between 5.0-7.8 with interval of 0.2 using HCl or NaOH. All fluids were prepared on the day before the assay and stored at 4°C until use.

Table A1.1 Composition of the simulated fluids (mM)

	FaSSGF	FaSSIF	FeSSIF
NaTc	0.08	3	15
Lecithin	0.02	0.75	3.75
NaCl	34.2	105.9	203.3
NaOH	-	8.7	102
NaH_2PO_4	-	8.2	-
Acetic acid	-	-	144

FaSSGF, fasted state simulated gastric fluid; FaSSIF, fasted state simulated intestinal fluid; FeSSIF, fed state simulated intestinal fluid.

Solubility assay

On the day of assay, 198 µL of test medium (FaSSGF, FaSSIF, FeSSIF and water) was aliquoted into centrifugal tubes (Costar Spin-X Centrifuge Tube, Fisher Scientific, Leicestershire, UK). A volume of 2 µL of 20 mM stock solution in DMSO was then spiked into each tube to yield 200 µM of test concentration. The tubes were incubated at 37°C shaking at 250 rpm for 2 h using a shaking incubator (Thermo Scientific MaxQ4000, Thermo Scientific, OH, USA). After the incubation, the samples were immediately centrifuged for 5 min at 2400 *g* (Heraeus Fresco 17 Centrifuge, Thermo Electron, MA, USA). The filtrate was collected and subjected to analysis as described below. The assay was performed in triplicate.

Sample analysis

To 50 µL of sample, 10 µL of internal standard stock solution (100 µM dexamethasone, 50% acetonitrile in water) was spiked. For FaSSGF samples, 200 µL of

1 M NaOH was added and for FaSSIF, FeSSIF and water samples, 200 µL of 0.1 M NaOH was added. Two mL of methyl-tert-butyl ether was then added and the mixture was vortex-mixed for 10 min and centrifuged at 1160 *g* for 10 min. The organic layer was transferred and evaporated to dryness under N_2 gas at 40°C. Hundred µL of 40% acetonitrile in water was then added for reconstitution and vortex-mixed for 10 min before being transferred to HPLC vial for analysis.

The prepared samples were analyzed by a HPLC-UV system consisting of a Waters 600 Pump, Waters 717 Autosampler and Waters 2996 Photodiode Array Detector. A separate column oven was used to maintain the column temperature at 40°C. The stationary phase was a Gemini C18 250 × 4.6 mm, 5 µm particle size equipped with a SecurityGuard 2 × 4 mm, 3 µm particle size (Phenomenex, Macclesfield, UK). Mobile phase was a mixture of acetonitrile and 10 mM ammonium acetate buffer with pH adjusted to 5.0 with glacial acetic acid (40:60, v/v). The flow rate was 0.5 mL/min and 60 µL was injected. Chromatograms were observed at 256.5 nm of UV wavelength.

A1.2.3 *In-vivo* pharmacokinetic experiment

Animals

This study was conducted in accordance with an approved protocol by the Institutional Animal Use and Care Committee at Rutgers, The State University of New Jersey (#16-001). Male Sprague Dawley rats (Envigo, Inc., Indianapolis, IN) weighing 300-350 g were used for the experiment. Animals were housed at controlled temperature, 12 h light/dark cycle and with free access to food and water. The acclimatization of the animals was at least for four days. Surgical procedures were performed under general anesthesia induced by inhalation of isoflurane with an air carrier (3% for induction and <3% for maintenance). All rats underwent right jugular vein cannulation for blood sampling. For the group that received colonic administration, cannulation of the cecum was performed based on a previously reported protocol (275). Laparotomy was performed to gain access

to the large intestine. A small hole in the cecum was made with a 19 G needle and the cannula was inserted. Animals were allowed to recover for two days and were fasted up to 12 h before the pharmacokinetic experiment (except postprandial conditions experiment) with free access to drinking water.

Pharmacokinetic experiments

Formulations of DF030263 were prepared in PEG400:water (50:50, v/v) in concentrations of 2 or 4 mg/mL. For intravenous administration, formulation of 2 mg/mL was delivered at 1 mL/kg via the jugular vein cannula followed by 0.3 mL of heparinized saline (50 IU/mL) to ensure complete administration. Oral administration was conducted with the formulation of 4 mg/mL at 3 mL/kg using an oral gavage tube. Colonic administration was also performed with the formulation of 4 mg/mL at 3 mL/kg delivered via the cannula inserted into the cecum. The formulation was infused using a syringe pump (PHD Ultra, Harvard Apparatus, Holliston, MA, USA) at a constant rate for 1 h for colonic administration. Following the administration, blood samples (250 µL) were collected from the jugular vein cannula at pre-determined time points. Blood samples were centrifuged (3000 *g*, 10 min) and plasma samples were stored in -80°C until analysis.

Sample analysis

A volume of 100 µL of plasma was used for sample preparation procedure. The plasma samples were spiked with 10 µL of internal standard stock solution (5 µg/mL chlorpromazine, 50% acetonitrile in water). Three hundred µL of 0.1 M NaOH and 2 mL of methyl-tert-butyl ether were then added. The mixture was vortex-mixed for 1 min and centrifuged at 1160 *g* for 10 min. The supernatant organic layer was transferred to new glass tubes and evaporated to dryness under gentle stream of N_2 gas at 40°C. Hundred µL of 40% acetonitrile in water was added to dried samples for reconstitution and vortex-mixed for 30 s before being transferred to HPLC vial for analysis.

The HPLC-UV system was composed of Agilent 1260 Infinity equipped with quaternary pump, high performance autosampler, thermostated column compartment and diode array detector. The stationary phase was a Gemini C18 250 × 4.6 mm, 5 µm particle size equipped with a SecurityGuard 2 × 4 mm, 3 µm particle size (Phenomenex, Macclesfield, UK) and the column temperature was maintained at 40°C. Mobile phase was a mixture of acetonitrile, methanol and 10 mM ammonium acetate buffer with pH adjusted to 5.0 with glacial acetic acid (30:20:50, v/v). The flow rate was 0.4 mL/min and 80 µL was injected. Chromatograms were observed at 256.5 nm of UV wavelength.

Sample stability was tested prior to the pharmacokinetic experiment to ensure sample integrity during sample storage and analysis. Samples of rat plasma (n = 4) spiked with low (25 ng/mL) and high (8 µg/mL) quality control concentrations were prepared and stored at following conditions: 4 h at room temperature to test bench-top stability; 1, 2 and 4 weeks at -80°C to test storage condition stability. Autosampler stability was tested at the same concentrations with processed samples stored at 5°C for 24 h. All stability results were within ±15% relative error. Accordingly, all sample storage and preparation were performed within the limit of stability tested.

A1.2.4 Deconvolution of plasma concentration-time profiles

Deconvolution of plasma concentration-time profiles was conducted using Phoenix WinNonlin version 6.3 (Pharsight, Mountain View, CA, USA). The mean plasma concentration-time profiles following oral and intravenous administrations were used for the deconvolution. The results of deconvolution were expressed by cumulative input vs time and input rate vs time.

A1.2.5 In silico simulation of absorption sites

Intestinal absorption of DF030263 compound in different compartments of the gastrointestinal tract was simulated *in silico* using GastroPlus™ version 9.0.0007 with built-in ADMET Predictor™ version 7.2.0.0 module (Simulations Plus, Inc., Lancaster, CA,

USA). The input parameters are listed in **Table A1.2**. Parameters and settings not mentioned in the **Table A1.2** were used as predicted by the ADMET Predictor™ or as given by software default. The physiology setting was selected as “Rat-Fasted” or “Rat-Fed” and paracellular permeation option was turned on. Percentages of the dose absorbed at different compartments of the gastrointestinal tract were simulated at both fasted and fed states for rats.

Table A1.2 Input parameters for *in silico* simulation of DF030263 compound

Parameters	Value
Molecular weight (g/mol)	435.6
Log P	3.1
pK_a	10.7
Human jejunal permeability ($\times 10^{-4}$ cm/s)	1.37[a]
Diffusion coefficient ($\times 10^{-5}$ cm^2/s)	0.6288[a]
Drug particle density (g/mL)	1.2[b]
Mean precipitation time (sec)	900[b]
Reference solubility (mg/mL)	0.03846[c]
Biorelevant solubilities (mg/mL)	
FaSSGF (pH 1.6)	0.6737[c]
FaSSIF (pH 6.6)	0.04935[c]
FeSSIF (pH 5.0)	0.06529[c]

[a] Predicted by GastroPlus™
[b] GastroPlus™ default values
[c] Experimental results

A1.2.6 Statistical analysis

Data were expressed as mean ± standard error of the mean (SEM). Statistical significance of differences between two groups was determined by two-tailed unpaired t-test. A *p*-value of less than 0.05 was defined as statistically significant. Statistical analysis was performed using GraphPad Prism version 7.01 (GraphPad Software, Inc., La Jolla, CA, USA). Plasma pharmacokinetic parameters were obtained by non-compartmental analysis using Phoenix WinNonlin 6.3 software (Pharsight, Mountain View, CA, USA).

A1.3 RESULTS

A1.3.1 *In-vivo* oral bioavailability evaluation of DF030263

In-vivo oral bioavailability of DF030263 was evaluated in rats and the mean plasma concentration-time profiles are shown in **Figure A1.2**. The plasma concentration-time profile obtained following oral administration showed a distinct double-peak phenomenon, which was not apparent following intravenous administration. The first peak appeared after rapid absorption of the compound at 0.5 h while the second peak followed a delayed absorption, appearing at 4 h. Although the time between the two peaks varied for individual animals, this double-peak phenomenon was observed in all rats tested for oral administration (n = 4). The mean oral bioavailability of DF030263 was determined to be 23.8% and other pharmacokinetic parameters obtained from the plasma concentration-time profiles are shown in **Table A1.3**.

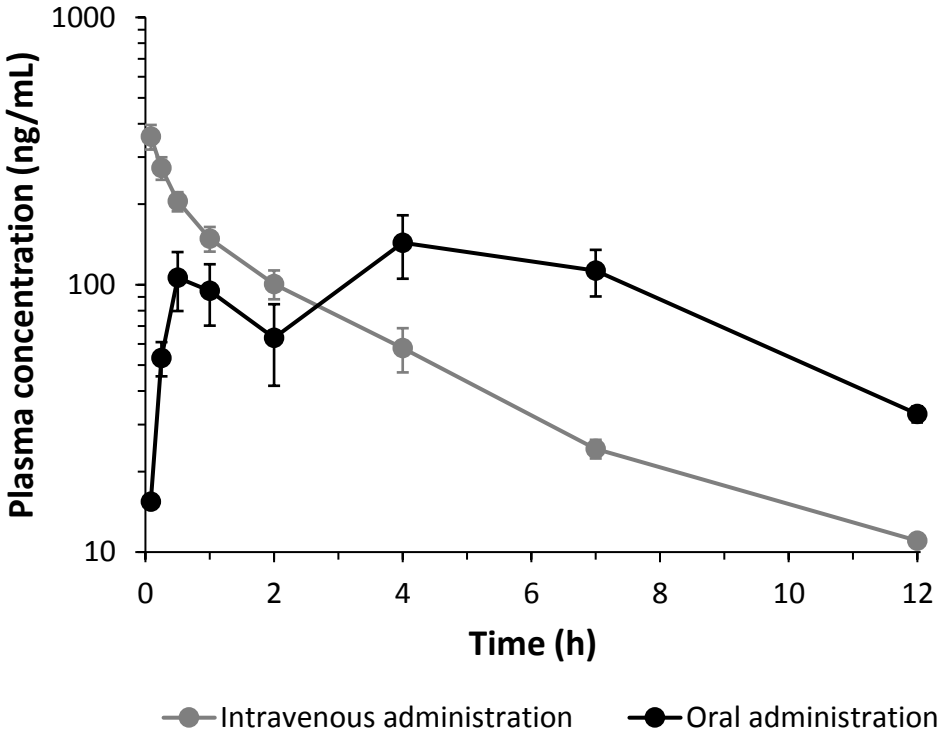

Figure A1.2 Mean plasma concentration-time profiles of DF030263 in rats following intravenous (2 mg/kg) and oral (12 mg/kg) administration (n = 4, each group).

Table A1.3 Plasma pharmacokinetic parameters obtained from *in-vivo* pharmacokinetic experiments

Parameters	**Intravenous administration (n = 4)**	**Oral administration at fasted state (n = 4)**	**Oral administration at fed state (n = 6)**	**Colonic administration (n = 3)***
Dose (mg/kg)	2	12	12	12
C_0 (ng/mL)	410.8 ± 46.4	-	-	-
C_{max} (ng/mL)	-	149.9 ± 34.8	346.6 ± 50.3**	302.2 ± 37.1
T_{max} (h)	-	4	7	1.5
CL (L/h/kg)	2.9 ± 0.4	-	-	-
V_{ss} (L/kg)	9.9 ± 1.1	-	-	-
$AUC_{0\rightarrow t}$ (h·ng/mL)	673.1 ± 98.1	960.9 ± 231.2	2570.2 ± 382.4**	978.9 ± 143.8
Bioavailability (%)	-	23.8 ± 5.7	63.6 ± 9.5**	24.2 ± 3.6

* Colonic administration was performed by infusion for 1 h through a cannula inserted to the cecum.
** Significantly different compared to oral administration at fasted state (p <0.05).
C_0, concentration extrapolated to time zero; C_{max}, maximum concentration observed; T_{max}, time of maximum concentration observed; $t_{1/2}$, elimination half-life; CL, clearance; V_{ss}, volume of distribution at steady state; $AUC_{0\rightarrow t}$, area under the curve from time zero to the last observed point.

A1.3.2 Deconvolution of plasma concentration-time profiles

Deconvolution of the plasma concentration-time profiles obtained from *in-vivo* oral bioavailability evaluation was performed in order to understand the absorption or input function of DF030263 following oral administration. The results of cumulative input or input rate vs time are shown in **Figure A1.3**. It can be seen from **Figure A1.3A** that the

absorption shows a biphasic input function; the first phase between 0-1 h and the second phase between 2-6 h. This becomes more apparent in **Figure A1.3B** where two peaks are shown from the input rate vs time graph. These results indicated possibility of existence of two absorption windows for DF030263 along the gastrointestinal tract.

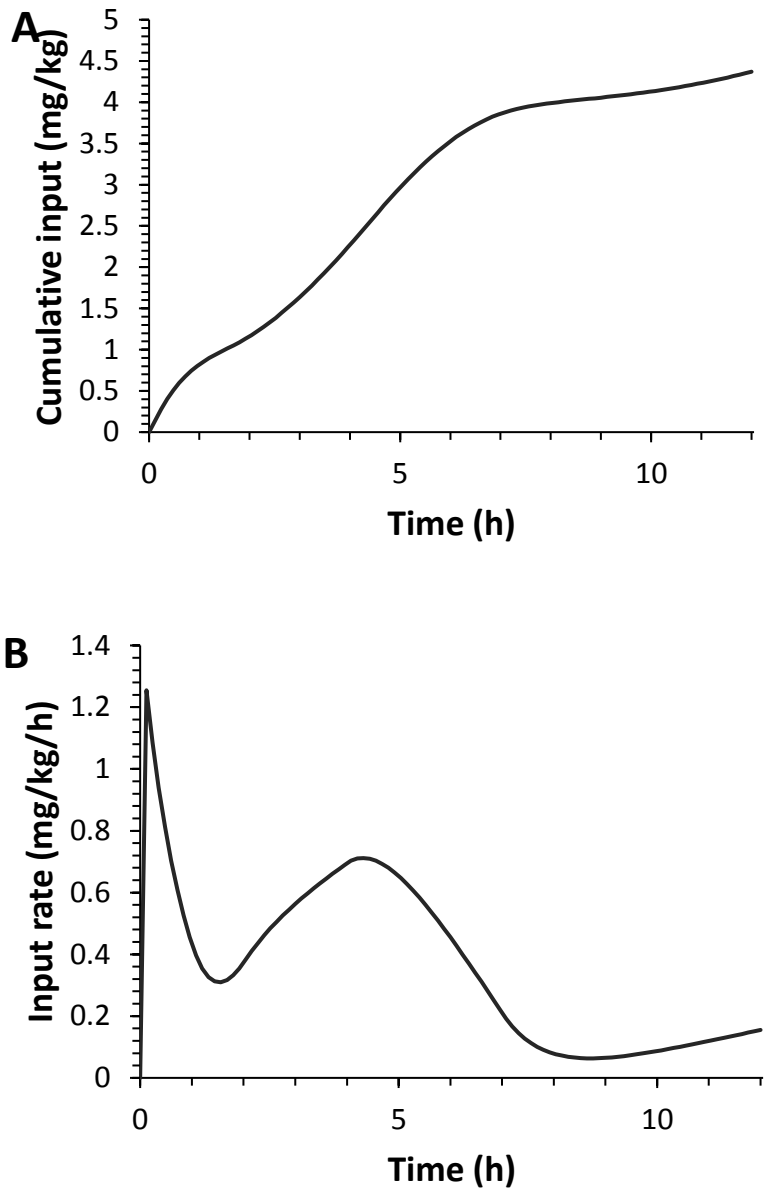

Figure A1.3 Deconvolution results of plasma concentration-time profiles obtained from oral bioavailability evaluation of DF030263. **A**, cumulative input vs time; **B**, input rate vs time.

A1.3.3 *In-vitro* solubility tests

In-vitro solubility tests were conducted with simulated fluids of FaSSGF, FaSSIF and FeSSIF to provide information on solubilization behavior of DF030263 along the gastrointestinal tract. The pH values of these simulated fluids are commonly used to represent the mean pH found in the gastrointestinal tract. However, different pH values are observed in different segments of the gastrointestinal tract *in-vivo* (276-278). Therefore, in this study, the pH of each simulated fluid was adjusted to represent the pH range found *in-vivo* and solubility of DF030263 was tested at each pH level. In general, DF030263 showed higher solubility in acidic environment (**Figure A1.4**). DF030263 exhibited pH-dependent solubility especially in FaSSIF where the solubility decreased steeply when the pH increased above 6.6. This indicated that there could be high probability of precipitation in segments of gastrointestinal tract with higher pH levels. This pH-dependent decrease was less apparent in FeSSIF. Solubility in water was 88.3 ± 2.6 μM.

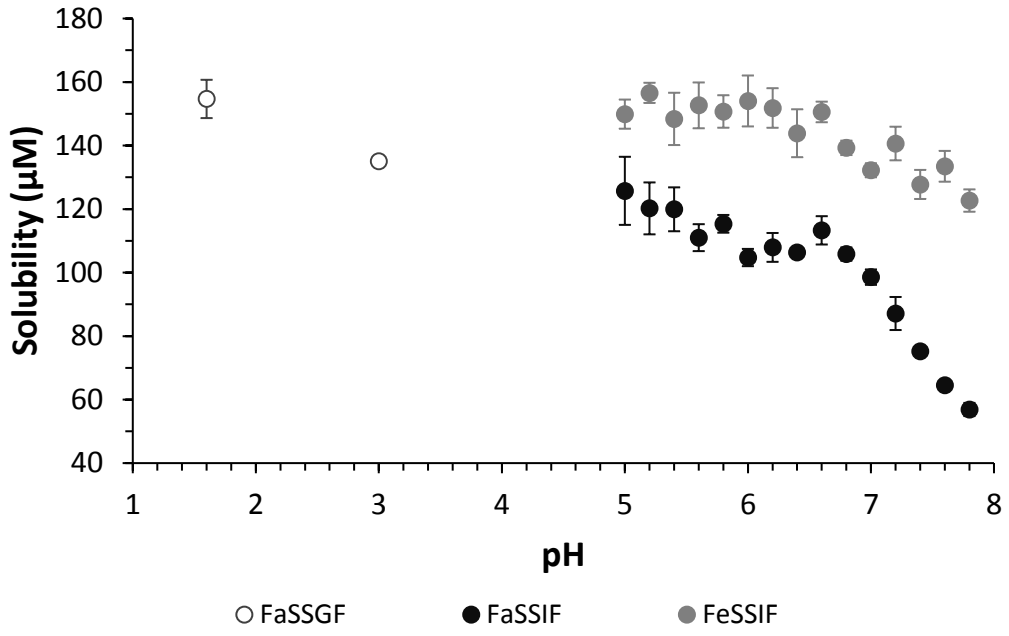

Figure A1.4 Solubility of DF030263 in FaSSGF, FaSSIF and FeSSIF at various pH (n = 3). FaSSGF, fasted state simulated gastric fluid; FaSSIF, fasted state simulated intestinal fluid; FeSSIF, fed state simulated intestinal fluid.

A1.3.4 In silico simulation of intestinal absorption

In silico simulation was performed to predict intestinal absorption of DF030263 *in-vivo*. GastroPlus™ utilizes advanced compartmental absorption and transit (ACAT) model for their intestinal absorption simulation (279), which compartmentalizes the gastrointestinal tract into nine different compartments. Therefore, it was able to predict the fraction of the dose that will be absorbed at the different compartments. The simulation results at both fasted and fed states of the rat are shown in **Figure A1.5**. The results show that DF030263 is predicted to be firstly absorbed at the proximal regions of the small intestine and then has an additional absorption window in the cecum and colon.

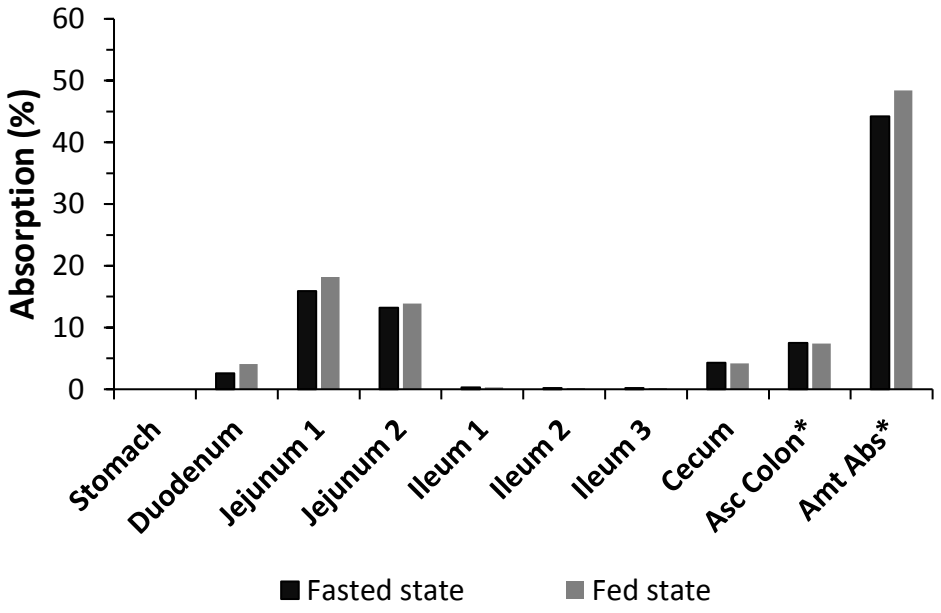

Figure A1.5 *In silico* simulation of intestinal absorption of DF030263 at each compartment of the gastrointestinal tract. *Asc Colon, ascending colon; Amt Abs, total amount absorbed in the gastrointestinal tract.

A1.3.5 Colonic and postprandial administration of DF030263

Following the above results, colonic and postprandial administration of DF030263 were evaluated in order to improve oral bioavailability of DF030263. Colonic administration was delivered by infusion through the cannula inserted to the cecum for 1 h to mimic controlled release of the drug in the large intestine. Postprandial oral gavage administration was performed on rats that had free access to food and water throughout the experiment. The double-peak phenomenon observed after administration by oral gavage at fasted state was not seen in the case of postprandial administration or colonic delivery (**Figure A1.6**). Colonic administration resulted in rapid absorption (T_{max} = 1.5 h) but no improvement in bioavailability was noted (**Table A1.3**). On the other hand, oral administration at fed state resulted in significantly higher C_{max} and bioavailability compared to fasted state.

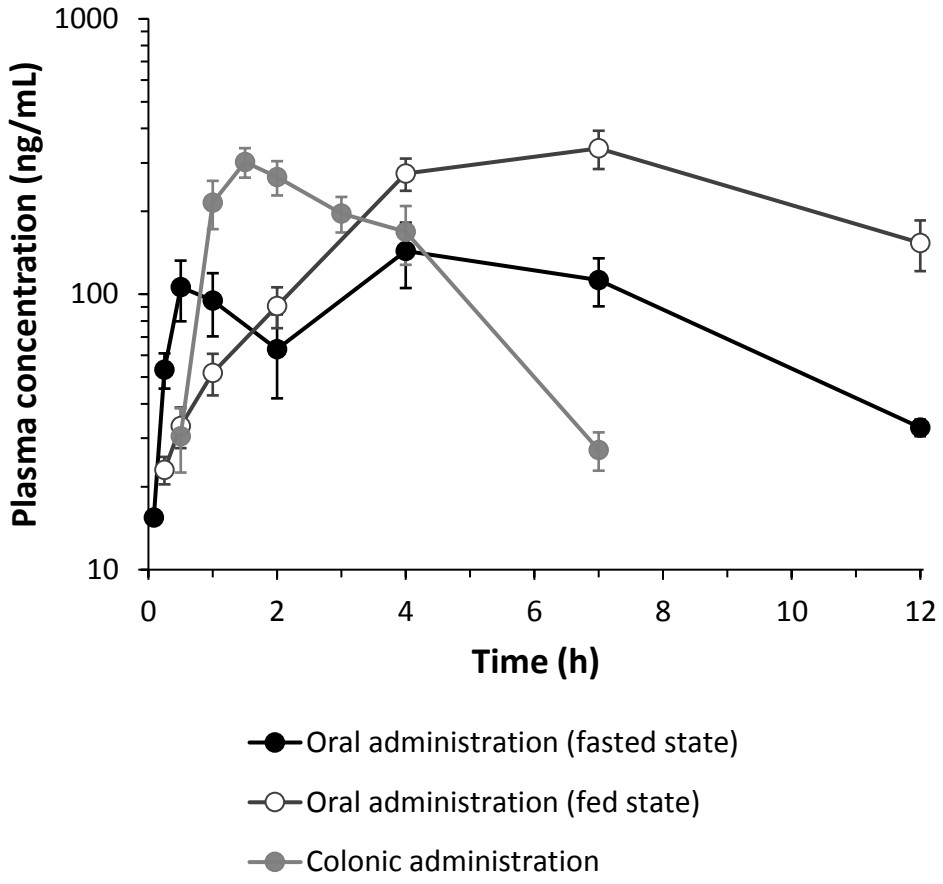

Figure A1.6 Mean plasma concentration-time profiles of DF030263 in rats following oral administration at fed state (12 mg/kg, n = 6) and colonic administration (12 mg/kg, n = 3).

A1.4 DISCUSSION

In the initial *in-vivo* oral bioavailability evaluation, DF030263 showed mean oral bioavailability of 23.8%. Interestingly, a distinct double-peak phenomenon was observed and it only appeared after oral administration of DF030263 (**Figure A1.2**). Similar double-peak phenomenon following oral administration has been reported for a number of drugs including acetaminophen (280), alprazolam (281), cimetidine (282), epinastine (283), furosemide (284), pafenolol (285), ranitidine (286) and veralipride (287). This phenomenon is usually attributed to the following three main causes (281, 286, 288-291): 1) enterohepatic recirculation where the drug in the systemic circulation is secreted via bile and reabsorbed from the gastrointestinal tract; 2) variable absorption properties along the gastrointestinal tract (also called “absorption windows”); 3) gastric emptying time is varied depending on motility of the gastrointestinal tract, gastric pH or the lipidic formulation effect. In all cases, this erratic pattern of absorption can potentially be problematic for CDK9 inhibitors as relatively narrow therapeutic window is known to be one of their potential drawbacks (292).

In the case of DF030263 compound, enterohepatic recirculation was excluded from the possible reasons because the plasma concentration-time profile following intravenous administration did not show a double peak. Variance in gastric emptying time was also unlikely to be the reason because the time between the two peaks was as long as 3-6.5 h. Moreover, all four rats orally administered at fasted state displayed double-peaks. Therefore, absorption window of DF030263 in the gastrointestinal tract was thought to be discontinuous and further studies were conducted to elaborate the two-site absorption windows hypothesis.

Deconvolution of the plasma concentration-time profiles were conducted to elucidate absorption rate over time for DF030263 following oral administration. Deconvolution represents a mathematical process that can inversely uncover the input

function when the oral administration profile is known and drug disposition characteristics are defined by the intravenous administration profile (293). This allows determination of the absorption characteristics which can often be challenging to measure or quantify *in situ* (294). As shown in **Figure A1.3**, the absorption function of DF030263 exhibited a biphasic process which leads to the two-site absorption.

The two-site absorption windows hypothesis was further supported with the results of the *in silico* simulation using GastroPlus^{TM}. The built-in ACAT and generic physiologically-based pharmacokinetic models in the software provide effective predictions of pharmacokinetic profiles in preclinical species and humans (295-298). In this study, intestinal absorption of DF030263 in different compartments of the rat gastrointestinal tract was predicted. The simulation results predicted clear discontinuation of absorption in the distal region of the small intestine and a second absorption window in the large intestine (**Figure A1.5**). Additionally, the secondary absorption phase following oral administration also corresponded to the oral-to-cecal transit time in rats (2-3 h) (285, 299). This corroborated the assumption that a second absorption window exists in the large intestine. Such site-specific absorption of drugs is known to occur due to properties related to solubility, stability or interaction with luminal contents (300).

The luminal pH levels can differ in different segments of the gastrointestinal tract and therefore *in-vitro* solubility tests were carried out in a range of pH using simulated biorelevant media of FaSSGF, FaSSIF and FeSSIF. The solubility of DF030263 was maintained at the highest levels in the acidic environment of FaSSGF and the lower pH ranges of FaSSIF and FeSSIF (**Figure A1.4**). This is explained by the fact that DF030263 is a weak base with a pK_a of 10.7 (predicted by ACD/Labs, Toronto, Canada) and therefore would be solubilized more efficiently in such acidic environment. When the pH level was increased above 6.6, DF030263 showed pH-dependent solubility with decreasing solubility especially in the FaSSIF. This suggested that DF030263 could be precipitating

in the regions of the gastrointestinal tract where the pH is relatively high, such as the distal small intestine. The luminal pH in the rat small intestine increases as it reaches the distal region; from pH 6.5 in the duodenum to 7.1 in the ileum (276). This possibility of precipitation in the small intestine with higher pH has been acknowledged especially for weakly basic compounds and it has been put forward as a critical drug development obstacle, significantly limiting the oral bioavailability of these compounds (301). The luminal pH drops again when it reaches the colon to 6.6 (276), which can provide opportunity for DF030263 to resolubilize and be available for absorption again. The pH-dependent solubility was therefore thought to be the main reason behind the two-site absorption windows. Since humans have a similar luminal pH levels pattern to rats, this phenomenon is likely to occur in humans as well (278).

In order to improve the oral bioavailability of DF030263, the pH-dependent solubility and potential precipitation in the distal region of the small intestine had to be mitigated. Colonic administration mimicking controlled release of DF030263 in the large intestine and postprandial oral administration were tested for this purpose. Deconvolution and *in silico* simulation of the intestinal absorption both indicated a second absorption window in the large intestine. Additionally, when partial area under the curve (AUC) is calculated for the oral administration profile at fasted state, the window between 2-12 h accounts for 86% of the total AUC. With all the above-mentioned factors, colonic administration was thought to possibly improve the bioavailability of DF030263.

Colonic administration was performed via a cannula inserted into the cecum and DF030263 solubilized in the dosing vehicle was infused for 1 h. Therefore, it would not pass through the distal region of the small intestine where the pH is relatively higher and the solubility of DF030263 is lower. Consequently, potential loss in absorption of DF030263 due to the precipitation-resolubilization process can be avoided.

As shown in **Figure A1.6**, colonic administration resulted in rapid absorption and only single peaks were observed in all rats tested. This is consistent with a previous study where pafenolol, which had double-peak following oral administration, showed a single peak when administered through an intraintestinal cannula to target a specific absorption window in the gastrointestinal tract (285). In spite of the single peak, colonic delivery did not improve the bioavailability of DF030263, but it was rather comparable to the oral administration at fasted state (**Table A1.3**). As a result, it was confirmed that the large intestine is indeed an absorption window but oral bioavailability cannot be improved by controlled release to this site. It is likely that the amount of dose that can be absorbed from the large intestine has been already absorbed from simple oral administration.

Postprandial oral administration was also tested mainly based on the premise that solubility is enhanced in fed conditions. The *in-vitro* solubility results in **Figure A1.4** clearly show that in FeSSIF, the solubility was higher and was less dependent on the change of pH. The presence of food in the gastrointestinal tract modifies the luminal contents which leads to changes in pH, buffer capacity and surface tension thereby affecting solubilization of drugs (301). Therefore less precipitation of drugs can be anticipated at fed state especially for weak bases with poor solubility (301) which means that more drug can be available for absorption. Also an important food-effect is the delay in gastric emptying which alters the gastrointestinal transit time (300). This delay can allow the drug to reside longer time at the first absorption window which is the proximal region of the small intestine (**Figure A1.5**).

The plasma concentration-time profile following postprandial oral administration showed a single-peak with substantially improved bioavailability (**Figure A1.6** and **Table A1.3**). Avoidance of the double-peak phenomenon by the food-effect has been previously reported (291, 299) but did not necessarily relate to increase in bioavailability. In the case of DF030263, higher solubility, less precipitation and prolonged exposure to the first

absorption window had significantly positive effects towards improving the oral bioavailability. Delayed gastric emptying had also caused extended absorption phase resulting in T_{max} of 7 h. It is also noteworthy that the variability in the bioavailability was reduced at fed state (**Table A1.3**), which is crucial for drugs such as CDK inhibitors where the narrow therapeutic window is a limitation (292).

To note, there could be interspecies differences between the rats and the humans in the gastrointestinal physiology and luminal contents which might result in different food effects. However, the changes of pH between fasted and fed states are similar between the two species and the rat intestinal fluid has slightly higher concentration of bile salt and phospholipid compared to the FeSSIF (277, 302, 303). Therefore, similar pattern of food effect could be expected in humans although the extent might vary.

A1.5 CONCLUSION

In conclusion, this study demonstrates an *in vitro-in vivo-in silico* approach in improving the oral bioavailability of DF030263, a promising candidate for treatment of CLL. The two-site absorption windows hypothesis was suggested and supported by *in-vitro* and *in-silico* studies following observation of a double-peak phenomenon *in-vivo*. Exploitation of the two-site absorption was attempted in order to improve the bioavailability. Colonic administration confirmed that the large intestine is a second absorption window but indicated that controlled release to the colon would not enhance the drug exposure. Instead, oral administration at fed state took advantage of the food-effect in terms of improved solubilization, reduced precipitation and delayed gastrointestinal transit time, thereby increasing the bioavailability.

REFERENCE

1. Miller KD, Siegel RL, Lin CC, Mariotto AB, Kramer JL, Rowland JH, Stein KD, Alteri R, Jemal A. Cancer treatment and survivorship statistics, 2016. CA Cancer J Clin. 2016;66(4):271-89. doi: 10.3322/caac.21349. PubMed PMID: 27253694.
2. Flatters SJL, Dougherty PM, Colvin LA. Clinical and preclinical perspectives on Chemotherapy-Induced Peripheral Neuropathy (CIPN): a narrative review. Br J Anaesth. 2017;119(4):737-49. doi: 10.1093/bja/aex229. PubMed PMID: 29121279.
3. Torrance N, Lawson KD, Afolabi E, Bennett MI, Serpell MG, Dunn KM, Smith BH. Estimating the burden of disease in chronic pain with and without neuropathic characteristics: does the choice between the EQ-5D and SF-6D matter? Pain. 2014;155(10):1996-2004. doi: 10.1016/j.pain.2014.07.001. PubMed PMID: 25020004; PMCID: PMC4220009.
4. Starobova H, Vetter I. Pathophysiology of Chemotherapy-Induced Peripheral Neuropathy. Front Mol Neurosci. 2017;10:174. doi: 10.3389/fnmol.2017.00174. PubMed PMID: 28620280; PMCID: PMC5450696.
5. Grisold W, Cavaletti G, Windebank AJ. Peripheral neuropathies from chemotherapeutics and targeted agents: diagnosis, treatment, and prevention. Neuro Oncol. 2012;14 Suppl 4:iv45-54. doi: 10.1093/neuonc/nos203. PubMed PMID: 23095830; PMCID: PMC3480245.
6. Seretny M, Currie GL, Sena ES, Ramnarine S, Grant R, MacLeod MR, Colvin LA, Fallon M. Incidence, prevalence, and predictors of chemotherapy-induced peripheral neuropathy: A systematic review and meta-analysis. Pain. 2014;155(12):2461-70. doi: 10.1016/j.pain.2014.09.020. PubMed PMID: 25261162.
7. Fallon MT. Neuropathic pain in cancer. Br J Anaesth. 2013;111(1):105-11. doi: 10.1093/bja/aet208. PubMed PMID: 23794652.
8. Farquhar-Smith P. Chemotherapy-induced neuropathic pain. Curr Opin Support Palliat Care. 2011;5(1):1-7. doi: 10.1097/SPC.0b013e328342f9cc. PubMed PMID: 21192267.
9. Balayssac D, Ferrier J, Descoeur J, Ling B, Pezet D, Eschalier A, Authier N. Chemotherapy-induced peripheral neuropathies: from clinical relevance to preclinical evidence. Expert Opin Drug Saf. 2011;10(3):407-17. doi: 10.1517/14740338.2011.543417. PubMed PMID: 21210753.
10. Han Y, Smith MT. Pathobiology of cancer chemotherapy-induced peripheral neuropathy (CIPN). Front Pharmacol. 2013;4:156. doi: 10.3389/fphar.2013.00156. PubMed PMID: 24385965; PMCID: PMC3866393.
11. Gutierrez-Gutierrez G, Sereno M, Miralles A, Casado-Saenz E, Gutierrez-Rivas E. Chemotherapy-induced peripheral neuropathy: clinical features, diagnosis, prevention and treatment strategies. Clin Transl Oncol. 2010;12(2):81-91. doi: 10.1007/S12094-010-0474-z. PubMed PMID: 20156778.
12. Pike CT, Birnbaum HG, Muehlenbein CE, Pohl GM, Natale RB. Healthcare costs and workloss burden of patients with chemotherapy-associated peripheral neuropathy in breast, ovarian, head and neck, and nonsmall cell lung cancer. Chemother Res Pract. 2012;2012:913848. doi: 10.1155/2012/913848. PubMed PMID: 22482054; PMCID: PMC3312207.
13. Hershman DL, Lacchetti C, Dworkin RH, Lavoie Smith EM, Bleeker J, Cavaletti G, Chauhan C, Gavin P, Lavino A, Lustberg MB, Paice J, Schneider B, Smith ML, Smith T, Terstriep S, Wagner-Johnston N, Bak K, Loprinzi CL, American Society of Clinical O. Prevention and management of chemotherapy-induced peripheral neuropathy in survivors

of adult cancers: American Society of Clinical Oncology clinical practice guideline. J Clin Oncol. 2014;32(18):1941-67. doi: 10.1200/JCO.2013.54.0914. PubMed PMID: 24733808.
14. Albers JW, Chaudhry V, Cavaletti G, Donehower RC. Interventions for preventing neuropathy caused by cisplatin and related compounds. Cochrane Database Syst Rev. 2011(2):CD005228. doi: 10.1002/14651858.CD005228.pub3. PubMed PMID: 21328275; PMCID: PMC3715044.
15. Tsavaris N, Kopterides P, Kosmas C, Efthymiou A, Skopelitis H, Dimitrakopoulos A, Pagouni E, Pikazis D, Zis PV, Koufos C. Gabapentin monotherapy for the treatment of chemotherapy-induced neuropathic pain: a pilot study. Pain Med. 2008;9(8):1209-16. doi: 10.1111/j.1526-4637.2007.00325.x. PubMed PMID: 19067834.
16. Rao RD, Michalak JC, Sloan JA, Loprinzi CL, Soori GS, Nikcevich DA, Warner DO, Novotny P, Kutteh LA, Wong GY, North Central Cancer Treatment G. Efficacy of gabapentin in the management of chemotherapy-induced peripheral neuropathy: a phase 3 randomized, double-blind, placebo-controlled, crossover trial (N00C3). Cancer. 2007;110(9):2110-8. doi: 10.1002/cncr.23008. PubMed PMID: 17853395.
17. Rao RD, Flynn PJ, Sloan JA, Wong GY, Novotny P, Johnson DB, Gross HM, Renno SI, Nashawaty M, Loprinzi CL. Efficacy of lamotrigine in the management of chemotherapy-induced peripheral neuropathy: a phase 3 randomized, double-blind, placebo-controlled trial, N01C3. Cancer. 2008;112(12):2802-8. doi: 10.1002/cncr.23482. PubMed PMID: 18428211.
18. Kautio AL, Haanpaa M, Saarto T, Kalso E. Amitriptyline in the treatment of chemotherapy-induced neuropathic symptoms. J Pain Symptom Manage. 2008;35(1):31-9. doi: 10.1016/j.jpainsymman.2007.02.043. PubMed PMID: 17980550.
19. Hammack JE, Michalak JC, Loprinzi CL, Sloan JA, Novotny PJ, Soori GS, Tirona MT, Rowland KM, Jr., Stella PJ, Johnson JA. Phase III evaluation of nortriptyline for alleviation of symptoms of cis-platinum-induced peripheral neuropathy. Pain. 2002;98(1-2):195-203. PubMed PMID: 12098632.
20. Anand P, Bley K. Topical capsaicin for pain management: therapeutic potential and mechanisms of action of the new high-concentration capsaicin 8% patch. Br J Anaesth. 2011;107(4):490-502. doi: 10.1093/bja/aer260. PubMed PMID: 21852280; PMCID: PMC3169333.
21. Coutaux A, Adam F, Willer JC, Le Bars D. Hyperalgesia and allodynia: peripheral mechanisms. Joint Bone Spine. 2005;72(5):359-71. doi: 10.1016/j.jbspin.2004.01.010. PubMed PMID: 16214069.
22. Dubner R. Pain research in animals. Ann N Y Acad Sci. 1983;406:128-32. PubMed PMID: 6410957.
23. Kaplow R, Iyere K. Grading chemotherapy-induced peripheral neuropathy in adults. Nursing. 2017;47(2):67-8. doi: 10.1097/01.NURSE.0000511823.41645.a1. PubMed PMID: 28121792.
24. Mogil JS. Animal models of pain: progress and challenges. Nat Rev Neurosci. 2009;10(4):283-94. doi: 10.1038/nrn2606. PubMed PMID: 19259101.
25. Sandkuhler J. Models and mechanisms of hyperalgesia and allodynia. Physiol Rev. 2009;89(2):707-58. doi: 10.1152/physrev.00025.2008. PubMed PMID: 19342617.
26. Deuis JR, Dvorakova LS, Vetter I. Methods Used to Evaluate Pain Behaviors in Rodents. Front Mol Neurosci. 2017;10:284. doi: 10.3389/fnmol.2017.00284. PubMed PMID: 28932184; PMCID: PMC5592204.
27. Hargreaves K, Dubner R, Brown F, Flores C, Joris J. A new and sensitive method for measuring thermal nociception in cutaneous hyperalgesia. Pain. 1988;32(1):77-88. PubMed PMID: 3340425.

28. Banik RK, Kabadi RA. A modified Hargreaves' method for assessing threshold temperatures for heat nociception. J Neurosci Methods. 2013;219(1):41-51. doi: 10.1016/j.jneumeth.2013.06.005. PubMed PMID: 23796910; PMCID: PMC3759573.
29. Ugo Basile Von Frey Plantar Aesthesiometer 2018 [cited 2018 09.09]. Available from: https://glo-bio.com/index.php?route=product/product&product_id=111.
30. Plantar test (Hargreaves apparatus) [cited 2018 09.09]. Available from: http://www.lintoninst.co.uk/Products/tabid/63/ProdID/267/Language/en-US/CatID/85/37370__Plantar_Test_Hargreaves_Apparatus.aspx.
31. Argyriou AA, Kyritsis AP, Makatsoris T, Kalofonos HP. Chemotherapy-induced peripheral neuropathy in adults: a comprehensive update of the literature. Cancer Manag Res. 2014;6:135-47. doi: 10.2147/CMAR.S44261. PubMed PMID: 24672257; PMCID: PMC3964029.
32. Rowinsky EK, Donehower RC. The clinical pharmacology of paclitaxel (Taxol). Seminars in oncology. 1993;20(4 Suppl 3):16-25. Epub 1993/08/01. PubMed PMID: 8102014.
33. Wani MC, Taylor HL, Wall ME, Coggon P, McPhail AT. Plant antitumor agents. VI. The isolation and structure of taxol, a novel antileukemic and antitumor agent from Taxus brevifolia. J Am Chem Soc. 1971;93(9):2325-7. Epub 1971/05/05. PubMed PMID: 5553076.
34. Singla AK, Garg A, Aggarwal D. Paclitaxel and its formulations. Int J Pharm. 2002;235:179-92.
35. Mathew AE, Mejillano MR, Nath JP, Himes RH, Stella VJ. Synthesis and evaluation of some water-soluble prodrugs and derivatives of taxol with antitumor activity. J Med Chem. 1992;35(1):145-51. PubMed PMID: 1346275.
36. Ringel I, Horwitz SB. Studies with RP 56976 (taxotere): a semisynthetic analogue of taxol. Journal of the National Cancer Institute. 1991;83(4):288-91. PubMed PMID: 1671606.
37. Swindell CS, Krauss NE, Horwitz SB, Ringel I. Biologically active taxol analogues with deleted A-ring side chain substituents and variable C-2' configurations. J Med Chem. 1991;34(3):1176-84. PubMed PMID: 1672157.
38. Tarr BD, Yalkowsky SH. A new parenteral vehicle for the administration of some poorly water soluble anti-cancer drugs. J Parenter Sci Technol. 1987;41(1):31-3. PubMed PMID: 3559832.
39. TAXOL® (paclitaxel) INJECTION [package insert] [Internet]. Bristol-Myers Squibb Company. 2011.
40. Lexicomp online, Hudson, Ohio: Lexi-Comp, Inc.; 2013; January 29, 2017.
41. Gelderblom H, Verweij J, Nooter K, Sparreboom A. Cremophor EL: the drawbacks and advantages of vehicle selection for drug formulation. Eur J Cancer. 2001;37(13):1590-8. PubMed PMID: 11527683.
42. Speck RM, Sammel MD, Farrar JT, Hennessy S, Mao JJ, Stineman MG, DeMichele A. Impact of chemotherapy-induced peripheral neuropathy on treatment delivery in nonmetastatic breast cancer. J Oncol Pract. 2013;9(5):e234-40. doi: 10.1200/JOP.2012.000863. PubMed PMID: 23943894.
43. Boulikas T. Clinical overview on lipoplatin: a successful liposomal formulation of cisplatin. Expert Opin Investig Drugs. 2009;18(8):1197-218.
44. PLATINOL® (cisplatin for injection, USP) [package insert] [Internet]. Bristol-Myers Squibb Company. 2010.
45. Caglar K, Kinalp C, Arpaci F, Turan M, Saglam K, Ozturk B, Komurcu S, Yavuz I, Yenicesu M, Ozet A, Vural A. Cumulative prior dose of cisplatin as a cause of the nephrotoxicity of high-dose chemotherapy followed by autologous stem-cell transplantation. Nephrol Dial Transplant. 2002;17(11):1931-5. PubMed PMID: 12401849.

46. van der Hoop RG, van der Burg ME, ten Bokkel Huinink WW, van Houwelingen C, Neijt JP. Incidence of neuropathy in 395 patients with ovarian cancer treated with or without cisplatin. Cancer. 1990;66(8):1697-702. PubMed PMID: 2119878.
47. Argyriou AA, Bruna J, Marmiroli P, Cavaletti G. Chemotherapy-induced peripheral neurotoxicity (CIPN): an update. Crit Rev Oncol Hematol. 2012;82(1):51-77. doi: 10.1016/j.critrevonc.2011.04.012. PubMed PMID: 21908200.
48. Glendenning JL, Barbachano Y, Norman AR, Dearnaley DP, Horwich A, Huddart RA. Long-term neurologic and peripheral vascular toxicity after chemotherapy treatment of testicular cancer. Cancer. 2010;116(10):2322-31. doi: 10.1002/cncr.24981. PubMed PMID: 20225230.
49. Roelofs RI, Hrushesky W, Rogin J, Rosenberg L. Peripheral sensory neuropathy and cisplatin chemotherapy. Neurology. 1984;34(7):934-8. PubMed PMID: 6330613.
50. Dorr RT. Pharmacology of the taxanes. Pharmacotherapy. 1997;17(5 Pt 2):96S-104S. PubMed PMID: 9322876.
51. Dasari S, Tchounwou PB. Cisplatin in cancer therapy: molecular mechanisms of action. Eur J Pharmacol. 2014;740:364-78. doi: 10.1016/j.ejphar.2014.07.025. PubMed PMID: 25058905; PMCID: PMC4146684.
52. Bennett GJ, Liu GK, Xiao WH, Jin HW, Siau C. Terminal arbor degeneration--a novel lesion produced by the antineoplastic agent paclitaxel. Eur J Neurosci. 2011;33(9):1667-76. doi: 10.1111/j.1460-9568.2011.07652.x. PubMed PMID: 21395870; PMCID: PMC3086946.
53. Boehmerle W, Huehnchen P, Peruzzaro S, Balkaya M, Endres M. Electrophysiological, behavioral and histological characterization of paclitaxel, cisplatin, vincristine and bortezomib-induced neuropathy in C57Bl/6 mice. Sci Rep. 2014;4:6370. doi: 10.1038/srep06370. PubMed PMID: 25231679; PMCID: PMC5377307.
54. Boyette-Davis JA, Cata JP, Driver LC, Novy DM, Bruel BM, Mooring DL, Wendelschafer-Crabb G, Kennedy WR, Dougherty PM. Persistent chemoneuropathy in patients receiving the plant alkaloids paclitaxel and vincristine. Cancer Chemother Pharmacol. 2013;71(3):619-26. doi: 10.1007/s00280-012-2047-z. PubMed PMID: 23228992; PMCID: PMC3581748.
55. Cavaletti G, Tredici G, Marmiroli P, Petruccioli MG, Barajon I, Fabbrica D. Morphometric study of the sensory neuron and peripheral nerve changes induced by chronic cisplatin (DDP) administration in rats. Acta Neuropathol. 1992;84(4):364-71. PubMed PMID: 1441917.
56. Sahenk Z, Barohn R, New P, Mendell JR. Taxol neuropathy. Electrodiagnostic and sural nerve biopsy findings. Arch Neurol. 1994;51(7):726-9. PubMed PMID: 7912506.
57. Amos LA, Lowe J. How Taxol stabilises microtubule structure. Chem Biol. 1999;6(3):R65-9. PubMed PMID: 10074470.
58. Kavallaris M. Microtubules and resistance to tubulin-binding agents. Nat Rev Cancer. 2010;10(3):194-204. doi: 10.1038/nrc2803. PubMed PMID: 20147901.
59. Shemesh OA, Spira ME. Paclitaxel induces axonal microtubules polar reconfiguration and impaired organelle transport: implications for the pathogenesis of paclitaxel-induced polyneuropathy. Acta Neuropathol. 2010;119(2):235-48. doi: 10.1007/s00401-009-0586-0. PubMed PMID: 19727778.
60. Flatters SJ, Bennett GJ. Studies of peripheral sensory nerves in paclitaxel-induced painful peripheral neuropathy: evidence for mitochondrial dysfunction. Pain. 2006;122(3):245-57. doi: 10.1016/j.pain.2006.01.037. PubMed PMID: 16530964; PMCID: PMC1805481.
61. Jin HW, Flatters SJ, Xiao WH, Mulhern HL, Bennett GJ. Prevention of paclitaxel-evoked painful peripheral neuropathy by acetyl-L-carnitine: effects on axonal mitochondria, sensory nerve fiber terminal arbors, and cutaneous Langerhans cells. Exp Neurol.

2008;210(1):229-37. doi: 10.1016/j.expneurol.2007.11.001. PubMed PMID: 18078936; PMCID: PMC2323600.
62. Thompson SW, Davis LE, Kornfeld M, Hilgers RD, Standefer JC. Cisplatin neuropathy. Clinical, electrophysiologic, morphologic, and toxicologic studies. Cancer. 1984;54(7):1269-75. PubMed PMID: 6088023.
63. Look MP, Musch E. Lipid peroxides in the polychemotherapy of cancer patients. Chemotherapy. 1994;40(1):8-15. doi: 10.1159/000239163. PubMed PMID: 8306820.
64. McDonald ES, Windebank AJ. Cisplatin-induced apoptosis of DRG neurons involves bax redistribution and cytochrome c release but not fas receptor signaling. Neurobiol Dis. 2002;9(2):220-33. doi: 10.1006/nbdi.2001.0468. PubMed PMID: 11895373.
65. Sangeetha P, Das UN, Koratkar R, Suryaprabha P. Increase in free radical generation and lipid peroxidation following chemotherapy in patients with cancer. Free Radic Biol Med. 1990;8(1):15-9. PubMed PMID: 2157633.
66. Weijl NI, Hopman GD, Wipkink-Bakker A, Lentjes EG, Berger HM, Cleton FJ, Osanto S. Cisplatin combination chemotherapy induces a fall in plasma antioxidants of cancer patients. Ann Oncol. 1998;9(12):1331-7. PubMed PMID: 9932164.
67. Canta A, Pozzi E, Carozzi VA. Mitochondrial Dysfunction in Chemotherapy-Induced Peripheral Neuropathy (CIPN). Toxics. 2015;3(2):198-223. doi: 10.3390/toxics3020198. PubMed PMID: 29056658; PMCID: PMC5634687.
68. Doyle T, Chen Z, Muscoli C, Bryant L, Esposito E, Cuzzocrea S, Dagostino C, Ryerse J, Rausaria S, Kamadulski A, Neumann WL, Salvemini D. Targeting the overproduction of peroxynitrite for the prevention and reversal of paclitaxel-induced neuropathic pain. J Neurosci. 2012;32(18):6149-60. doi: 10.1523/JNEUROSCI.6343-11.2012. PubMed PMID: 22553021; PMCID: PMC3752044.
69. Xiao WH, Bennett GJ. Effects of mitochondrial poisons on the neuropathic pain produced by the chemotherapeutic agents, paclitaxel and oxaliplatin. Pain. 2012;153(3):704-9. doi: 10.1016/j.pain.2011.12.011. PubMed PMID: 22244441; PMCID: PMC3288606.
70. Carozzi VA, Canta A, Chiorazzi A. Chemotherapy-induced peripheral neuropathy: What do we know about mechanisms? Neurosci Lett. 2015;596:90-107. doi: 10.1016/j.neulet.2014.10.014. PubMed PMID: 25459280.
71. Kidd JF, Pilkington MF, Schell MJ, Fogarty KE, Skepper JN, Taylor CW, Thorn P. Paclitaxel affects cytosolic calcium signals by opening the mitochondrial permeability transition pore. The Journal of biological chemistry. 2002;277(8):6504-10. doi: 10.1074/jbc.M106802200. PubMed PMID: 11724773.
72. Mironov SL, Ivannikov MV, Johansson M. [Ca2+]i signaling between mitochondria and endoplasmic reticulum in neurons is regulated by microtubules. From mitochondrial permeability transition pore to Ca2+-induced Ca2+ release. The Journal of biological chemistry. 2005;280(1):715-21. doi: 10.1074/jbc.M409819200. PubMed PMID: 15516333.
73. Nieto FR, Entrena JM, Cendan CM, Pozo ED, Vela JM, Baeyens JM. Tetrodotoxin inhibits the development and expression of neuropathic pain induced by paclitaxel in mice. Pain. 2008;137(3):520-31. doi: 10.1016/j.pain.2007.10.012. PubMed PMID: 18037242.
74. Leo M, Schmitt LI, Erkel M, Melnikova M, Thomale J, Hagenacker T. Cisplatin-induced neuropathic pain is mediated by upregulation of N-type voltage-gated calcium channels in dorsal root ganglion neurons. Exp Neurol. 2017;288:62-74. doi: 10.1016/j.expneurol.2016.11.003. PubMed PMID: 27823926.
75. Tomaszewski A, Busselberg D. Cisplatin modulates voltage gated channel currents of dorsal root ganglion neurons of rats. Neurotoxicology. 2007;28(1):49-58. doi: 10.1016/j.neuro.2006.07.005. PubMed PMID: 16945417.
76. Feng SS, Chien S. Chemotherapeutic engineering: Application and further development of chemical engineering principles for chemotherapy of cancer and other

diseases. Chem Eng Sci. 2003;58(18):4087-114. doi: 10.1016/S0009-2509(03)00234-3. PubMed PMID: WOS:000185375200001.
77. Maeda H. The enhanced permeability and retention (EPR) effect in tumor vasculature: the key role of tumor-selective macromolecular drug targeting. Adv Enzyme Regul. 2001;41:189-207. PubMed PMID: 11384745.
78. Jing S, qiang Z. Advances in the formulation and delivery technology of paclitaxel for injection. Journal of Chinese Pharmaceutical Sciences. 2015;24(8). doi: 10.5246/jcps.2015.08.063.
79. Park K, Lee S, Kang E, Kim K, Choi K, Kwon IC. New Generation of Multifunctional Nanoparticles for Cancer Imaging and Therapy. Advanced Functional Materials. 2009;19(10):1553-66. doi: 10.1002/adfm.200801655. PubMed PMID: WOS:000266626100007.
80. Wang X, Yang L, Chen ZG, Shin DM. Application of nanotechnology in cancer therapy and imaging. CA Cancer J Clin. 2008;58(2):97-110. doi: 10.3322/CA.2007.0003. PubMed PMID: 18227410.
81. De Jong WH, Borm PJ. Drug delivery and nanoparticles:applications and hazards. Int J Nanomedicine. 2008;3(2):133-49. PubMed PMID: 18686775; PMCID: PMC2527668.
82. Jones A, Harris AL. New developments in angiogenesis: a major mechanism for tumor growth and target for therapy. Cancer J Sci Am. 1998;4(4):209-17. PubMed PMID: 9689977.
83. Lasic DD. Novel applications of liposomes. Trends Biotechnol. 1998;16(7):307-21. PubMed PMID: 9675915.
84. Drummond DC, Meyer O, Hong K, Kirpotin DB, Papahadjopoulos D. Optimizing liposomes for delivery of chemotherapeutic agents to solid tumors. Pharmacol Rev. 1999;51(4):691-743. PubMed PMID: 10581328.
85. Gregoriadis G. Overview of liposomes. J Antimicrob Chemother. 1991;28 Suppl B:39-48. PubMed PMID: 1778891.
86. Medina OP, Zhu Y, Kairemo K. Targeted liposomal drug delivery in cancer. Curr Pharm Des. 2004;10(24):2981-9. PubMed PMID: 15379663.
87. Alexis F, Pridgen E, Molnar LK, Farokhzad OC. Factors affecting the clearance and biodistribution of polymeric nanoparticles. Mol Pharm. 2008;5(4):505-15. doi: 10.1021/mp800051m. PubMed PMID: 18672949; PMCID: PMC2663893.
88. Storm G, Belliot SO, Daemen T, Lasic DD. Surface Modification of Nanoparticles to Oppose Uptake by the Mononuclear Phagocyte System. Advanced Drug Delivery Reviews. 1995;17(1):31-48. doi: Doi 10.1016/0169-409x(95)00039-A. PubMed PMID: WOS:A1995TH26500004.
89. Owens DE, 3rd, Peppas NA. Opsonization, biodistribution, and pharmacokinetics of polymeric nanoparticles. Int J Pharm. 2006;307(1):93-102. doi: 10.1016/j.ijpharm.2005.10.010. PubMed PMID: 16303268.
90. Bulbake U, Doppalapudi S, Kommineni N, Khan W. Liposomal Formulations in Clinical Use: An Updated Review. Pharmaceutics. 2017;9(2). doi: 10.3390/pharmaceutics9020012. PubMed PMID: 28346375; PMCID: PMC5489929.
91. Gill PS, Espina BM, Muggia F, Cabriales S, Tulpule A, Esplin JA, Liebman HA, Forssen E, Ross ME, Levine AM. Phase I/II clinical and pharmacokinetic evaluation of liposomal daunorubicin. J Clin Oncol. 1995;13(4):996-1003. doi: 10.1200/JCO.1995.13.4.996. PubMed PMID: 7707129.
92. Schmidt PG, Adler-Moore JP, Forssen E, Profitt R. Medical Applications of Liposomes. In: Lasic DD, Papahadjopoulos D, editors.: Elsevier; 1998. p. 703-31.
93. Lasic DD, Needham D. The "Stealth" liposome: A prototypical biomaterial. Chemical Reviews. 1995;95(8):2601-28. doi: DOI 10.1021/cr00040a001. PubMed PMID: WOS:A1995TL94500001.

94. Kuhl TL, Leckband DE, Lasic DD, Israelachvili JN. Modulation of interaction forces between bilayers exposing short-chained ethylene oxide headgroups. Biophys J. 1994;66(5):1479-88. doi: 10.1016/S0006-3495(94)80938-5. PubMed PMID: 8061197; PMCID: PMC1275868.
95. Lasic DD. Doxorubicin in sterically stabilized liposomes. Nature. 1996;380(6574):561-2. doi: 10.1038/380561a0. PubMed PMID: 8606781.
96. Xu X, Wang L, Xu HQ, Huang XE, Qian YD, Xiang J. Clinical comparison between paclitaxel liposome (Lipusu(R)) and paclitaxel for treatment of patients with metastatic gastric cancer. Asian Pac J Cancer Prev. 2013;14(4):2591-4. PubMed PMID: 23725180.
97. Fetterly GJ, Grasela TH, Sherman JW, Dul JL, Grahn A, Lecomte D, Fiedler-Kelly J, Damjanov N, Fishman M, Kane MP, Rubin EH, Tan AR. Pharmacokinetic/pharmacodynamic modeling and simulation of neutropenia during phase I development of liposome-entrapped paclitaxel. Clin Cancer Res. 2008;14(18):5856-63. doi: 10.1158/1078-0432.CCR-08-1046. PubMed PMID: 18794097.
98. Fasol U, Frost A, Buchert M, Arends J, Fiedler U, Scharr D, Scheuenpflug J, Mross K. Vascular and pharmacokinetic effects of EndoTAG-1 in patients with advanced cancer and liver metastasis. Ann Oncol. 2012;23(4):1030-6. doi: 10.1093/annonc/mdr300. PubMed PMID: 21693769.
99. Matsumura Y, Maeda H. A new concept for macromolecular therapeutics in cancer chemotherapy: mechanism of tumouritropic accumulation of proteins and the antitumour agent smancs. Cancer Res. 1986;46:6387 - 92.
100. Celia C, Cosco D, Paolino D, Fresta M. Gemcitabine-loaded innovative nanocarriers vs GEMZAR: biodistribution, pharmacokinetic features and in vivo antitumor activity. Expert Opin Drug Deliv. 2011;8(12):1609-29. doi: 10.1517/17425247.2011.632630. PubMed PMID: 22077480.
101. Rizzo J, Riley C, von Hoff D, Kuhn J, Phillips J, Brown T. Analysis of anticancer drugs in biological fluids: determination of taxol with application to clinical pharmacokinetics. Journal of pharmaceutical and biomedical analysis. 1990;8(2):159-64. Epub 1990/01/01. PubMed PMID: 1982732.
102. Rowinsky EK, Cazenave LA, Donehower RC. Taxol: a novel investigational antimicrotubule agent. Journal of the National Cancer Institute. 1990;82(15):1247-59. Epub 1990/08/01. PubMed PMID: 1973737.
103. Wiernik PH, Schwartz EL, Einzig A, Strauman JJ, Lipton RB, Dutcher JP. Phase I trial of taxol given as a 24-hour infusion every 21 days: responses observed in metastatic melanoma. J Clin Oncol. 1987;5(8):1232-9. Epub 1987/08/01. doi: 10.1200/jco.1987.5.8.1232. PubMed PMID: 2887641.
104. Walle T, Walle UK, Kumar GN, Bhalla KN. Taxol metabolism and disposition in cancer patients. Drug Metab Dispos. 1995;23(4):560-12.
105. Farris FF, Dedrick RL, King FG. Cisplatin pharmacokinetics: applications of a physiological model. Toxicol Lett. 1988;43:117-37.
106. Farris FF, King FG, Dedrick RL, Litterst CL. Phsiological model for the pharmacokinetics of cis-dichlorodiammineplatinum(II) (DDP) in the tumored rat. J Pharmcokinet Biopharm. 1985;13(1):13-39.
107. Gibaldi M, Perrier D. Pharmacokinetics. 2nd ed. New York, NY, USA: Marcel Dekker, Inc.; 1982.
108. Gillespie WR. Noncompartmental versus compartmental modelling in clinical pharmacokinetics. Clin Pharmacokinet. 1991;20(4):253-62. doi: 10.2165/00003088-199120040-00001. PubMed PMID: 2036746.
109. Yamaoka K, Nakagawa T, Uno T. Statistical moments in pharmacokinetics. J Pharmacokinet Biopharm. 1978;6(6):547-58. PubMed PMID: 731417.

110. Rowland Yeo K, Aarabi M, Jamei M, Rostami-Hodjegan A. Modeling and predicting drug pharmacokinetics in patients with renal impairment. Expert Rev Clin Pharmacol. 2011;4(2):261-74. doi: 10.1586/ecp.10.143. PubMed PMID: 22115405.
111. Berezhkovskiy LM. Determination of volume of distribution at steady state with complete consideration of the kinetics of protein and tissue binding in linear pharmacokinetics. J Pharm Sci. 2004;93(2):364-74. doi: 10.1002/jps.10539. PubMed PMID: 14705193.
112. Poulin P, Theil FP. Prediction of pharmacokinetics prior to in vivo studies. 1. Mechanism-based prediction of volume of distribution. J Pharm Sci. 2002;91(1):129-56. PubMed PMID: 11782904.
113. Rodgers T, Rowland M. Mechanistic approaches to volume of distribution predictions: understanding the processes. Pharm Res. 2007;24(5):918-33. doi: 10.1007/s11095-006-9210-3. PubMed PMID: 17372687.
114. Huang SM, Abernethy DR, Wang Y, Zhao P, Zineh I. The utility of modeling and simulation in drug development and regulatory review. J Pharm Sci. 2013;102(9):2912-23. doi: 10.1002/jps.23570. PubMed PMID: 23712632.
115. Guideline for industry. Drug interaction studies - study design, data analysis, implications, for dosing, and labeling recommendations: Food and Drug Administration, US. Department of Health and Human Services; 2012 [09.01.2018]. Available from: http://www.fda.gov/downloads/Drugs/GuidanceComplianceRegulatoryInformation/Guidances/ucm292362.pdf.
116. Guideline on the qualification and reporting of physiologically based pharmacokinetic (PBPK) modelling and simulation: European Medicines Agency; 2016 [cited 2018 09.01.2018]. Available from: http://www.ema.europa.eu/docs/en_GB/document_library/Scientific_guideline/2016/07/WC500211315.pdf.
117. Jones H, Rowland-Yeo K. Basic concepts in physiologically based pharmacokinetic modeling in drug discovery and development. CPT Pharmacometrics Syst Pharmacol. 2013;2:e63. doi: 10.1038/psp.2013.41. PubMed PMID: 23945604; PMCID: PMC3828005.
118. Jones HM, Gardner IB, Collard WT, Stanley PJ, Oxley P, Hosea NA, Plowchalk D, Gernhardt S, Lin J, Dickins M, Rahavendran SR, Jones BC, Watson KJ, Pertinez H, Kumar V, Cole S. Simulation of human intravenous and oral pharmacokinetics of 21 diverse compounds using physiologically based pharmacokinetic modelling. Clin Pharmacokinet. 2011;50(5):331-47. doi: 10.2165/11539680-000000000-00000. PubMed PMID: 21456633.
119. Jones HM, Parrott N, Jorga K, Lave T. A novel strategy for physiologically based predictions of human pharmacokinetics. Clin Pharmacokinet. 2006;45(5):511-42. doi: 10.2165/00003088-200645050-00006. PubMed PMID: 16640456.
120. Brown RP, Delp MD, Lindstedt SL, Rhomberg LR, Beliles RP. Physiological parameter values for physiologically based pharmacokinetic models. Toxicol Ind Health. 1997;13(4):407-84.
121. Davies B, Morris T. Physiological parameters in laboratory animals and humans. Pharm Res. 1993;10(7):1093-5.
122. Gerlowski LE, Jain RK. Physiologically based pharmacokinetic modeling: principles and application. J Pharm Sci. 1983;72(10):1103-27.
123. Mahmood I, Sahajwalla C. Interspecies scaling of biliary excreted drugs. J Pharm Sci. 2002;91(8):1908-14. doi: 10.1002/jps.10174. PubMed PMID: 12115817.
124. Paine SW, Menochet K, Denton R, McGinnity DF, Riley RJ. Prediction of human renal clearance from preclinical species for a diverse set of drugs that exhibit both active secretion and net reabsorption. Drug Metab Dispos. 2011;39(6):1008-13. doi: 10.1124/dmd.110.037267. PubMed PMID: 21357702.

125. Rowland M, Peck C, Tucker G. Physiologically-based pharmacokinetics in drug development and regulatory science. Annual review of pharmacology and toxicology. 2011;51:45-73. Epub 2010/09/22. doi: 10.1146/annurev-pharmtox-010510-100540. PubMed PMID: 20854171.
126. Abdel-Rahman SM, Kauffman RE. The integration of pharmacokinetics and pharmacodynamics: understanding dose-response. Annual review of pharmacology and toxicology. 2004;44:111-36. doi: 10.1146/annurev.pharmtox.44.101802.121347. PubMed PMID: 14744241.
127. Gabrielsson J, Weiner D. Pharmacokinetic and pharmacodynamic data analysis: concentps and applications. 5th edition ed. Stockholm, Sweden: Apotekarsocieteten; 2016.
128. Sheiner LB, Stanski DR, Vozeh S, Miller RD, Ham J. Simultaneous modeling of pharmacokinetics and pharmacodynamics: application to d-tubocurarine. Clin Pharmacol Ther. 1979;25(3):358-71. PubMed PMID: 761446.
129. Sharma A, Jusko WJ. Characteristics of indirect pharmacodynamic models and applications to clinical drug responses. Br J Clin Pharmacol. 1998;45(3):229-39. PubMed PMID: 9517366; PMCID: PMC1873365.
130. Felmlee MA, Morris ME, Mager DE. Mechanism-based pharmacodynamic modeling. Methods Mol Biol. 2012;929:583-600. doi: 10.1007/978-1-62703-050-2_21. PubMed PMID: 23007443; PMCID: PMC3684160.
131. Hamaguchi T, Matsumura Y, Suzuki M, Shimizu K, Goda R, Nakamura I, Nakatomi I, Yokoyama M, Kataoka K, Kakizoe T. NK105, a paclitaxel-incorporating micellar nanoparticle formulation, can extend in vivo antitumour activity and reduce the neurotoxicity of paclitaxel. Br J Cancer. 2005;92(7):1240-6. doi: 10.1038/sj.bjc.6602479. PubMed PMID: 15785749; PMCID: PMC2361981.
132. Rowinsky EK, Donehower RC. Paclitaxel (taxol). The New England journal of medicine. 1995;332(15):1004-14. doi: 10.1056/NEJM199504133321507. PubMed PMID: 7885406.
133. Schiff PB, Horwitz SB. Taxol stabilizes microtubules in mouse fibroblast cells. Proc Natl Acad Sci U S A. 1980;77(3):1561-5. Epub 1980/03/01. PubMed PMID: 6103535; PMCID: Pmc348536.
134. Hamel E, del Campo AA, Lowe MC, Lin CM. Interactions of taxol, microtubule-associated proteins, and guanine nucleotides in tubulin polymerization. The Journal of biological chemistry. 1981;256(22):11887-94. Epub 1981/11/25. PubMed PMID: 6117556.
135. Schiff PB, Fant J, Horwitz SB. Promotion of microtubule assembly in vitro by taxol. Nature. 1979;277(5698):665-7. Epub 1979/02/22. PubMed PMID: 423966.
136. Wang TH, Wang HS, Soong YK. Paclitaxel-induced cell death: where the cell cycle and apoptosis come together. Cancer. 2000;88(11):2619-28. Epub 2000/06/22. PubMed PMID: 10861441.
137. Authier N, Gillet JP, Fialip J, Eschalier A, Coudore F. Description of a short-term Taxol-induced nociceptive neuropathy in rats. Brain Res. 2000;887(2):239-49.
138. Saif MW, Podoltsev NA, Rubin MS, Figueroa JA, Lee MY, Kwon J, Rowen E, Yu J, Kerr RO. Phase II clinical trial of paclitaxel loaded polymeric micelle in patients with advanced pancreatic cancer. Cancer Invest. 2010;28(2):186-94. doi: 10.3109/07357900903179591. PubMed PMID: 19968498.
139. Gradishar WJ, Tjulandin S, Davidson N, Shaw H, Desai N, Bhar P, Hawkins M, O'Shaughnessy J. Phase III trial of nanoparticle albumin-bound paclitaxel compared with polyethylated castor oil-based paclitaxel in women with breast cancer. J Clin Oncol. 2005;23(31):7794-803. doi: 10.1200/JCO.2005.04.937. PubMed PMID: 16172456.
140. Gianni L, Kearns CM, Capri G, Vigano L, Locatelli A, Bonadonna G, Egorin MJ. Nonlinear pharmacokinetics and metabolism of paclitaxel and its

pharmacokinetic/pharmacodynamic relationships in humans. J Clin Oncol. 1995;13(1):180-90.
141. Karlsson MO, Monlnar V, Freijs A, Nygren P, Bergh J, Larsson R. Pharmacokinetic models for the saturable distribution of paclitaxel. Drug Metab Dispos. 1999;27(10):1220-3.
142. Henningsson A, Karlsson MO, Vigano L, Gianni L, Verweij J, Sparreboom A. Mechanism-based pharmacokinetic model for paclitaxel. J Clin Oncol. 2001;19(20):4065-73.
143. Shin BS, Kim HJ, Hong SH, Lee JB, Hwang SW, Lee MH, Yoo SD. Enhanced absorption and tissue distribution of paclitaxel following oral administration of DHP 107, a novel mucoadhesive lipid dosage form. Cancer Chemother Pharmacol. 2009;64(1):87-94. doi: 10.1007/s00280-008-0849-9. PubMed PMID: 18941747.
144. Gong C, Xie Y, Wu Q, Wang Y, Deng S, Xiong D, Liu L, Xiang M, Qian Z, Wei Y. Improving anti-tumor activity with polymeric micelles entrapping paclitaxel in pulmonary carcinoma. Nanoscale. 2012;4(19):6004-17. doi: 10.1039/c2nr31517c. PubMed PMID: 22910790.
145. Li S, Su Z, Sun M, Xiao Y, Cao F, Huang A, Li H, Ping Q, Zhang C. An arginine derivative contained nanostructure lipid carriers with pH-sensitive membranolytic capability for lysosomolytic anti-cancer drug delivery. Int J Pharm. 2012;436(1-2):248-57. doi: 10.1016/j.ijpharm.2012.06.040. PubMed PMID: 22732672.
146. Yang XY, Li YX, Li M, Zhang L, Feng LX, Zhang N. Hyaluronic acid-coated nanostructured lipid carriers for targeting paclitaxel to cancer. Cancer Lett. 2013;334(2):338-45. doi: 10.1016/j.canlet.2012.07.002. PubMed PMID: 22776563.
147. Gu G, Xia H, Hu Q, Liu Z, Jiang M, Kang T, Miao D, Tu Y, Pang Z, Song Q, Yao L, Chen H, Gao X, Chen J. PEG-co-PCL nanoparticles modified with MMP-2/9 activatable low molecular weight protamine for enhanced targeted glioblastoma therapy. Biomaterials. 2013;34(1):196-208. doi: 10.1016/j.biomaterials.2012.09.044. PubMed PMID: 23069707.
148. Wang Y, Wang C, Gong C, Wang Y, Guo G, Luo F, Qian Z. Polysorbate 80 coated poly (varepsilon-caprolactone)-poly (ethylene glycol)-poly (varepsilon-caprolactone) micelles for paclitaxel delivery. Int J Pharm. 2012;434(1-2):1-8. doi: 10.1016/j.ijpharm.2012.05.015. PubMed PMID: 22609127.
149. Zhang W, Shi Y, Chen Y, Yu S, Hao J, Luo J, Sha X, Fang X. Enhanced antitumor efficacy by paclitaxel-loaded pluronic P123/F127 mixed micelles against non-small cell lung cancer based on passive tumor targeting and modulation of drug resistance. Eur J Pharm Biopharm. 2010;75(3):341-53. doi: 10.1016/j.ejpb.2010.04.017. PubMed PMID: 20451605.
150. Han LM, Guo J, Zhang LJ, Wang QS, Fang XL. Pharmacokinetics and biodistribution of polymeric micelles of paclitaxel with Pluronic P123. Acta Pharmacol Sin. 2006;27(6):747-53. doi: 10.1111/j.1745-7254.2006.00340.x. PubMed PMID: 16723095.
151. Tong X, Zhou J, Tan Y. Liquid chromatography/tandem triple-quadrupole mass spectrometry for determination of paclitaxel in rat tissues. Rapid Commun Mass Spectrom. 2006;20(12):1905-12. doi: 10.1002/rcm.2525. PubMed PMID: 16715470.
152. Wang Y, Li Y, Wang Q, Wu J, Fang X. Pharmacokinetics and biodistribution of pacliatxel-loaded pluronic P105/L101 mixed polymeric micelles. Yakugaku Zasshi. 2008;128(6):941-50.
153. Peltier S, Oger JM, Lagarce F, Couet W, Benoit JP. Enhanced oral paclitaxel bioavailability after administration of paclitaxel-loaded lipid nanocapsules. Pharm Res. 2006;23(6):1243-50. doi: 10.1007/s11095-006-0022-2. PubMed PMID: 16715372.
154. Lee SW, Chang DH, Shim MS, Kim BO, Kim SO, Seo MH. Ionically fixed polymeric nanoparticles as a novel drug carrier. Pharm Res. 2007;24(8):1508-16. doi: 10.1007/s11095-007-9269-5. PubMed PMID: 17380262.

155. Yang T, Choi MK, Cui FD, Kim JS, Chung SJ, Shim CK, Kim DD. Preparation and evaluation of paclitaxel-loaded PEGylated immunoliposome. J Control Release. 2007;120(3):169-77. doi: 10.1016/j.jconrel.2007.05.011. PubMed PMID: 17586082.
156. Forrest ML, Yanez JA, Remsberg CM, Ohgami Y, Kwon GS, Davies NM. Paclitaxel prodrugs with sustained release and high solubility in poly(ethylene glycol)-b-poly(epsilon-caprolactone) micelle nanocarriers: pharmacokinetic disposition, tolerability, and cytotoxicity. Pharm Res. 2008;25(1):194-206. doi: 10.1007/s11095-007-9451-9. PubMed PMID: 17912488; PMCID: PMC4872624.
157. Nornoo AO, Chow DS. Cremophor-free intravenous microemulsions for paclitaxel II. Stability, in vitro release and pharmacokinetics. Int J Pharm. 2008;349(1-2):117-23. doi: 10.1016/j.ijpharm.2007.07.043. PubMed PMID: 17869458.
158. Zhang Z, Lee SH, Gan CW, Feng SS. In vitro and in vivo investigation on PLA-TPGS nanoparticles for controlled and sustained small molecule chemotherapy. Pharm Res. 2008;25(8):1925-35. doi: 10.1007/s11095-008-9611-6. PubMed PMID: 18509603.
159. Zhang C, Qu G, Sun Y, Wu X, Yao Z, Guo Q, Ding Q, Yuan S, Shen Z, Ping Q, Zhou H. Pharmacokinetics, biodistribution, efficacy and safety of N-octyl-O-sulfate chitosan micelles loaded with paclitaxel. Biomaterials. 2008;29(9):1233-41. doi: 10.1016/j.biomaterials.2007.11.029. PubMed PMID: 18093646.
160. Gelderblom H, Verweij J, van Zomeren DM, Ouwens L, Nooter K, Stoter G, Sparreboom A. Influence of Cremophor EL on the bioavailability of intraperitoneal paclitaxel. Clin Cancer Res. 2002;8(4):1237-41.
161. Bulitta JB, Zhao P, Arnold RD, Kessler DR, Daifuku R, Pratt J, Luciano G, Hanauske AR, Gelderblom H, Awada A, Jusko WJ. Mechanistic population pharmacokinetics of total and unbound paclitaxel for a new nanodroplet formulation versus Taxol in cancer patients. Cancer Chemother Pharmacol. 2009;63(6):1049-63. doi: 10.1007/s00280-008-0827-2. PubMed PMID: 18791718.
162. Gardner ER, Dahut W, Figg WD. Quantitative determination of total and unbound paclitaxel in human plasma following Abraxane treatment. J Chromatogr B Analyt Technol Biomed Life Sci. 2008;862(1-2):213-8. doi: 10.1016/j.jchromb.2007.12.013. PubMed PMID: 18191625; PMCID: PMC2259285.
163. Chen KJ, Chen WY, Chen X, Jia YM, Peng GQ, Chen L. Increased elimination of paclitaxel by magnesium isoglycyrrhizinate in epithelial ovarian cancer patients treated with paclitaxel plus cisplatin: a pilot clinical study. Eur J Drug Metab Pharmacokinet. 2014;39(1):25-31. doi: 10.1007/s13318-013-0136-y. PubMed PMID: 23681836.
164. Veltkamp SA, Thijssen B, Garrigue JS, Lambert G, Lallemand F, Binlich F, Huitema AD, Nuijen B, Nol A, Beijnen JH, Schellens JH. A novel self-microemulsifying formulation of paclitaxel for oral administration to patients with advanced cancer. Br J Cancer. 2006;95(6):729-34. doi: 10.1038/sj.bjc.6603312. PubMed PMID: 16926835; PMCID: PMC2360510.
165. Bissery MC, Nohynek G, Sanderink GJ, Lavelle F. Docetaxel (Taxotere): a review of preclinical and clinical experience. Part I: Preclinical experience. Anticancer Drugs. 1995;6(3):339-55, 63-8. PubMed PMID: 7670132.
166. Eiseman JL, Eddington ND, Leslie J, MacAuley C, Sentz DL, Zuhowski M, Kujawa JM, Young D, Egorin MJ. Plasma pharmacokinetics and tissue distribution of paclitaxel in CD2F1 mice. Cancer Chemother Pharmacol. 1994;34(6):465-71.
167. Fetterly GJ, Straubinger RM. Pharmacokinetics of paclitaxel-containing liposomes in rats. AAPS PharmSci. 2003;5(4):E32.
168. Sparreboom A, Van Tellingen O, Nooijen WJ, Beijnen J. Preclinical pharmacokinetics of paclitaxel and docetaxel. Anticancer Drugs. 1998;9(1):1-17.

169. Sparreboom A, van Tellingen O, Nooijen WJ, Beijnen JH. Tissue distribution, metabolism and excretion of paclitaxel in mice. Anticancer Drugs. 1996;7(1):78-86. PubMed PMID: 8742102.
170. Walle T, Kumar GN, McMillan JM, Thornburg KR, Walle UK. Taxol metabolism in rat hepatocytes. Biochem Pharmacol. 1993;46(9):1661-4. PubMed PMID: 7902091.
171. Monsarrat B, Royer I, Wright M, Cresteil T. Biotransformation of taxoids by human cytochromes P450: structure-activity relationship. Bull Cancer. 1997;84(2):125-33. PubMed PMID: 9180834.
172. Sparreboom A, van Asperen J, Mayer U, Schinkel AH, Smit JW, Meijier DK, Borst P, Nooijen WJ, Beijnen JH, Van Tellingen O. Limited oral bioavailability and active epithelial excretion of paclitaxel (Taxol) caused by P-glycoprotein in the intestine. Proc Natl Acad Sci U S A. 1997;94(5):2031-5.
173. Kagan L, Gershkovich P, Wasan KM, Mager DE. Physiologically based pharmacokinetic model of amphotericin B disposition in rats following administration of deoxycholate formulation (Fungizone(R)): pooled analysis of published data. AAPS J. 2011;13(2):255-64. doi: 10.1208/s12248-011-9267-8. PubMed PMID: 21431453; PMCID: PMC3085707.
174. Kagan L, Gershkovich P, Wasan KM, Mager DE. Dual physiologically based pharmacokinetic model of liposomal and nonliposomal amphotericin B disposition. Pharm Res. 2014;31(1):35-45. doi: 10.1007/s11095-013-1127-z. PubMed PMID: 23793994.
175. Kawai R, Lemaire M, Steimer JL, Bruelisauer A, Niederberger W, Rowland M. Physiologically based pharmacokinetic study on a cyclosporin derivative, SDZ IMM 125. J Pharmacokinet Biopharm. 1994;22(5):327-65. PubMed PMID: 7791036.
176. Wei Y, Xue Z, Ye Y, Wang P, Huang Y, Zhao L. Pharmacokinetic and tissue distribution of paclitaxel in rabbits assayed by LC-UV after intravenous administration of its novel liposomal formulation. Biomed Chromatogr. 2014;28(2):204-12. doi: 10.1002/bmc.3005. PubMed PMID: 23893887.
177. Ait-Oudhia S, Straubinger RM, Mager DE. Meta-analysis of nanoparticulate paclitaxel delivery system pharmacokinetics and model prediction of associated neutropenia. Pharm Res. 2012;29(10):2833-44. doi: 10.1007/s11095-012-0775-8. PubMed PMID: 22588463.
178. Rowinsky EK, Jiroutek M, Bonomi P, Johnson D, Baker SD. Paclitaxel steady-state plasma concentration as a determinant of disease outcome and toxicity in lung cancer patients treated with paclitaxel and cisplatin. Clin Cancer Res. 1999;5(4):767-74. PubMed PMID: 10213211.
179. Liebmann JE, Cook JA, Lipschultz C, Teague D, Fisher J, Mitchell JB. Cytotoxic studies of paclitaxel (Taxol) in human tumour cell lines. Br J Cancer. 1993;68(6):1104-9. PubMed PMID: 7903152; PMCID: PMC1968657.
180. Pushkarev VM, Starenki DV, Saenko VA, Yamashita S, Kovzun OI, Popadiuk ID, Pushkarev VV, Tronko MD. Effects of low and high concentrations of antitumour drug taxol in anaplastic thyroid cancer cells. Exp Oncol. 2009;31(1):16-21. PubMed PMID: 19300411.
181. Joerger M, Huitema AD, Richel DJ, Dittrich C, Pavlidis N, Briasoulis E, Vermorken JB, Strocchi E, Martoni A, Sorio R, Sleeboom HP, Izquierdo MA, Jodrell DI, Calvert H, Boddy AV, Hollema H, Fety R, Van der Vijgh WJ, Hempel G, Chatelut E, Karlsson M, Wilkins J, Tranchand B, Schrijvers AH, Twelves C, Beijnen JH, Schellens JH. Population pharmacokinetics and pharmacodynamics of paclitaxel and carboplatin in ovarian cancer patients: a study by the European organization for research and treatment of cancer-pharmacology and molecular mechanisms group and new drug development group. Clin Cancer Res. 2007;13(21):6410-8. doi: 10.1158/1078-0432.CCR-07-0064. PubMed PMID: 17975154.

182. Rowinsky EK, Chaudhry V, Cornblath DR, Donehower RC. Neurotoxicity of Taxol. J Natl Cancer Inst Monogr. 1993(15):107-15. PubMed PMID: 7912516.
183. Polomano RC, Mannes AJ, Clark US, Bennett GJ. A painful peripheral neuropathy in the rat produced by the chemotherapeutic drug, paclitaxel. Pain. 2001;94(3):293-304.
184. Lee JB, Zgair A, Taha DA, Zang X, Kagan L, Kim TH, Kim MG, Yun HY, Fischer PM, Gershkovich P. Quantitative analysis of lab-to-lab variability in Caco-2 permeability assays. Eur J Pharm Biopharm. 2017. doi: 10.1016/j.ejpb.2016.12.027. PubMed PMID: 28088633.
185. Straubinger RM. Biopharmaceutics of paclitaxel (Taxol): formulation, activity, and pharmacokinetics. In: M. S, editor. Taxol: Science and Applications. illustrated ed. Boca Raton, Florida: CRC Press; 1995. p. 448.
186. Waugh WN, Trissel LA, Stella VJ. Stability, compatibility, and plasticizer extraction of taxol (NSC-125973) injection diluted in infusion solutions and stored in various containers. Am J Hosp Pharm. 1991;48(7):1520-4. PubMed PMID: 1679294.
187. Adams JD, Flora KP, Goldspiel BR, Wilson JW, Arbuck SG, Finley R. Taxol: a history of pharmaceutical development and current pharmaceutical concerns. J Natl Cancer Inst Monogr. 1993(15):141-7. PubMed PMID: 7912520.
188. Song D, Hsu LF, Au JL. Binding of taxol to plastic and glass containers and protein under in vitro conditions. J Pharm Sci. 1996;85(1):29-31.
189. Sonnichsen DS, Hurwitz CA, Pratt CB, Shuster JJ, Relling MV. Saturable pharmacokinetics and paclitaxel pharmacodynamics in children with solid tumors. J Clin Oncol. 1994;12(3):532-8. doi: 10.1200/JCO.1994.12.3.532. PubMed PMID: 7907130.
190. Sparreboom A, Van Tellingen O, Nooijen WJ, Beijnen JH. Nonlinear pharmacokinetics of paclitaxel in mice results from the pharmaceutical vehicle Cremophor EL. Cancer Res. 1996;56(9):2112-5.
191. Van Tellingen O, Huizing MT, Panday VR, Schellens JH, Nooijen WJ, Beijnen JH. Cremophor EL causes (pseudo-) non-linear pharmacokineitcs of paclitaxel in patients. Br J Cancer. 1999;81(2):330-5.
192. Cao Y, Jusko WJ. Applications of minimal physiologically-based pharmacokinetic models. J Pharmacokinet Pharmacodyn. 2012;39(6):711-23. doi: 10.1007/s10928-012-9280-2).
193. Lu XF, Bi K, Chen X. Physiologically based pharmacokinetic model of docetaxel and interspecies scaling: comparison of simple injection with folate receptor-targeting amphiphilic copolymer-modified liposomes. Xenobiotica. 2016;46(12):1093-104. doi: 10.3109/00498254.2016.1155128. PubMed PMID: 26986924.
194. Kawai R, Mathew D, Tanaka C, Rowland M. Physiologically based pharmacokinetics of cyclosporine A: extension to tissue distribution kinetics in rats and scale-up to human. J Pharmacol Exp Ther. 1998;287(2):457-68. PubMed PMID: 9808668.
195. Tang H, Mayersohn M. A global examination of allometric scaling for predicting human drug clearance and the prediction of large vertical allometry. J Pharm Sci. 2006;95(8):1783-99. doi: 10.1002/jps.20481. PubMed PMID: 16795013.
196. Hu TM, Hayton WL. Allometric scaling of xenobiotic clearance: uncertainty versus universality. AAPS PharmSci. 2001;3(4):E29.
197. DeSantis CE, Lin CC, Mariotto AB, Siegel RL, Stein KD, Kramer JL, Alteri R, Robbins AS, Jemal A. Cancer treatment and survivorship statistics, 2014. CA Cancer J Clin. 2014;64(4):252-71. doi: 10.3322/caac.21235. PubMed PMID: 24890451.
198. Farquhar-Smith P, Brown MRD. Persistent Pain in Cancer Survivors: Pathogenesis and Treatment Options. Pain Clinical Updates XXIV. 2016;4:1-8.
199. Cavaletti G, Alberti P, Marmiroli P. Chemotherapy-induced peripheral neurotoxicity in cancer survivors: an underdiagnosed clinical entity? Am Soc Clin Oncol Educ Book. 2015:e553-60. doi: 10.14694/EdBook_AM.2015.35.e553. PubMed PMID: 25993222.

200. Beijers AJ, Mols F, Tjan-Heijnen VC, Faber CG, van de Poll-Franse LV, Vreugdenhil G. Peripheral neuropathy in colorectal cancer survivors: the influence of oxaliplatin administration. Results from the population-based PROFILES registry. Acta Oncol. 2015;54(4):463-9. doi: 10.3109/0284186X.2014.980912. PubMed PMID: 25417732.
201. Finnerup NB, Attal N, Haroutounian S, McNicol E, Baron R, Dworkin RH, Gilron I, Haanpaa M, Hansson P, Jensen TS, Kamerman PR, Lund K, Moore A, Raja SN, Rice AS, Rowbotham M, Sena E, Siddall P, Smith BH, Wallace M. Pharmacotherapy for neuropathic pain in adults: a systematic review and meta-analysis. Lancet Neurol. 2015;14(2):162-73. doi: 10.1016/S1474-4422(14)70251-0. PubMed PMID: 25575710; PMCID: PMC4493167.
202. Kaley TJ, Deangelis LM. Therapy of chemotherapy-induced peripheral neuropathy. Br J Haematol. 2009;145(1):3-14. doi: 10.1111/j.1365-2141.2008.07558.x. PubMed PMID: 19170681.
203. Lao J, Madani J, Puertolas T, Alvarez M, Hernandez A, Pazo-Cid R, Artal A, Anton Torres A. Liposomal Doxorubicin in the treatment of breast cancer patients: a review. J Drug Deliv. 2013;2013:456409. doi: 10.1155/2013/456409. PubMed PMID: 23634302; PMCID: PMC3619536.
204. Rahman AM, Yusuf SW, Ewer MS. Anthracycline-induced cardiotoxicity and the cardiac-sparing effect of liposomal formulation. Int J Nanomedicine. 2007;2(4):567-83. PubMed PMID: 18203425; PMCID: PMC2676818.
205. O'Brien ME, Wigler N, Inbar M, Rosso R, Grischke E, Santoro A, Catane R, Kieback DG, Tomczak P, Ackland SP, Orlandi F, Mellars L, Alland L, Tendler C, Group CBCS. Reduced cardiotoxicity and comparable efficacy in a phase III trial of pegylated liposomal doxorubicin HCl (CAELYX/Doxil) versus conventional doxorubicin for first-line treatment of metastatic breast cancer. Ann Oncol. 2004;15(3):440-9. PubMed PMID: 14998846.
206. Stone NR, Bicanic T, Salim R, Hope W. Liposomal Amphotericin B (AmBisome((R))): A Review of the Pharmacokinetics, Pharmacodynamics, Clinical Experience and Future Directions. Drugs. 2016;76(4):485-500. doi: 10.1007/s40265-016-0538-7. PubMed PMID: 26818726; PMCID: PMC4856207.
207. Koudelka S, Turanek J. Liposomal paclitaxel formulations. J Control Release. 2012;163(3):322-34. doi: 10.1016/j.jconrel.2012.09.006. PubMed PMID: 22989535.
208. Saad M, Garbuzenko OB, Ber E, Chandna P, Khandare JJ, Pozharov VP, Minko T. Receptor targeted polymers, dendrimers, liposomes: which nanocarrier is the most efficient for tumor-specific treatment and imaging? J Control Release. 2008;130(2):107-14. doi: 10.1016/j.jconrel.2008.05.024. PubMed PMID: 18582982; PMCID: PMC3590109.
209. Yilmaz E, Gold MS. Sensory neuron subpopulation-specific dysregulation of intracellular calcium in a rat model of chemotherapy-induced peripheral neuropathy. Neuroscience. 2015;300:210-8. doi: 10.1016/j.neuroscience.2015.05.019. PubMed PMID: 25982563; PMCID: PMC4485584.
210. Thangamani D, Edafiogho IO, Masocha W. The anticonvulsant enaminone E139 attenuates paclitaxel-induced neuropathic pain in rodents. ScientificWorldJournal. 2013;2013:240508. doi: 10.1155/2013/240508. PubMed PMID: 24385872; PMCID: PMC3872104.
211. Aydin TH, Can OD, Demir Ozkay U, Turan N. Effect of subacute agomelatine treatment on painful diabetic neuropathy: involvement of catecholaminergic mechanisms. Fundam Clin Pharmacol. 2016;30(6):549-67. doi: 10.1111/fcp.12224. PubMed PMID: 27421789.

212. Sisignano M, Baron R, Scholich K, Geisslinger G. Mechanism-based treatment for chemotherapy-induced peripheral neuropathic pain. Nat Rev Neurol. 2014;10(12):694-707. doi: 10.1038/nrneurol.2014.211. PubMed PMID: 25366108.
213. Quasthoff S, Hartung HP. Chemotherapy-induced peripheral neuropathy. J Neurol. 2002;249(1):9-17.
214. Yamashita Y, Egashira N, Masuguchi K, Ushio S, Kawashiri T, Oishi R. Comparison of Peripheral Neuropathy Induced by Standard and Nanoparticle Albumin–Bound Paclitaxel in Rats. Journal of Pharmacological Sciences. 2011;117(2):116-20. doi: 10.1254/jphs.11062SC.
215. Park IH, Sohn JH, Kim SB, Lee KS, Chung JS, Lee SH, Kim TY, Jung KH, Cho EK, Kim YS, Song HS, Seo JH, Ryoo HM, Lee SA, Yoon SY, Kim CS, Kim YT, Kim SY, Jin MR, Ro J. An Open-Label, Randomized, Parallel, Phase III Trial Evaluating the Efficacy and Safety of Polymeric Micelle-Formulated Paclitaxel Compared to Conventional Cremophor EL-Based Paclitaxel for Recurrent or Metastatic HER2-Negative Breast Cancer. Cancer Res Treat. 2017;49(3):569-77. doi: 10.4143/crt.2016.289. PubMed PMID: 27618821; PMCID: PMC5512366.
216. Paclitaxel liposome for injection [package insert in Chinese]. Nanjing, China. Luye Pharma Group.2007.
217. Meerum Terwogt JM, ten Bokkel Huinink WW, Schellens JH, Schot M, Mandjes IA, Zurlo MG, Rocchetti M, Rosing H, Koopman FJ, Beijnen JH. Phase I clinical and pharmacokinetic study of PNU166945, a novel water-soluble polymer-conjugated prodrug of paclitaxel. Anticancer Drugs. 2001;12(4):315-23. PubMed PMID: 11335787.
218. Zang X, Kagan L. Physiologically-based modeling and interspecies prediction of paclitaxel pharmacokinetics. J Pharmacokinet Pharmacodyn. 2018. doi: 10.1007/s10928-018-9586-9. PubMed PMID: 29671170.
219. Masocha W. Gene expression profile of sodium channel subunits in the anterior cingulate cortex during experimental paclitaxel-induced neuropathic pain in mice. PeerJ. 2016;4:e2702. doi: 10.7717/peerj.2702. PubMed PMID: 27896032; PMCID: PMC5119229.
220. Alvarez P, Ferrari LF, Levine JD. Muscle pain in models of chemotherapy-induced and alcohol-induced peripheral neuropathy. Ann Neurol. 2011;70(1):101-9. doi: 10.1002/ana.22382. PubMed PMID: 21786301; PMCID: PMC3145965.
221. Winer EP, Berry DA, Woolf S, Duggan D, Kornblith A, Harris LN, Michaelson RA, Kirshner JA, Fleming GF, Perry MC, Graham ML, Sharp SA, Keresztes R, Henderson IC, Hudis C, Muss H, Norton L. Failure of higher-dose paclitaxel to improve outcome in patients with metastatic breast cancer: cancer and leukemia group B trial 9342. J Clin Oncol. 2004;22(11):2061-8. doi: 10.1200/JCO.2004.08.048. PubMed PMID: 15169793.
222. Chan JK, Brady MF, Penson RT, Huang H, Birrer MJ, Walker JL, DiSilvestro PA, Rubin SC, Martin LP, Davidson SA, Huh WK, O'Malley DM, Boente MP, Michael H, Monk BJ. Weekly vs. Every-3-Week Paclitaxel and Carboplatin for Ovarian Cancer. The New England journal of medicine. 2016;374(8):738-48. doi: 10.1056/NEJMoa1505067. PubMed PMID: 26933849; PMCID: PMC5081077.
223. Baldwin RM, Owzar K, Zembutsu H, Chhibber A, Kubo M, Jiang C, Watson D, Eclov RJ, Mefford J, McLeod HL, Friedman PN, Hudis CA, Winer EP, Jorgenson EM, Witte JS, Shulman LN, Nakamura Y, Ratain MJ, Kroetz DL. A genome-wide association study identifies novel loci for paclitaxel-induced sensory peripheral neuropathy in CALGB 40101. Clin Cancer Res. 2012;18(18):5099-109. doi: 10.1158/1078-0432.CCR-12-1590. PubMed PMID: 22843789; PMCID: PMC3445665.
224. de Graan AJ, Elens L, Sprowl JA, Sparreboom A, Friberg LE, van der Holt B, de Raaf PJ, de Bruijn P, Engels FK, Eskens FA, Wiemer EA, Verweij J, Mathijssen RH, van Schaik RH. CYP3A4*22 genotype and systemic exposure affect paclitaxel-induced

neurotoxicity. Clin Cancer Res. 2013;19(12):3316-24. doi: 10.1158/1078-0432.CCR-12-3786. PubMed PMID: 23640974; PMCID: PMC3686845.
225. Mielke S, Sparreboom A, Steinberg SM, Gelderblom H, Unger C, Behringer D, Mross K. Association of Paclitaxel pharmacokinetics with the development of peripheral neuropathy in patients with advanced cancer. Clin Cancer Res. 2005;11(13):4843-50. doi: 10.1158/1078-0432.CCR-05-0298. PubMed PMID: 16000582.
226. Ochi-ishi R, Nagata K, Inoue T, Tozaki-Saitoh H, Tsuda M, Inoue K. Involvement of the chemokine CCL3 and the purinoceptor P2X7 in the spinal cord in paclitaxel-induced mechanical allodynia. Mol Pain. 2014;10:53. doi: 10.1186/1744-8069-10-53. PubMed PMID: 25127716; PMCID: PMC4141668.
227. Mehrotra S, Sharma MR, Gray E, Wu K, Barry WT, Hudis C, Winer EP, Lyss AP, Toppmeyer DL, Moreno-Aspitia A, Lad TE, Valasco M, Overmoyer B, Rugo H, Ratain MJ, Gobburu JV. Kinetic-Pharmacodynamic Model of Chemotherapy-Induced Peripheral Neuropathy in Patients with Metastatic Breast Cancer Treated with Paclitaxel, Nab-Paclitaxel, or Ixabepilone: CALGB 40502 (Alliance). AAPS J. 2017;19(5):1411-23. doi: 10.1208/s12248-017-0101-9. PubMed PMID: 28620884; PMCID: PMC5711539.
228. Woolf CJ. Central sensitization: implications for the diagnosis and treatment of pain. Pain. 2011;152(3 Suppl):S2-15. doi: 10.1016/j.pain.2010.09.030. PubMed PMID: 20961685; PMCID: PMC3268359.
229. Woo S, Pawaskar D, Jusko WJ. Methods of utilizing baseline values for indirect response models. J Pharmacokinet Pharmacodyn. 2009;36(5):381-405. doi: 10.1007/s10928-009-9128-6. PubMed PMID: 19697107; PMCID: PMC3712653.
230. Dansirikul C, Silber HE, Karlsson MO. Approaches to handling pharmacodynamic baseline responses. J Pharmacokinet Pharmacodyn. 2008;35(3):269-83. doi: 10.1007/s10928-008-9088-2. PubMed PMID: 18446428.
231. Qin LF, Ng IO. Induction of apoptosis by cisplatin and its effect on cell cycle-related proteins and cell cycle changes in hepatoma cells. Cancer Lett. 2002;175(1):27-38. PubMed PMID: 11734333.
232. Siddik ZH, Jones M, Boxall FE, Harrap KR. Comparative distribution and excretion of carbopaltin and cisplatin in mice. Cancer Chemother Pharmacol. 1988;21:19-24.
233. Korst AE, Boven E, van der Sterre ML, Fichtinger-Schepman AM, van der Vijgh WJ. Pharmacokinetics of cisplatin with and without amifostine in tumour-bearing nude mice. Eur J Cancer. 1998;34(3):412-6.
234. Ichinose K, Tomiyama N, Nakashima M, Ohya Y, Ichikawa M, Ouchi T, Kanematsu T. Antitumor activity of dextran derivatives immobilizing platinum complex (II). Anticancer Drugs. 2000;11(1):33-8.
235. Nishiyama N, Kato Y, Sugiyama Y, Kataoka K. Cisplatin-loaded polymer-metal complex micelle with time-modulated decaying property as a novel drug delivery system. Pharm Res. 2001;18(7):1035-41.
236. Zamboni WC, Gervais AC, Egorin MJ, Schellens JH, Hamburger DR, Delauter BJ, Grim A, Zuhowski EG, Joseph E, Pluim D, Potter DM, Eiseman JL. Inter- and intratumoral disposition of platinum in solid tumors after administration of cisplatin. Clin Cancer Res. 2002;8(9):2992-9.
237. Nishiyama N, Okazaki S, Cabral H, Miyamoto M, Kato Y, Sugiyama Y, Nishio K, Matsumura Y, Kataoka K. Novel cisplatin-incorporated polymeric micelles can eradicate solid tumors in mice. Cancer Res. 2003;63(24):8977-83.
238. Staffhorst RW, van der Born K, Erkelens CA, Hamelers IH, Peters GJ, Boven E, de Kroon AI. Antitumor activity and biodistribution of cisplatin nanocapsules in nude mice bearing human ovarian carcinoma xenografts. Anticancer Drugs. 2008;19(7):721-7.

239. Kuang Y, Liu J, Liu Z, Zhuo R. Cholesterol-based anionic long-circulating cisplatin liposomes with reduced renal toxicity. Biomaterials. 2012;33(5):1596-606. doi: 10.1016/j.biomaterials.2011.10.081. PubMed PMID: 22079777.
240. Oberoi HS, Nukolova NV, Laquer FC, Poluektova LY, Huang J, Alnouti Y, Yokohira M, Arnold LL, Kabanov AV, Cohen SM, Bronich TK. Cisplatin-loaded core cross-linked micelles: comparative pharmacokinetics, antitumor activity, and toxicity in mice. Int J Nanomedicine. 2012;7:2557-71. doi: 10.2147/IJN.S29145. PubMed PMID: 22745537; PMCID: PMC3383348.
241. Xiao H, Song H, Yang Q, Cai H, Qi R, Yan L, Liu S, Zheng Y, Huang Y, Liu T, Jing X. A prodrug strategy to deliver cisplatin(IV) and paclitaxel in nanomicelles to improve efficacy and tolerance. Biomaterials. 2012;33(27):6507-19. doi: 10.1016/j.biomaterials.2012.05.049. PubMed PMID: 22727463.
242. Yu H, Tang Z, Zhang D, Song W, Zhang Y, Yang Y, Ahmad Z, Chen X. Pharmacokinetics, biodistribution and in vivo efficacy of cisplatin loaded poly(L-glutamic acid)-g-methoxy poly(ethylene glycol) complex nanoparticles for tumor therapy. J Control Release. 2015;205:89-97. doi: 10.1016/j.jconrel.2014.12.022. PubMed PMID: 25529533.
243. Zhang JS, Imai T, Otagiri M. Effects of a cisplatin-chondroitin sulfate A complex in reducing the nephrotoxicity of cisplatin. Arch Toxicol. 2000;74(6):300-7.
244. Zhang JS, Imai T, Suenaga A, Otagiri M. Molecular-weight-dependent pharmacokinetics and cytotoxic properties of cisplatin complexes prepared with chondroitin sulfate A and C. Int J Pharm. 2002;240(1-2):23-31.
245. Uchino H, Matsumura Y, Negishi T, Koizumi F, Hayashi T, Honda T, Nishiyama N, Kataoka K, Naito S, Kakizoe T. Cisplatin-incorporating polymeric micelles (NC-6004) can reduce nephrotoxicity and neurotoxicity of cisplatin in rats. Br J Cancer. 2005;93(6):678-87. doi: 10.1038/sj.bjc.6602772. PubMed PMID: 16222314; PMCID: PMC2361620.
246. Gormley PE, Bull JM, LeRoy AF, Cysyk R. Kinetics of cis-dichlorodiammineplatinum. Clin Pharmacol Ther. 1979;25(3):351-7. PubMed PMID: 761445.
247. Jehn CF, Boulikas T, Kourvetaris A, Possinger K, Luftner D. Pharmacokinetics of liposomal cisplatin (lipoplatin) in combination with 5-FU in patients with advanced head and neck cancer: first results of a phase III study. Anticancer Res. 2007;27(1A):471-5. PubMed PMID: 17352269.
248. Verschraagen M, Boven E, Ruijter R, van der Born K, Berkhof J, Hausheer FH, van der Vijgh WJ. Pharmacokinetics and preliminary clinical data of the novel chemoprotectant BNP7787 and cisplatin and their metabolites. Clin Pharmacol Ther. 2003;74(2):157-69. doi: 10.1016/S0009-9236(03)00150-4. PubMed PMID: 12891226.
249. Krarup-Hansen A, Rietz B, Krarup C, Heydorn K, Rorth M, Schmalbruch H. Histology and platinum content of sensory ganglia and sural nerves in patients treated with cisplatin and carboplatin: an autopsy study. Neuropathol Appl Neurobiol. 1999;25:29-40.
250. Stewart DJ, Mikhael NZ, Nair RC, Kacew S, Montpetit V, Nanji A, Maroun JA, Howard K. Platinum concentrations in human autopsy tumor samples. Am J Clin Oncol. 1988;11(2):152-8.
251. Tanaka H, Ishikawa E, Teshima S, Shimizu E. Histopathological study of human cisplatin nephropathy. Toxicol Pathol. 1986;14(2):247-57.
252. Litterst CL, LeRoy AF, Guarino AM. Disposition and distribution of platinum following parenteral administration of cis-dichlorodiammineplatinum(II) to animals. Cancer treatment reports. 1979;63(9-10):1485-92. PubMed PMID: 498147.
253. LeRoy AF, Lutz RJ, Dedrick RL, Litterst CL, Guarino AM. Pharmacokinetic study of cis-dichlorodiammineplatinum(II) (DDP) in the beagle dog: thermodynamic and kinetic

behavior of DDP in a biologic millieu. Cancer treatment reports. 1979;63(1):59-71. PubMed PMID: 421234.
254. Casper ES, Kelsen DP, Alcock NW, Young CW. Platinum concentrations in bile and plasma following rapid and 6-hour infusions of cis-dichlorodiammineplatinum(II). Cancer treatment reports. 1979;63(11-12):2023-5. PubMed PMID: 575066.
255. Z. Q, D. BM. Measurement of Glomerular Filtration Rate in Conscious Mice. In: G. B, T. H, editors. Kidney Research Methods in Molecular Biology (Methods and Protocols): Humana Press; 2009. p. 61-72.
256. Glomerular Filtration Rate (GFR) 2018 [cited 2018 09.20]. Available from: https://www.kidney.org/atoz/content/gfr.
257. King FG, Dedrick RL, Farris FF. Physiological pharmacokinetic modeling of cis-dichlorodiammineplatinum(II) (DDP) in several species. J Pharmacokinet Biopharm. 1986;14(2):131-55.
258. Hanada K, Ninomiya K, Ogata H. Pharmacokinetics and toxicodynamics of cisplatin and its metabolites in rats: relationship between renal handling and nephrotoxicity of cisplatin. J Pharm Pharmacol. 2000;52(11):1345-53. PubMed PMID: 11186242.
259. Waterlow JC. Protein turnover with special reference to man. Q J Exp Physiol. 1984;69(3):409-38. PubMed PMID: 6382379.
260. Ostrow S, Egorin MJ, Hahn D, Markus S, Aisner J, Chang P, LeRoy A, Bachur NR, Wiernik PH. High-dose cisplatin therapy using mannitol versus furosemide diuresis: comparative pharmacokinetics and toxicity. Cancer treatment reports. 1981;65(1-2):73-8. PubMed PMID: 6784924.
261. Lammers T, Hennink WE, Storm G. Tumour-targeted nanomedicines: principles and practice. Br J Cancer. 2008;99(3):392-7. Epub 2008/07/24. doi: 10.1038/sj.bjc.6604483. PubMed PMID: 18648371; PMCID: 2527811.
262. Thanki K, Gangwal RP, Sangamwar AT, Jain S. Oral delivery of anticancer drugs: challenges and opportunities. J Control Release. 2013;170(1):15-40. Epub 2013/05/08. doi: 10.1016/j.jconrel.2013.04.020. PubMed PMID: 23648832.
263. Singh Y, Palombo M, Sinko PJ. Recent trends in targeted anticancer prodrug and conjugate design. Curr Med Chem. 2008;15(18):1802-26. Epub 2008/08/12. PubMed PMID: 18691040; PMCID: 2802226.
264. Li J, Chen F, Cona MM, Feng Y, Himmelreich U, Oyen R, Verbruggen A, Ni Y. A review on various targeted anticancer therapies. Target Oncol. 2012;7(1):69-85. Epub 2012/02/22. doi: 10.1007/s11523-012-0212-2. PubMed PMID: 22350489.
265. Ruddy K, Mayer E, Partridge A. Patient adherence and persistence with oral anticancer treatment. CA Cancer J Clin. 2009;59(1):56-66. Epub 2009/01/17. doi: 10.3322/caac.20004. PubMed PMID: 19147869.
266. Banna GL, Collova E, Gebbia V, Lipari H, Giuffrida P, Cavallaro S, Condorelli R, Buscarino C, Tralongo P, Ferrau F. Anticancer oral therapy: emerging related issues. Cancer Treat Rev. 2010;36(8):595-605. Epub 2010/06/24. doi: 10.1016/j.ctrv.2010.04.005. PubMed PMID: 20570443.
267. O'Neill VJ, Twelves CJ. Oral cancer treatment: developments in chemotherapy and beyond. Br J Cancer. 2002;87(9):933-7. Epub 2002/11/16. doi: 10.1038/sj.bjc.6600591. PubMed PMID: 12434279; PMCID: 2364332.
268. Lapenna S, Giordano A. Cell cycle kinases as therapeutic targets for cancer. Nat Rev Drug Discov. 2009;8(7):547-66. doi: 10.1038/nrd2907. PubMed PMID: 19568282.
269. Shao H, Shi S, Huang S, Hole AJ, Abbas AY, Baumli S, Liu X, Lam F, Foley DW, Fischer PM, Noble M, Endicott JA, Pepper C, Wang S. Substituted 4-(thiazol-5-yl)-2-(phenylamino)pyrimidines are highly active CDK9 inhibitors: synthesis, X-ray crystal structures, structure-activity relationship, and anticancer activities. J Med Chem.

2013;56(3):640-59. doi: 10.1021/jm301475f. PubMed PMID: 23301767; PMCID: PMC3579313.
270. Shao H, Shi S, Foley DW, Lam F, Abbas AY, Liu X, Huang S, Jiang X, Baharin N, Fischer PM, Wang S. Synthesis, structure-activity relationship and biological evaluation of 2,4,5-trisubstituted pyrimidine CDK inhibitors as potential anti-tumour agents. Eur J Med Chem. 2013;70:447-55. doi: 10.1016/j.ejmech.2013.08.052. PubMed PMID: 24185375.
271. Wang S, Fischer PM. Cyclin-dependent kinase 9: a key transcriptional regulator and potential drug target in oncology, virology and cardiology. Trends Pharmacol Sci. 2008;29(6):302-13. doi: 10.1016/j.tips.2008.03.003. PubMed PMID: 18423896.
272. Dressman JB, Vertzoni M, Goumas K, Reppas C. Estimating drug solubility in the gastrointestinal tract. Adv Drug Deliv Rev. 2007;59(7):591-602. doi: 10.1016/j.addr.2007.05.009. PubMed PMID: 17599644.
273. Vertzoni M, Dressman J, Butler J, Hempenstall J, Reppas C. Simulation of fasting gastric conditions and its importance for the in vivo dissolution of lipophilic compounds. Eur J Pharm Biopharm. 2005;60(3):413-7. doi: 10.1016/j.ejpb.2005.03.002. PubMed PMID: 15893920.
274. Merchant HA, Afonso-Pereira F, Rabbie SC, Youssef SA, Basit AW. Gastrointestinal characterisation and drug solubility determination in animals. J Pharm Pharmacol. 2015;67(5):630-9. doi: 10.1111/jphp.12361. PubMed PMID: 25560785.
275. Kagan L, Hoffman A. Selection of drug candidates for gastroretentive dosage forms: pharmacokinetics following continuous intragastric mode of administration in a rat model. Eur J Pharm Biopharm. 2008;69(1):238-46. doi: 10.1016/j.ejpb.2007.10.019. PubMed PMID: 18068342.
276. Smith HW. Observations on the Flora of the Alimentary Tract of Animals and Factors Affecting Its Composition. The Journal of pathology and bacteriology. 1965;89:95-122. Epub 1965/01/01. PubMed PMID: 14263502.
277. Ward FW, Coates ME. Gastrointestinal pH measurement in rats: influence of the microbial flora, diet and fasting. Laboratory animals. 1987;21(3):216-22. Epub 1987/07/01. PubMed PMID: 3626468.
278. Evans DF, Pye G, Bramley R, Clark AG, Dyson TJ, Hardcastle JD. Measurement of gastrointestinal pH profiles in normal ambulant human subjects. Gut. 1988;29(8):1035-41. Epub 1988/08/01. PubMed PMID: 3410329; PMCID: 1433896.
279. Agoram B, Woltosz WS, Bolger MB. Predicting the impact of physiological and biochemical processes on oral drug bioavailability. Advanced Drug Delivery Reviews. 2001;50:S41-S67.
280. Clements JA, Heading RC, Nimmo WS, Prescott LF. Kinetics of acetaminophen absorption and gastric emptying in man. Clin Pharmacol Ther. 1978;24(4):420-31. PubMed PMID: 688732.
281. Wang Y, Roy A, Sun L, Lau CE. A double-peak phenomenon in the pharmacokinetics of alprazolam after oral administration. Drug Metab Dispos. 1999;27(8):855-9. PubMed PMID: 10421610.
282. Takamatsu N, Welage LS, Hayashi Y, Yamamoto R, Barnett JL, Shah VP, Lesko LJ, Ramachandran C, Amidon GL. Variability in cimetidine absorption and plasma double peaks following oral administration in the fasted state in humans: correlation with antral gastric motility. Eur J Pharm Biopharm. 2002;53(1):37-47. PubMed PMID: 11777751.
283. Ogiso T, Kasutani M, Tanaka H, Iwaki M, Tanino T. Pharmacokinetics of epinastine and a possible mechanism for double peaks in oral plasma concentration profiles. Biol Pharm Bull. 2001;24(7):790-4. PubMed PMID: 11456119.
284. Hammarlund MM, Paalzow LK, Odlind B. Pharmacokinetics of furosemide in man after intravenous and oral administration. Application of moment analysis. Eur J Clin Pharmacol. 1984;26(2):197-207. PubMed PMID: 6723758.

285. Lennernas H, Regardh CG. Regional gastrointestinal absorption of the beta-blocker pafenolol in the rat and intestinal transit rate determined by movement of 14C-polyethylene glycol (PEG) 4000. Pharm Res. 1993;10(1):130-5. PubMed PMID: 8094244.
286. Yin OQ, Tomlinson B, Chow AH, Chow MS. A modified two-portion absorption model to describe double-peak absorption profiles of ranitidine. Clin Pharmacokinet. 2003;42(2):179-92. doi: 10.2165/00003088-200342020-00005. PubMed PMID: 12537516.
287. Plusquellec Y, Campistron G, Staveris S, Barre J, Jung L, Tillement JP, Houin G. A double-peak phenomenon in the pharmacokinetics of veralipride after oral administration: a double-site model for drug absorption. J Pharmacokinet Biopharm. 1987;15(3):225-39. PubMed PMID: 3668801.
288. Wagner JG. Unusual pharmacokinetics. In: Benet LZ, Levy G, Ferraiolo BL, editors. Pharmacokinetics: A Modern View. New York: Plenum Press; 1984. p. 173-89.
289. Godfrey KR, Arundel PA, Dong Z, Bryant R. Modelling the Double Peak Phenomenon in pharmacokinetics. Comput Methods Programs Biomed. 2011;104(2):62-9. doi: 10.1016/j.cmpb.2010.03.007. PubMed PMID: 20381191.
290. Williams MF, Dukes GE, Heizer W, Han YH, Hermann DJ, Lampkin T, Hak LJ. Influence of gastrointestinal site of drug delivery on the absorption characteristics of ranitidine. Pharm Res. 1992;9(9):1190-4. PubMed PMID: 1409403.
291. Charman WN, Rogge MC, Boddy AW, Barr WH, Berger BM. Absorption of danazol after administration to different sites of the gastrointestinal tract and the relationship to single- and double-peak phenomena in the plasma profiles. J Clin Pharmacol. 1993;33(12):1207-13. PubMed PMID: 8126256.
292. Guha M. Cyclin-dependent kinase inhibitors move into Phase III. Nat Rev Drug Discov. 2012;11(12):892-4. doi: 10.1038/nrd3908. PubMed PMID: 23197022.
293. Roush JA. Evaluation of gastrointestinal motility directly from human pharmacokinetic data. International journal of pharmaceutics. 2011;419(1-2):43-51. Epub 2011/07/26. doi: 10.1016/j.ijpharm.2011.07.011. PubMed PMID: 21784142.
294. Kakhi M, Chittenden J. Modeling of pharmacokinetic systems using stochastic deconvolution. J Pharm Sci. 2013;102(12):4433-43. Epub 2013/11/01. doi: 10.1002/jps.23752. PubMed PMID: 24174399.
295. Heikkinen AT, Baneyx G, Caruso A, Parrott N. Application of PBPK modeling to predict human intestinal metabolism of CYP3A substrates - an evaluation and case study using GastroPlus. Eur J Pharm Sci. 2012;47(2):375-86. doi: 10.1016/j.ejps.2012.06.013. PubMed PMID: 22759901.
296. Mathias NR, Crison J. The use of modeling tools to drive efficient oral product design. AAPS J. 2012;14(3):591-600. doi: 10.1208/s12248-012-9372-3. PubMed PMID: 22644702; PMCID: PMC3385810.
297. Parrott N, Jones H, Paquereau N, Lave T. Application of full physiological models for pharmaceutical drug candidate selection and extrapolation of pharmacokinetics to man. Basic Clin Pharmacol Toxicol. 2005;96(3):193-9. doi: 10.1111/j.1742-7843.2005.pto960308.x. PubMed PMID: 15733214.
298. De Buck SS, Sinha VK, Fenu LA, Nijsen MJ, Mackie CE, Gilissen RA. Prediction of human pharmacokinetics using physiologically based modeling: a retrospective analysis of 26 clinically tested drugs. Drug Metab Dispos. 2007;35(10):1766-80. doi: 10.1124/dmd.107.015644. PubMed PMID: 17620347.
299. Suttle AB, Brouwer KL. Regional gastrointestinal absorption of ranitidine in the rat. Pharm Res. 1995;12(9):1311-5. PubMed PMID: 8570527.
300. Davis SS. Formulation strategies for absorption windows. Drug Discov Today. 2005;10(4):249-57. doi: 10.1016/S1359-6446(04)03351-3. PubMed PMID: 15708743.
301. Kostewicz ES, Wunderlich M, Brauns U, Becker R, Bock T, Dressman JB. Predicting the precipitation of poorly soluble weak bases upon entry in the small intestine.

J Pharm Pharmacol. 2004;56(1):43-51. doi: 10.1211/0022357022511. PubMed PMID: 14980000.
302. Berghausen J, Seiler FH, Gobeau N, Faller B. Simulated rat intestinal fluid improves oral exposure prediction for poorly soluble compounds over a wide dose range. Admet & Dmpk. 2016;4(1):35. doi: 10.5599/admet.4.1.258.
303. McConnell EL, Basit AW, Murdan S. Measurements of rat and mouse gastrointestinal pH, fluid and lymphoid tissue, and implications for in-vivo experiments. J Pharm Pharmacol. 2008;60(1):63-70. Epub 2007/12/20. doi: 10.1211/jpp.60.1.0008. PubMed PMID: 18088506.